RCA REVIEW

a technical journal

RADIO AND ELECTRONICS
RESEARCH • ENGINEERING

VOLUME XIII SEPTEMBER 1952 NO. 3

PRINTED IN U.S.A.

RCA REVIEW, published quarterly in March, June, September and December by RCA Laboratories Division, Radio Corporation of America, Princeton, New Jersey. Entered as second class matter July 3, 1950 at the Post Office at Princeton, New Jersey, under the act of March 3, 1879. Subscription price in the United States, Canada and Postal Union; one year $2.00, two years $3.50, three years $4.50: in other countries; one year $2.40, two years $4.30, three years $5.70. Single copies in the United States, $.75; in other countries, $.85.

RCA REVIEW

a technical journal

RADIO AND ELECTRONICS
RESEARCH • ENGINEERING

Published quarterly by
RCA Laboratories Division
Radio Corporation of America
in cooperation with

RCA Victor Division
Radiomarine Corporation of America
RCA International Division
RCA Communications, Inc.
National Broadcasting Company, Inc.
RCA Institutes, Inc.

VOLUME XIII SEPTEMBER, 1952 NUMBER 3

CONTENTS

RCA REVIEW is regularly abstracted and indexed by *Industrial Arts Index, Science Abstracts* (I.E.E.-Brit.), *Electronic Engineering Master Index, Chemical Abstracts, Proc. I.R.E.*, and *Wireless Engineer.*

RCA REVIEW

BOARD OF EDITORS

A HIGH-ACCURACY TIME-DIVISION MULTIPLIER*

By

Edwin A. Goldberg

Research Department, RCA Laboratories Division,
Princeton, N. J.

Summary—*An electronic multiplier is described which produces a pulse wave form whose amplitude is proportional to one variable, whose length relative to period is a function of another variable, and whose average value is proportional to the product of the two variables. This principle is an old one, but multipliers based on it have not heretofore been high-precision devices. Through the use of a novel high-precision electronic switch whose characteristics are essentially independent of tube characteristics, and a feed-back system for establishing the proper timing of the pulse wave form, a high-speed multiplier with a precision of the order of 0.01 per cent of full scale has been developed for use in analogue-type electronic computers. This work was done under contract with the Office of Naval Research, Special Devices Center, as part of the Typhoon Analog Computer project.*

Introduction

THE speed and accuracy obtainable with analogue computers has been principally limited by the multipliers available. A multiplier has been developed which has accuracy and speed capabilities superior to any other electronic multipliers with which the author is familiar.

The basic principles upon which this multiplier operates are not entirely new. A wave train consisting of rectangular pulses is generated. The amplitude of the pulses is made proportional to one of the variables (multiplicand), the ratio of pulse length to period is made a function of another variable (multiplier), and the average or direct-current component of the resultant wave train is then proportional to the product of the two variables. High precision is obtained through the use of a feed-back system to establish the proper pulse timing, and an electronic switch circuit with excellent characteristics.

Establishment of Pulse Timing

The system used for establishing the proper timing for the pulse wave form is illustrated in the block diagram of Figure 1. The electronic switch (block 1) has the following characteristic: If lead b is positive with respect to lead c, current k, proportional to voltage K,

*Decimal Classification: 621.375.2.

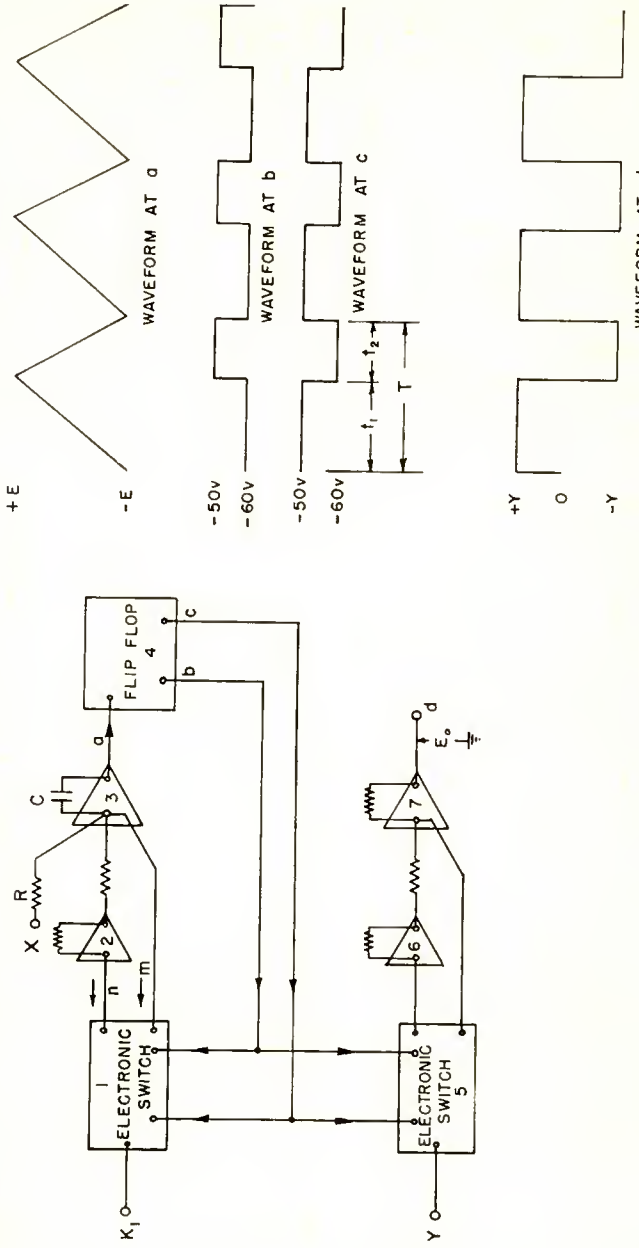

Fig. 1—Basic time-division multiplier.

will flow in lead m in the direction of the arrow and the current in lead n will be zero. If lead c is positive with respect to lead b, the same current k will flow in lead n, and the current in lead m will be zero. Let us call the former case I, and the latter case II. The flip-flop will produce output voltages per case I after the input at a has reached —E, and will produce output voltages per case II after the input at a has reached +E. The current input to the integrator (block 3) is $x - k$ for case I and $x + k$ for case II. The timing is computed as follows:

Let $2E$ = voltage excursion required at input of flip-flop to change its state,

C = capacity of condenser in integrator in farads,

X = value of multiplier factor in volts,

R = input resistor for multiplier in ohms,

$x = \frac{X}{R}$ = input current to integrator due to the multiplier factor X,

t_1 = duration per cycle case II applies,

t_2 = duration per cycle case I applies,

$T = t_1 + t_2$ = period in seconds,

$f = \frac{1}{T}$ = frequency in cycles per second.

Then $$t_1 = \frac{2CE}{k + x},$$

$$t_2 = \frac{2CE}{k - x},$$

$$T = \frac{4k\,CE}{k^2 - x^2},$$

$$f = \frac{k^2 - x^2}{4k\,CE},$$

Thus, it is apparent that the period is not constant, but varies as a function of the value of the multiplier factor, X.

The multiplicand, Y, is switched through the use of electronic

switch 5 which is actuated by the same switching pulses as switch 1. A wave train similar to that of Figure 1(d) appears at the output of amplifier 7. Its average value, E_o, may be computed as follows:

$$E_o = \frac{+Yt_1 - Yt_2}{T},$$

$$E_o = \frac{\dfrac{+Y\,2CE}{k+x} - \dfrac{Y2\,CE}{k-x}}{\dfrac{4k\,CE}{k^2-x^2}},$$

$$E_o = -\frac{xY}{k} = \frac{XY}{K_1},$$

where $K_1 =$ a constant.

Thus, it is apparent that the average value of the output voltage of amplifier 7 will be proportional to the product of the multiplier and multiplicand input voltages.

Electronic Switch

The heart of the multiplier lies in the electronic switch circuit. This switch differs from most electronic switches in that it is a current switch rather than a potential switch. It has the following characteristics. When the switch is turned off, the current output is zero, and when it is turned on, the current output is a linear function of the voltage input. In addition, the characteristics of the switch are essentially independent of the characteristics of the tubes employed.

Figure 2 is a diagram of the electronic switch. Amplifiers 1, 2, and 3 are wide-band, chopper-stabilized, direct-current amplifiers.[1] Switching signals are applied to the grids of the 6J5 triodes T_2 and T_3. If the control grid of T_2 is positive with respect to the control grid of T_3 by a sufficient amount, the plate current of the 6SJ7, T_1, will flow through tube T_2 and the output voltage E_2 will have a negative polarity. If the control grid of T_3 is positive with respect to the control grid of T_2 by a sufficient amount, the plate current of T_1 will flow through T_3 rather than through T_2, and E_2 will have the same

[1] E. A. Goldberg, "Stabilization of Wide-Band Direct-Current Amplifiers for Zero and Gain," *RCA Review*, Vol. XI, pp. 296-300, June, 1950.

magnitude as before, but it will have positive rather than negative polarity. The plate current of T_1 can thus be made to flow in either of two external circuits. The plate current of T_1 is made a linear function of an input voltage E_1 through use of a large amount of degenerative feedback. Feedback insures that the potential e_3 at the cathode end of R_3 will be given by

$$e_3 = -\frac{R_2}{R_1} E_1 .$$

The current in the cathode circuit of T_1 will be the algebraic sum of the currents in resistors R_2 and R_3, which in turn will be a linear function of the input voltage E_1 provided the —300-volt source voltage is held constant. Since the screen battery and the suppressor grid of

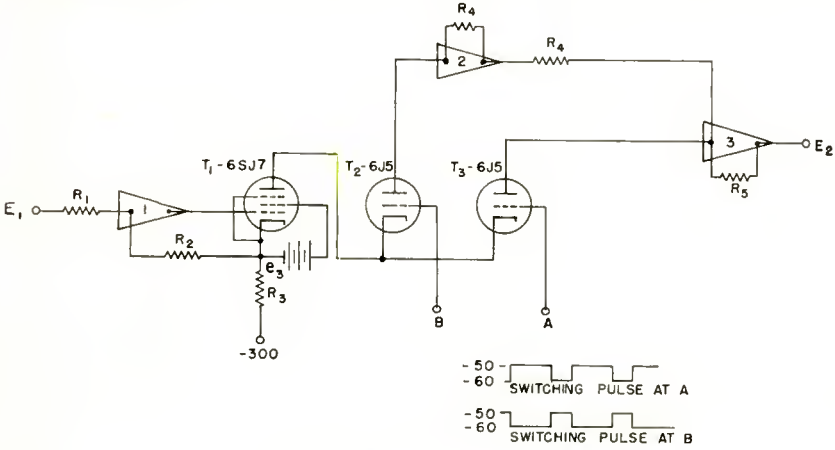

Fig. 2—Electronic switch.

the 6SJ7 are both returned directly to the cathode, the current in the plate circuit will be equal to the current in the cathode circuit.

A pentode rather than a triode is used for T_1 because of its inherently high dynamic-plate-resistance characteristic which makes the plate current essentially independent of the plate voltage for constant grid voltage. During switching, the cathode potential of T_2 and T_3 will vary in accordance with the switching potentials at A and B. Since switching occurs rapidly, amplifier 1 would have to be capable of handling high-frequency components to maintain the plate current of T_1 constant during switching if it were necessary to change the grid potential of T_1 to do so. Use of the pentode con-

sequently means less stringent requirements on the high-frequency response characteristics of amplifier 1.

The range of input voltage which may be handled is limited. For the arrangement shown, the plate of T_1 operates at about —50 volts. Allowing a minimum plate voltage of 50 volts on T_1 (relative to cathode) would limit the most positive potential for e_3 to —100 volts. The maximum negative potential for e_3 would occur when the plate current of T_1 is zero, and is a function of R_2, R_3, and the —300-volt potential. Normally, the range of operation should not be such that the plate current of T_1 is ever actually cut off. Since the range of input potentials is limited, a fixed voltage is added to the variable voltage at the input of each switch. The unwanted component in the resultant output of the multiplier is eliminated by a bridging system described later.

Sources of error are such items as (1) heater–cathode leakages, (2) excessive grid current in any of the three tubes of the switch proper, and (3) excessive capacity between the common cathodes of the 6J5's and ground. Item 1 may be controlled through the use of separate, well-insulated, heater transformers, and item 2 may be controlled through tube choice and proper operating range. Item 3 will cause switching errors which increase as the repetition rate increases, but is subject to control by either choosing matched 6J5's, or shifting the level of switching pulses A relative to B so that the common cathode potential does not change when the current is commutated from one 6J5 to the other.

Flip-Flop

Figure 3 is a schematic diagram of a flip-flop circuit which has been found satisfactory for use in the multiplier. The integrator output connects to terminal I, the input terminal to the flip-flop. A 6SN7, cathode-coupled, flip-flop stage generates square waves in accordance with the voltage variations applied to terminal I. These square waves actuate another flip-flop consisting of three 6AG7 tubes. The square-wave output of this flip-flop has extremely steep sides, and is applied to a pair of 6Y6-G's used as a push-pull power-output amplifier. Output from the unit is derived from Terminals A and B, and the voltage excursion on each output terminal is between —50 volts and —60 volts. The whole unit is direct-current coupled.

A simpler flip-flop circuit may be employed. The one described above was developed to produce switching waves with extremely short rise time to minimize multiplier errors due to finite switching time. The power-output stage was incorporated so that a large number of

electronic switches might be driven from the one pulser unit without having the resultant wiring capacity cause the switching pulse wave form to deteriorate.

Practical Multiplier

A practical multiplier diagram showing the method employed to permit bipolar operation with the precision switch is illustrated in Figure 4. The scale factors in terms of volts are as follows for the values of resistances and fixed reference voltages shown:

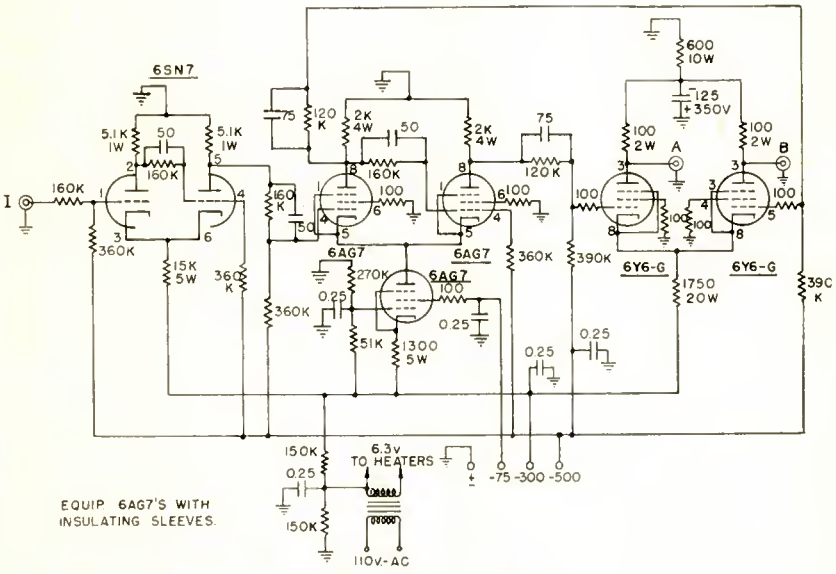

Fig. 3—Multiplier flip-flop.

$$\text{Nominal full scale } X \text{ input} = 75 \text{ volts},$$

$$\text{Nominal full scale } Y \text{ input} = 75 \text{ volts},$$

$$\text{Nominal full scale } E_o \text{ output} = 75 \text{ volts},$$

$$E_o = \frac{XY}{75} \text{ volts}.$$

A constant input voltage, K, is applied to the input circuit of each of the switches. It is so chosen that, for the case of the timing switch,

the cathode of T_1 will operate at a potential of —175 volts. The cathode of T_4 of the slave (lower) switch will operate at a potential of $-175-Y$ volts. The excursion of Y will be ±75 volts full scale resulting in an excursion from —100 to —250 volts for the cathode of T_4. If $Y=0$, the cathode of T_4 is at —175 volts, and the current through T_4 will be finite. Normally, this would result in a net direct-current output of amplifier 7 for values of X other than zero. This spurious term in the product is a linear function of X, and is eliminated by feeding a linear component of X into the input of amplifier 7 in addition to the output of the slave switch. In this manner, the average output voltage of amplifier 7 is made proportional to the product XY.

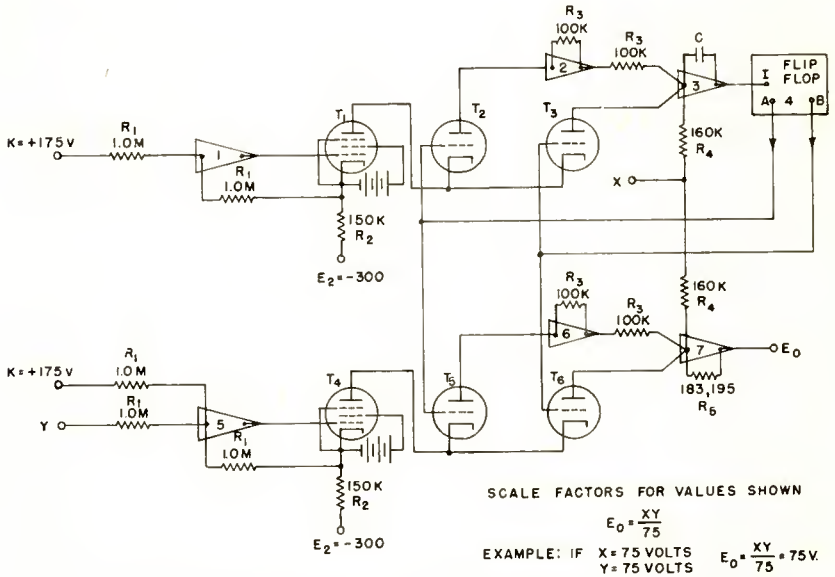

Fig. 4—Time-division multiplier incorporating switch of Figure 2.

For the arrangement shown, E_0 consists of pulses whose average component is the product desired. Quite frequently in analog computer applications, a multiplier is followed by an integrator. For such an application, R_3 might be replaced by a capacitor, and amplifier 7 would become the integrator. No filter would be required to remove the alternating-current components of the pulses because the integrator itself would perform this function.

For cases where the output of one multiplier is used as one of the inputs to another multiplier, it is normally necessary to remove the

alternating-current components due to pulse repetition rate, especially if the second multiplier is operating at a repetition rate either equal to, or close to, that of the first. If the alternating-current components are not removed, erroneous results will be obtained from the second multiplier. A low-pass filter on the output of the first multiplier is required to eliminate the alternating current.

Performance

The accuracy of this multiplier has been measured with a bridging system which makes it possible to measure linearity of output with respect to either variable without having to depend on the accuracy of calibration of potentiometers. The accuracy is a function of the repetition rate chosen. Since the repetition rate varies about two to one for full-scale variation of X, the repetition rate mentioned will be the repetition rate for $X = 0$ (maximum repetition rate).

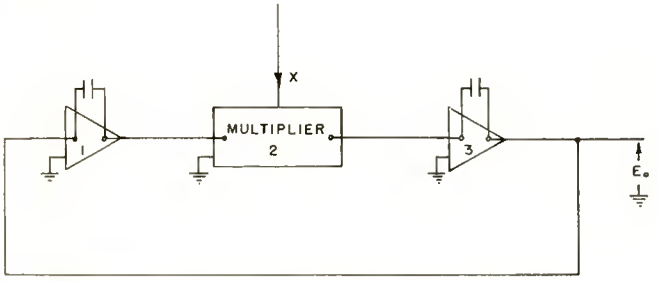

Fig. 5—Computing loop for measurement of delay characteristic of multiplier without filter.

Tests indicate that the accuracy obtainable is about ±0.01 per cent of full scale for a maximum pulse repetition rate of 2000 cycles, and ±0.1 per cent of full scale for a pulse repetition rate of 20,000 cycles.

When used with a filter to remove the pulses from the output, the delay of the multiplier is practically the same as the delay of the filter. When used without a filter, the delay is considerably less than the period of the repetition rate. Delay characteristics without the filter have been studied through the use of the computing circuit shown in Figure 5. The total phase shift consists of 180 degrees due to the two integrators plus an additional amount due to the multiplier. The amount due to the multiplier may be found by determining the decrement of the sine wave produced. If the Y input of the multiplier is in the loop, a resistance–capacitance (RC) circuit with lagging

phase shift with a time constant considerably less than the repetition-rate period inserted in the loop, must be used to compensate for the delay characteristic of the multiplier. This indicates that the multiplier has a leading phase-angle characteristic when so used. If the X input, rather than the Y input, of the multiplier is in the loop, an RC circuit with leading phase shift is required for compensation. This indicates a lagging phase characteristic for the multiplier when used in this manner. The delay is considerably less than the repetition rate period.

Conclusion

This multiplier circuit should find considerable application in the field of analogue computers. The accuracy and speed of response characteristics are considerably better than for any other analogue type of electronic multiplier known to the author. The superior performance is obtained by (1) use of a feed-back system for establishing accurate timing, (2) use of steep switching pulses, (3) use of an electronic switch circuit of predictable performance independent of tube characteristics, and (4) use of precision resistors and reference voltage sources.

Acknowledgment

The writer wishes to acknowledge the work done by A. W. Vance of RCA Laboratories Division, Princeton, in establishing the feed-back timing principle used. The writer also wishes to give due credit to Milo Wadlin of RCA Laboratories Division, Princeton, who has conducted the major portion of the experimental work on this multiplier.

A TIME-DIVISION MULTIPLEX TERMINAL*

By

Orville E. Dow

Research Department, RCA Laboratories Division,
Rocky Point, N. Y.

Summary—*A twenty-two channel, time-division multiplex terminal of the pulse-amplitude-modulated variety is described. The individual channels are suitable for the transmission of voice-frequency signals. Circuit details of the electronic distributor, which uses a step-wave timing voltage, are described. The method of reducing noise, a cross-talk balancing circuit, and performance results are explained.*

Introduction

MICROWAVE radio-relay systems are rapidly increasing in number and size. The services they provide vary from the extensive public-carrier networks to the smaller private-communication links. Whereas microwave radio-relay equipment may readily transmit a wide frequency band of the order of megacycles, most of the systems will be required to supply a number of narrow-band channels for telephone, teletype, telemetering, and remote control service. Thus, to obtain complete and efficient use, the wide band must be divided into narrow-band channels.

The process of multiplexing, that is, transmitting several narrow-band channels over a single wide-band circuit, may be accomplished by one of two general methods: frequency-band division and time division. In the frequency-band division method, each narrow-band channel uses part of the total frequency band of the common circuit all of the time. In the time-division method, each narrow-band channel uses the total frequency band of the common circuit part of the time, that is, each narrow-band channel is assigned to definite time intervals when it alone may occupy the common circuit. There are other sub-classifications under the two main methods which have been described and analyzed by Landon.[1] Of the many types of time-division multiplex systems, we will be concerned here with the one designated symbolically as PAM±FM. In such a circuit, the narrow-band channels are in effect connected momentarily to the common circuit in rapid succession. The resulting amplitude-modulated pulses, of both plus and minus polarities, are used to frequency modulate the radio-frequency carrier. A multi-

* Decimal Classification: R 460.

[1] V. D. Landon, "Theoretical Analysis of Various Systems of Multiplex Transmission," *RCA Review*, Vol. IX, June, 1948, pp. 287-351, and September, 1948, pp. 433-482.

plex terminal for such a system with a capacity of twenty-two voice-frequency channels plus a service channel will be described.

General Description

Each 22-channel terminal, which consists of a transmitter, receiver, all power supplies, test equipment, and terminal jacks, is contained in three standard seven-foot cabinet racks. A front view of such a terminal is shown in Figure 13. The construction is such as to make all parts of the multiplex circuits readily accessible from the back without removal from the cabinet.

The individual channels of this terminal have a transmission band extending from 100 to 3400 cycles per second. The normal input to or output from any channel is a level corresponding to zero dbm, which is one milliwatt across a balanced 600-ohm load.

In the multiplexing process, each channel is sampled 8333 times per second by means of an electronic distributor. One period of the

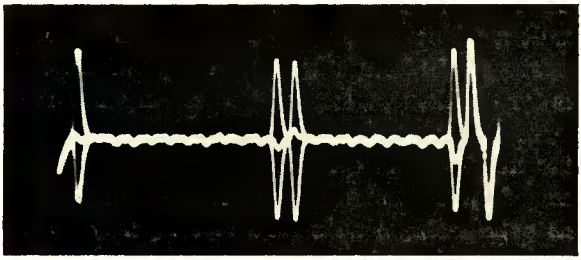

Fig. 1—One frame of the multiplex-transmitter output signal.

distributor is called a frame and contains twenty-two channel pulses and the synchronizing pulse. With a tone input to a channel terminal equal to zero dbm, the pulse in the frame corresponding to that channel has a peak-to-peak amplitude of three volts at the transmitter output. The synchronizing pulse consists of a positive pulse with a peak amplitude of one and one-half volts followed by a negative pulse with a peak amplitude of one and one-half volts. The positive half of the synchronizing pulse occupies the position of channel number twenty-three and the negative half the position of channel number twenty-four. The service channel shares time interval number twenty-three with the first half of the synchronizing pulse. Figure 1 is an oscilloscope picture of one frame of the transmitter output signal. Channels one, twelve, thirteen, and twenty-two are being modulated at their peak level with a common tone, the frequency of which is exactly one-third the sampling frequency. Each channel pulse is thus shown at three

different amplitudes corresponding to different phases of the modulating tone. One frame lasts for 120 microseconds (1/8333 second) and, since it contains twenty-four time intervals, each interval has a duration of five microseconds. Thus, duration is equal to the period of a 200,000 cycle per second sinusoidal wave which is the basic frequency of the transmitter and receiver distributors.

Transmitter

The function of the electronic distributor is to make each channel in succession operative for a short period during the five-microsecond time interval allotted to it in every frame. The distributor is made

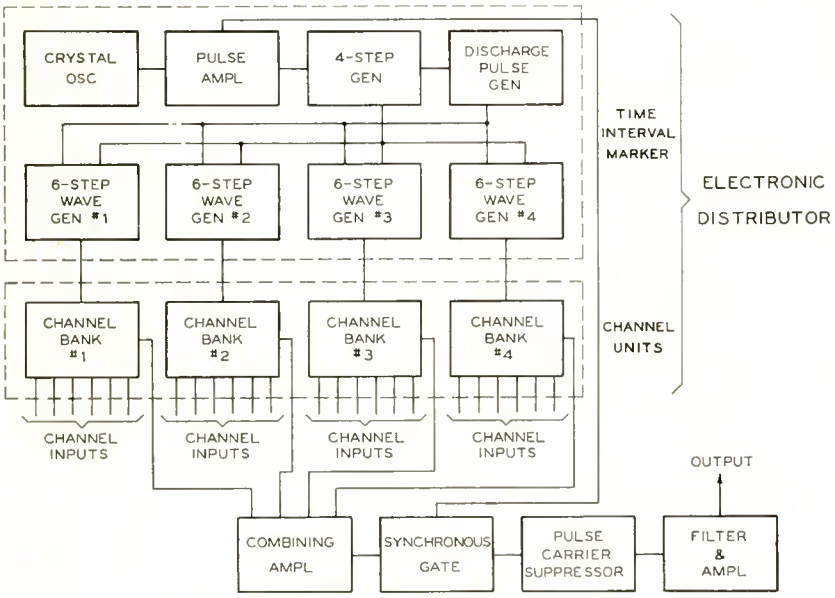

Fig. 2—Block diagram of transmitter.

up of two parts: first, the time-interval marker, and second, the channel unit as shown in the block diagram of the transmitter (Figure 2). The time-interval marker contains a two-stage step counter. The first stage is driven from crystal controlled pulses which have a repetition rate of 200,000 per second (Figure 3a) and it generates a series of step waves. Each step wave has four equal "risers" and is repeated 50,000 times per second as shown in Figure 3b. The second stage contains four identical branches. Each branch has a counter which generates a step-wave voltage with six risers as shown in Figure 3c. The risers of six-step wave number one coincide with the first risers

of the four-step wave; the risers of six-step wave number two coincide with the second risers of the four-step wave, and so on. Thus, each of the twenty-four risers of the four six-step wave voltage marks the beginning of a different time interval in the frame. The output of each six-step-wave generator is connected to a bank of six channels. Each riser initiates a gate pulse for a particular channel.

In the four-step counter-circuit, triode $V2$ of Figure 4 adds an increment of charge to the capacitor C each time its grid is made positive by the output from the pulse amplifier. Each increment of charge causes an increase in voltage across capacitor C. When the potential across C has reached a predetermined level, triode $V3$ becomes

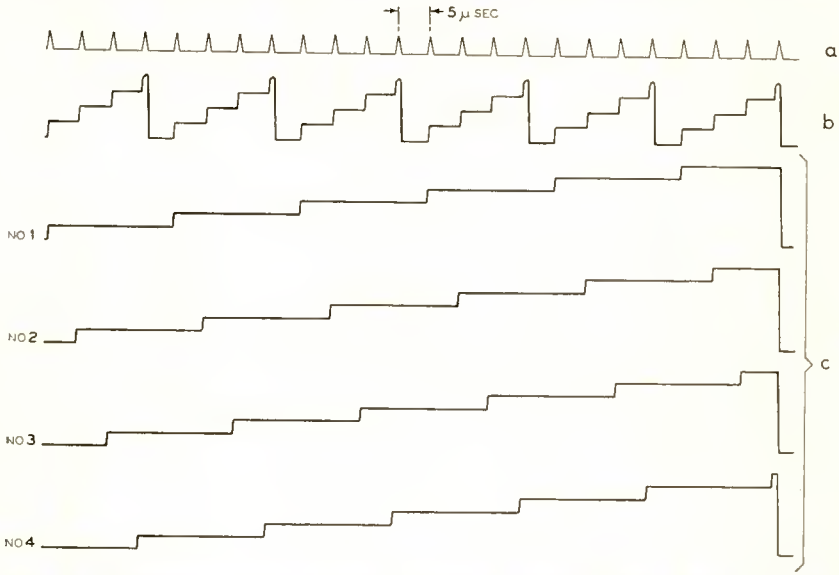

Fig. 3—Relative occurrence time of voltage waves in the interval marker.

conducting and, due to the regenerative action of the transformer $L1$, its grid is driven positive with respect to its cathode. The resulting grid current causes capacitor C to be discharged so that its high terminal is negative with respect to ground. The clamp diode connected across the capacitor returns the high terminal to ground potential so that number one riser always starts from zero potential. The four-step wave is coupled to the four six-step wave generators by a cathode follower. The 50,000 pulses per second generated in the transformer $L2$ when triode $V3$ discharges capacitor C, are coupled to a discharge pulse generator.

Each six-step wave generator (Figure 5) has a selector triode, 1, which is biased to become conducting on a particular riser of the four-

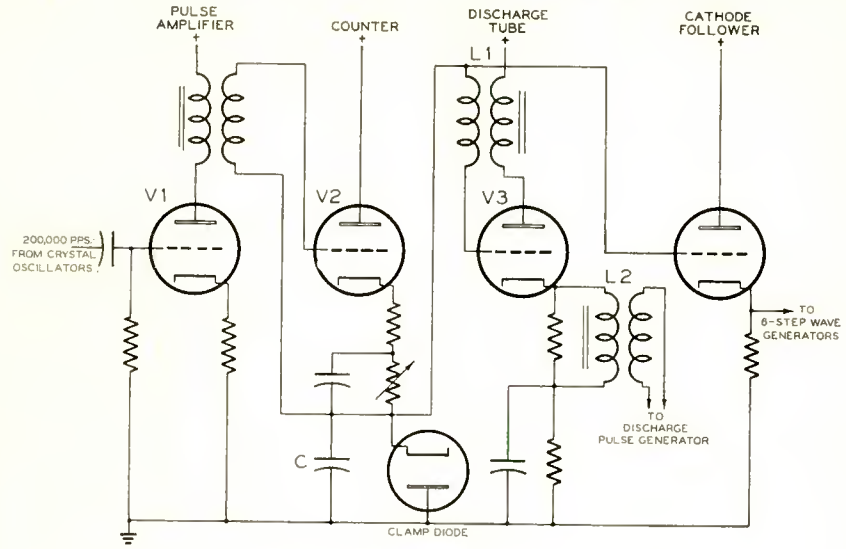

Fig. 4—Four-step wave-generator circuit.

step wave. Thus, generator number one is assigned to riser number one, generator number two is assigned to riser number two, etc. When the selector becomes conducting, it generates a pulse which is used to operate the six-step counter circuit. The limiting resistor in series with the grid of the selector triode, 1, prevents the generation

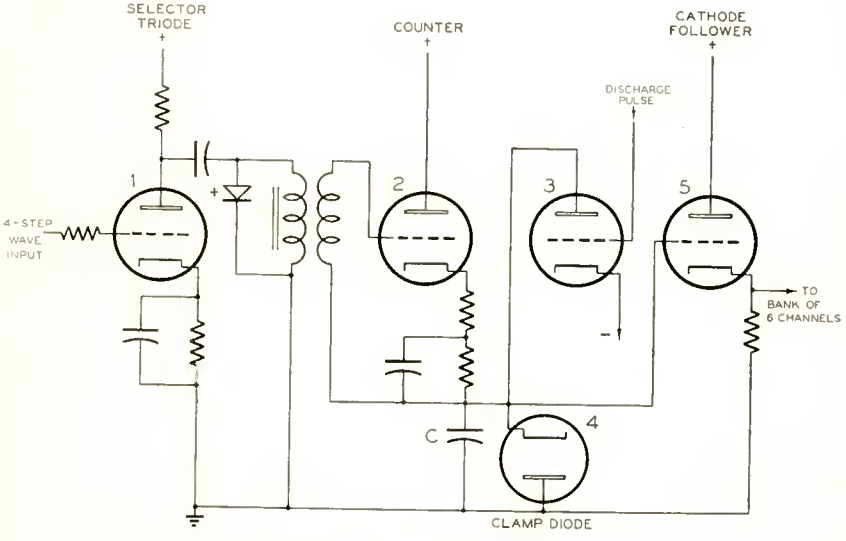

Fig. 5—Six-step wave-generator circuit.

of a pulse at the time of any riser which begins at a higher voltage than the assigned riser. The counter circuit performs as does the counter in the four-step wave generator. After every sixth riser the triode 3 is made conducting by a short plus pulse from the discharge pulse generator to discharge the capacitor C. To insure that the capacitor C is discharged below ground potential, the cathode of triode 3 is returned to a negative supply. This permits the clamp diode, 4, to return capacitor C to zero potential so that each riser of the step wave always occupies the same voltage range. Each of the four six-step waves is coupled to a bank of six channels by a cathode follower.

The discharge pulse generator produces a stable positive pulse which occurs following the last riser of number four four-step wave. The use of an independent discharge pulse permits the adjustment of

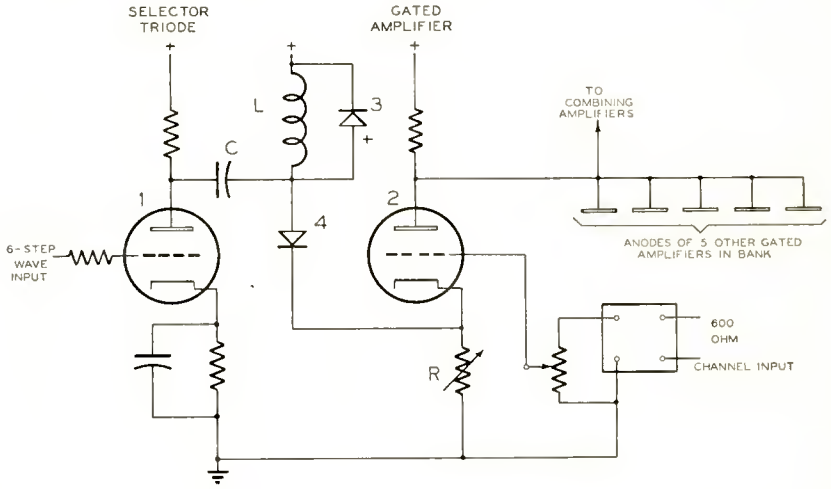

Fig. 6—Transmitter-channel unit.

the amplitudes of the six-step waves over a considerable range without altering their count.

Each of the twenty-four channel units in the transmitter has a selector triode and a gated amplifier (Figure 6). The selector triode generates a gate pulse at the time interval assigned to that particular channel. As in the six-step wave generator, the selector is biased so as to become conducting during the time of a particular riser. The amplitude of the riser and the plate-to-cathode voltage of the triode are such that the tube goes from the condition of zero plate current to grid conduction in the amplitude range of one riser. Any additional increase of the voltage input to the selector grid due to succeeding risers beginning at a higher potential appears almost entirely across

the limiting resistor in series with the grid of the selector triode, and hence, does not change the plate current appreciably. When the selector conducts, the negative voltage step generated in its anode circuit excites the tuned circuit L–C of Figure 6. The width of the resulting gate pulse is determined by the resonant frequency of L and C. Any positive voltage transient which would appear across L following the gate pulse or at the end of each step wave when the selector again becomes nonconducting is suppressed by diode 3.

The gated amplifier triode 2, Figure 6, is maintained in the cutoff condition due to current through its cathode resistor from a direct-current supply by way of inductor L and diode 4. When, due to the negative gate pulse on its anode, diode 4 becomes nonconducting, triode 2 operates as a class-A amplifier and produces in its anode circuit a negative pulse with an amplitude proportional to the amplitude of the channel input voltage on its grid at that instant. The six gated amplifiers of each of the four banks have a common plate-load resistor so that the bank output signal has, in one frame, six unidirectional amplitude-modulated negative pulses.

The synchronizing pulse is generated in channels twenty-three and twenty-four. The average or unmodulated amplitude of each of the channel pulses, except numbers 23 and 24, is adjusted to equality by a cathode resistor R in each of the gated amplifiers (Figure 6). The pulse output of channel twenty-three is made lower than average and the output of channel twenty-four is made higher than average, and in this way the synchronizing pulse is generated.

The four pulse signals from each bank are coupled into one common circuit by four combining triode amplifiers. At this point, one frame contains twenty-four unidirectional channel pulses. The pulses of individual channels differ slightly in shape due to the differences in the gating tubes. In order to make them uniform, the multiplex signal is transmitted through a synchronous gate which selects only the center portion of each channel pulse. The direct current or unvarying part of the resulting pulses is balanced to zero by a pulse carrier suppressor, which leaves only the modulated part of the channel pulses. The synchronous gate (Figure 7) is operated from the crystal-controlled pulse amplifier by pulses which are delayed so as to register with the centers of the channel pulses. The gate generator, 1, and the gated amplifier, 2, are similar to the circuits of the channel unit, except that the inductance L and the capacitance C are chosen so as to generate a gate narrower than any channel pulse. The pulse-carrier generator, 3, is also a gated amplifier, but whereas triode 2 has on its grid the multiplex signal from the combining amplifiers, triode 3 has a direct-current bias on its grid. The value of this bias is adjusted until the amplitude

of the pulses at the anode of tube 3 is equal to the average or unmodulated amplitude of the pulses at the anode of tube 2. Since both tubes are gated by the same voltage wave, the width of the pulse voltages at their anodes will be equal. The voltage at the anode of triode 3 is inverted by the unity gain amplifier 4, and combined with the output of triode 2. This balances out the pulse carrier from the output signal. The resulting signal is then amplified and transmitted through a low-pass filter to remove the high-frequency gating components, and the resulting output signal appears as in Figure 1.

The signal generated by the multiplex transmitter is used to frequency modulate the radio-frequency transmitter. When the pulse signal is recovered by demodulation in the radio-frequency receiver, it will have noise added to it which has a frequency distribution char-

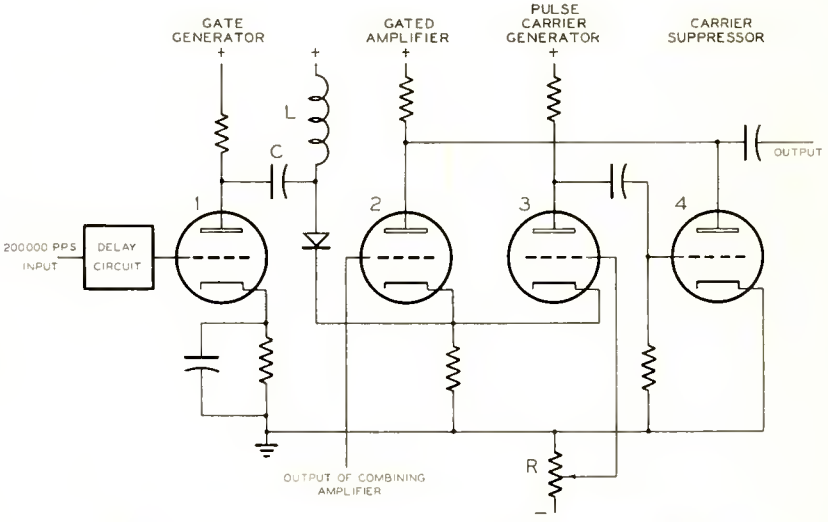

Fig. 7—Synchronous gate and pulse-carrier suppressor.

acteristic of a frequency-modulated system. The noise in the base frequency or modulation band will be zero at zero frequency and will increase linearly in amplitude with increase in frequency. The distribution of the energy of the multiplex signal in the modulation band is the reverse of the noise energy, that is, the greater part of the signal energy is in the low frequency end of the base frequency band. It is the function of the multiplex receiver to separate out the individual channel pulses and transmit the intelligence carried by them to the respective channel output terminals with the maximum signal-to-noise ratio obtainable.

Receiver

Preliminary to performing its primary function of separating the channel pulses, the receiver must first condition the pulse signal, that is, reduce the noise and cross talk to an acceptable value, and second, phase the locally generated channel gates with the received signal. The various functions of the receiver are indicated in the block diagram of Figure 8.

To reduce the noise on the received multiplex signal, it is transmitted through a low-pass filter with an attenuation characteristic similar to that shown in Figure 9. The approximate distribution of the sinusoidal components of the signal and the noise components are

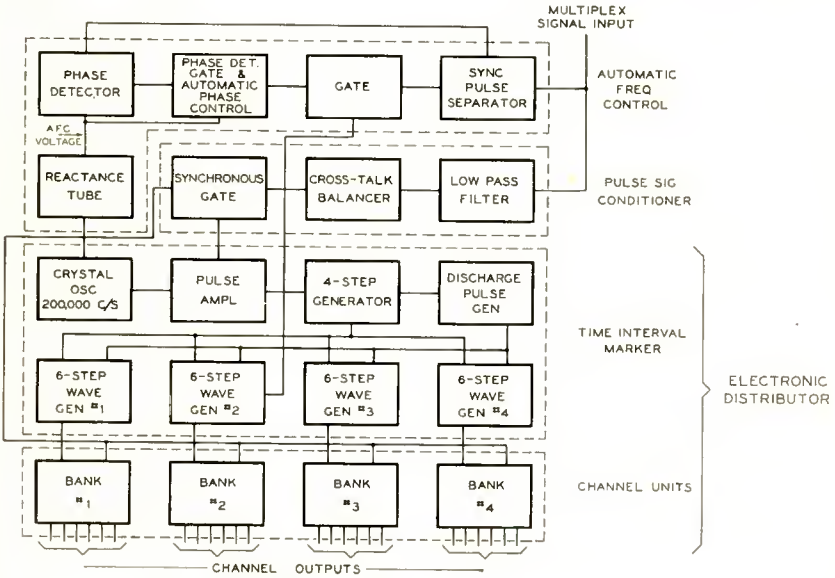

Fig. 8—Block diagram of receiver.

indicated in the figure; however, the actual or relative value of signal and noise is not shown. The action of this filter is to attenuate the noise more than the signal. A filter with this type of response transmits the pulses without oscillations in the "trail off," that is, the trailing edge of each pulse decreases rapidly and continuously toward zero. The width of the low-pass filter is chosen so that its equivalent noise band is one-half the number of channel intervals times the frequency of the channel repetition rate, or 100,000 cycles per second.

Due to the attenuation of the high-frequency components, the low-pass filter lengthens each channel pulse so that it trails off into the first and second following channel intervals. A cross-talk balancer

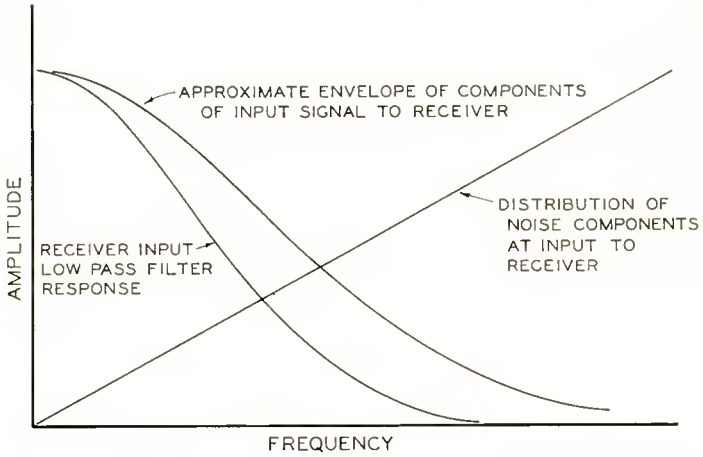

Fig. 9—Low-pass filter attenuation characteristic and distribution of sinusoidal components of pulses and noise at input to receiver.

circuit of the delay-line type (Figure 10) reduces the cross talk to an acceptable level. The action of this circuit is to peak the high frequencies and adjust the phase response. The peaking action is undesirable in that it increases the noise level, so the principal gain is derived from the change in the phase response. The operation of the cross-talk balancing circuit may be explained by considering the time response rather than the frequency response. The cutoff frequency of the delay line is high enough so that the shapes of the pulse waves are not

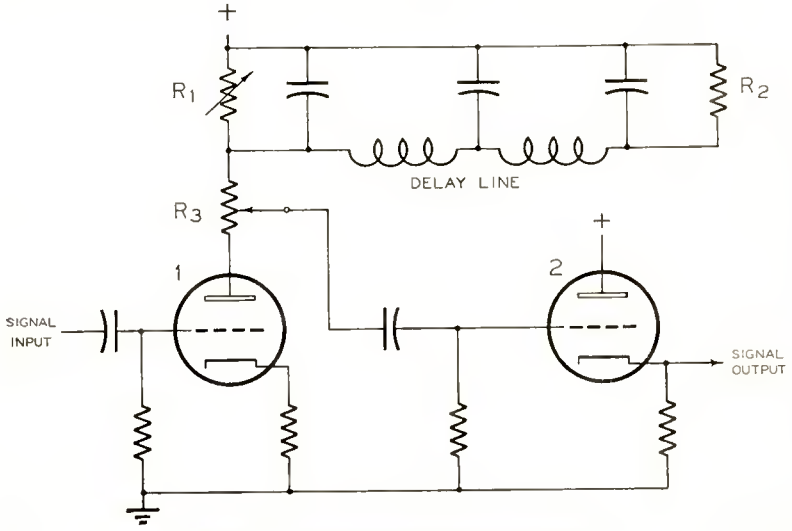

Fig. 10—Cross-talk balancer circuit.

materially changed by transmission over it. In Figure 11, the instantaneous values of a main signal pulse for channel one are shown trailing over into the time interval of channel two to cause cross talk. This cross talk is indicated by the shaded area above the base line. If a portion of this main signal pulse is delayed and inverted, it will appear as indicated by the curve below the base line. If the amplitude of the delayed and inverted pulse is adjusted until the shaded area below the base line is equal to the shaded area above the base line, the cross talk from channel one into channel two will be zero when these two signals are combined. The main portion of the signal pulse is transmitted directly from the output of triode 1 to the input of triode 2, Figure 10. The delayed portion is transmitted down the delay line and partially reflected with a reversal of polarity at resistor R_2.

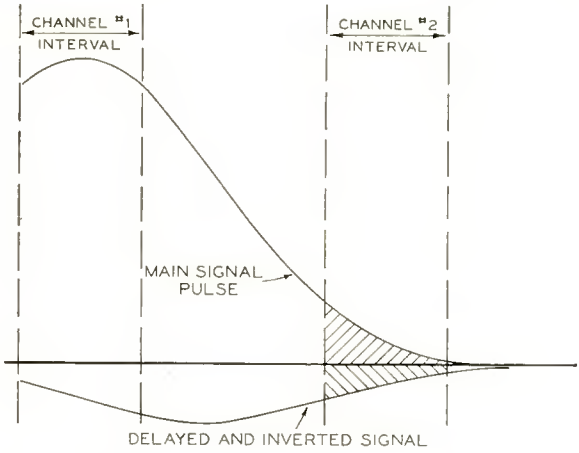

Fig. 11—Voltage waves in cross-talk balancer.

The reflected portion travels back over the line, where it is further delayed and finally combined with the main part of the signal at the grid of tube 2. The amplitude of the main part of the voltage wave relative to the delayed part is determined, in part, by the setting of potentiometer R_3. An additional reflection at the input terminals of the line may be produced by making resistor R_1 either larger or smaller than the characteristic impedance of the line. This adjustment may be used to remove cross talk from any channel into a second following channel. Since all channels are precisely spaced, the reduction of cross talk between one group of channels will reduce it for all channels in the terminal.

One more conditioning action must be performed on the input signal before the individual channel pulses are ready to be selected

by their respective channels. The signal is transmitted through a synchronous gate, which operates 200,000 times per second, and selects the center slice of each channel pulse for transmission to the channel units. This type of gate is a nonlinear device during the transition time when it is changing from the off to the on condition and, therefore, adds distortion to the signal. For this reason, the transition periods are made short relative to the total on time of the gate so that the amplitude distortion introduced by the gate will be small. The selected center portion of each channel pulse fits, with margin, into the channel gates so that the slower operating channel gates add no distortion to the output signal. The signal applied to the grids of the channel gated amplifiers is a series of short, unidirectional, amplitude-modulated pulses as represented in the oscilloscope picture of Figure 12.

The receiver channels are grouped in four banks of six channels each, as in the transmitter. Also, each channel has a selector triode and a gated amplifier which performs as in the transmitter. However,

Fig. 12—Input signal to receiver-channel units.

in the receiver, the grids of all the gated amplifiers are connected together and have impressed on them the conditioned multiplex signal. The plate of each gated amplifier is connected, via a low-pass filter and a two-stage audio amplifier, to a channel output terminal. The low-pass filter removes all frequencies above 3400 cycles per second from the individual channel pulse signals and leaves only a reproduction of the signal voltage applied to the input terminals of that channel at the transmitter.

The time-interval marker in the receiver is identical to the time-interval marker in the transmitter. To maintain the individual channel gates registered with the correct channel pulse, a phase detector generates a direct-current voltage which, by means of a reactance tube, makes the necessary corrections in the phase of a local crystal oscillator operating at 200,000 cycles per second. The direct-current output of the phase detector is proportional to the difference of occurrence time of the received synchronizing pulse and a locally generated gate pulse. Thus, if the frequency of the transmitter crystal

oscillator changes with respect to the receiver crystal oscillator, the resulting initial change in the timing of the two voltage waves compared in the phase detector varies the direct-current automatic-frequency-control voltage to the reactance tube in the direction to make the required frequency adjustment of the receiver crystal oscillator. However, the resulting error in timing required to generate the correcting voltage will throw the channel gates out of exact register with the received signal. To overcome this, an automatic phase-control circuit, operating in response to the direct-current output of the phase

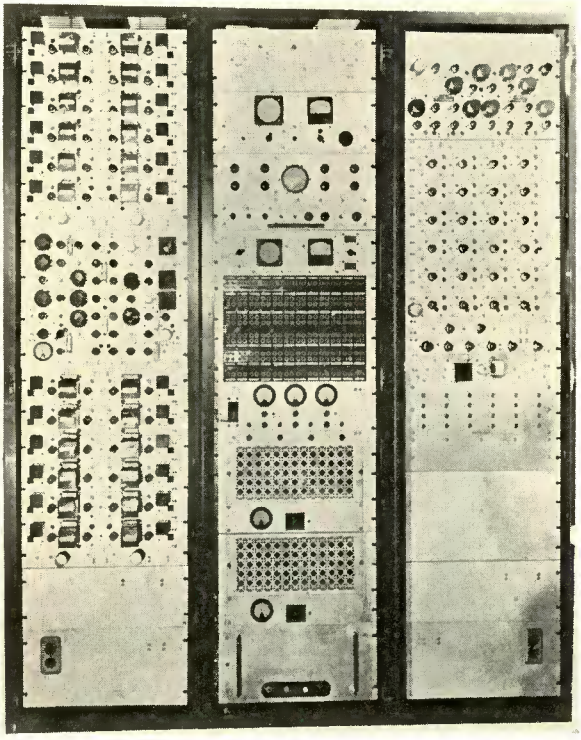

Fig. 13—Front view of 22-channel terminal.

detector, shifts the locally-generated phase-detector gate pulse by exactly the same amount as the timing error which produced the direct-current correcting voltage and in a direction to keep the channel gates registered with the received signal pulses. For example, if a change of —0.1 microsecond in the occurrence time of the phase-detector gate pulse with respect to the received synchronizing pulse produced a change of +0.1 volt in the direct-current output of the phase detector, then this change in the direct-current voltage acting

through the automatic phase-control circuit changes the occurrence time of the phase detector gate with respect to the channel gates by +0.1 microsecond. Thus, the occurrence time of the channel gates with respect to the received synchronizing and channel pulses remains unchanged.

The synchronizing pulse is selected from the received signal by delaying and inverting the positive pulse in channel 23 and adding it to the negative pulse in channel 24. The resulting synchronizing pulse is twice the amplitude of the maximum normal amplitude of a channel pulse and is selected by a clipper amplifier. To insure against improper synchronization from impulse-type interference, a locally generated gate makes the clipper amplifier inoperative except when the synchronizing pulse is expected.

Auxiliary Equipment

A monitor, which is equivalent to a single-channel receiver, is supplied with the terminal to check the performance of the transmitter. By means of timing waves derived from the transmitter and a 24-position switch, any one of the twenty-four channel intervals may be monitored to determine the modulation level, or the quality of the transmission. For operation and maintenance purposes, the terminal also contains an oscilloscope, an 800-cycle per second test oscillator, a volume level indicator (VU) meter, and a monitor speaker.

Each incoming and outgoing telephone pair is normally connected to an assigned channel, but by a system of jacks any telephone pair may be transferred to any channel. In addition, each channel is provided with a monitor jack.

Design Considerations

A 30-channel prototype terminal was completed in 1948. Tests of this unit showed that the greatest single cause of trouble was the rapid decrease of transconductance of the tubes. The decrease of transconductance was found to be caused by the increase of internal resistance in the cathode. Life tests running continuously for over two years have shown that tubes with a low silicon content in the nickel cathode sleeves are not subject to this pronounced decrease in transconductance even when operated under cutoff conditions. For this reason, miniature tubes with cathode sleeves made of nickel with a low silicon content were used in the construction of the 22-channel terminal. To further stabilize the performance of the terminal, all tubes in critical positions, and particularly where they are operating at low duty factors, have unbypassed cathode resistors to reduce the

percentage change of cathode-circuit resistance due to growth of internal cathode resistance.

The choice of twenty-four channel time intervals was made to provide flexibility of the terminal in regard to channel frequency band width. The basic channel-frequency band width is 3300 cycles per second but this may be increased by operating two or more channels in parallel. Thus, two channels may be operated in parallel to form a single channel with a band width twice that of the basic channel. However, the two channels which are paralleled must be so chosen that the elapsed time between the sampling of the first channel and the sampling of the second channel is exactly equal to the elapsed time between the sampling of the second channel and the sampling of the first channel. In other words, the paralleled channels must be so located in the frame that their combined repetition rate is single-valued, and this is only possible when the number of channel time intervals is even. If it is desired to parallel three channels to produce a single channel with a frequency band width three times that of the basic channel, the number of channel time intervals must be divisible by three. Twenty-four time intervals would permit the paralleling of two, three, or four channels.

The use of interlaced step-wave voltages in the time-interval markers results in higher amplitude risers for a given peak-to-peak amplitude of the total voltage wave. When receiver-type tubes are used, or if the direct-current supply is limited to 250 or 300 volts, the peak-to-peak amplitude of a linear step-wave voltage is limited to about 120 volts. A wave with twenty-four steps would have riser amplitudes of about five volts. It is desirable to have a riser amplitude of a least ten volts for good performance of the selector tubes. Two twelve-step waves would have been sufficient but it was believed that the extra diversity afforded by four channel banks was worth the extra tubes and circuit required.

Performance

The complete terminal draws 800 watts from a 115 or 230 volt, 50 or 60 cycles per second power source. The line voltage may vary ± 10 per cent from its mean value without affecting the performance of the terminal. In back-to-back operation, the signal-to-noise ratio in any channel is 60 decibels, measured with a line-weighted amplifier under the conditions of eleven channels being modulated at peak level with voice. The cross talk, measured with an 800 cycles per second tone modulating a channel at zero dbm level, is less than —60 dbm in any other channel. The amplitude distortion is less than 3 per cent.

Components of the 60 cycles per second power supply are less than —50 dbm measured with a flat-frequency-response meter. The signal-to-noise ratio in the service channel is 20 decibels lower than in the other channels. This is due to limiting the peak modulation of the service channel to a value 20 decibels lower than the peak allowed in other channels in order not to interfere with synchronization. The terminal has been tested at ambient temperatures ranging from 0 to +50 degrees centigrade. Due to the temperature coefficient of the crystal, which is not temperature controlled, the range of temperatures over which operation is possible without readjustment is limited to ±10 degrees centigrade. In most applications, the multiplex terminal will be operated in a room maintained at temperatures comfortable for personnel. If the terminal is operated in a room where the temperature varies widely, the crystal may be easily mounted in a temperature controlled oven or inclosure.

Acknowledgments

The time-division multiplex terminals referred to in this paper were developed in the RCA Laboratories at Rocky Point, New York under the direction of C. W. Hansell. The 30-channel prototype terminal was the result mainly of the work of W. D. Houghton. For the development of the 22-channel terminal, credit is given to H. L. Cooke and R. K. Gallup.

A HIGH-CONDUCTIVITY GLASS-TO-METAL SEAL*

By

J. C. Turnbull

Tube Department, RCA Victor Division,
Lancaster, Pa.

Summary—*A method is described for plating Kovar† with high-conductivity metals before sealing to glass to reduce seal heating at high frequencies. The effect of various thicknesses of copper and chromium plating on residual strain in the seals and on seal heating is discussed. For operation at frequencies of 100 to 120 megacycles, the conductivity of a Kovar-to-glass seal can be increased by a factor of 25, and its current-carrying capacity by a factor of 5.*

Introduction

KOVAR-to-glass seals, because of their resistance to mechanical and thermal shock and their ease of fabrication, are widely used in the construction of power tubes. At high frequencies, however, these seals may be subject to severe heating as a result of electrical losses in the glassed-metal surfaces. Seal heating may be reduced by plating the Kovar with a metal of higher conductivity before the seal is made. This article will discuss the properties of high-conductivity seals using Kovar plated with copper and chromium. In these seals, a relatively thick inner layer of copper is used to provide conductivity, and a thin outer layer of chromium to provide a surface to which glass can readily be sealed. Such high-conductivity seals, having diameters up to 6½ inches, have been used in several frequency-modulation and television transmitting tubes.

Description of Seals

The high-conductivity seals described above are prepared as follows:

1. The Kovar parts are cleaned thoroughly and are then plated with copper.

2. As a check on the quality of the copper plating, the parts are fired in hydrogen and examined for blisters.

3. The copper-plated Kovar parts are plated with chromium and fired in a dry-hydrogen atmosphere (dew point —50 degrees Centigrade).

---

* Decimal Classification: R 331.

† Trade mark Registered U. S. Patent Office by Westinghouse Electric Corp.

4. The finished parts are oxidized by firing in moist hydrogen. Standard factory procedures such as lathe sealing, stem pressing, or furnace sealing may be followed in sealing glass to the plated Kovar parts. The sealing conditions generally are less critical for the plated metal than for unplated Kovar.

Figure 1 is a photograph of a cross section of a glass-to-metal seal using Kovar plated with chromium and copper. In this seal, the thickness of the copper plating is 0.0013 inch, and the chromium-plating thickness is 0.00005 inch. These plating thicknesses are somewhat arbitrary. Copper-plating thickness is limited only by its effect on residual strain in the glass. Chromium plating should be thick enough so that it does not oxidize through to the copper because chromium oxide will not adhere to copper.

Defects in the chromium oxide, which may cause leaks, bubbles, or poor adherence on sealing, usually result from inadequate time,

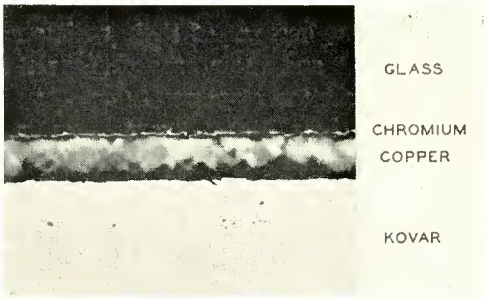

Fig. 1—Cross section (400×) of a glass-to-metal seal using Kovar plated with chromium and copper. The black area is glass, the light area Kovar. The chromium layer is the thin light area under the glass; the copper layer under the chromium was oxidized to emphasize the chromium.

temperature, or atmosphere during the dry-hydrogen firing schedule. For example, Figure 2a shows a typical system of microscopic cracks in a chromium-plated surface before firing. Oxidation of this surface by firing in air (and usually also by firing in an atmosphere of wet hydrogen) leaves an undesirable surface for glass sealing, as shown in Figure 2c. The oxide at the cracks is heavy and may be expected to be weakly adherent and permeable to air. Dry-hydrogen firing, at a temperature close to the melting point of copper, improves the structure of the chromium plating, as shown in Figure 2b, leaving it free of cracks and greatly reduced in porosity.

Residual Strains

Because copper has a higher thermal-expansion coefficient than

Kovar, the copper plating in a high-conductivity seal is subjected to strain as a result of temperature changes. The effect of this strain is relatively small in directions parallel to the plated layer. The increase in thermal-expansion coefficient for sheet Kovar caused by 12 per cent copper cladding on either side, measured in a parallel direction, was found to be 3×10^{-7} parts per degree centigrade, which represents a 6 per cent change in the thermal-expansion coefficient of Kovar. It is possible, therefore, that glass strains can be

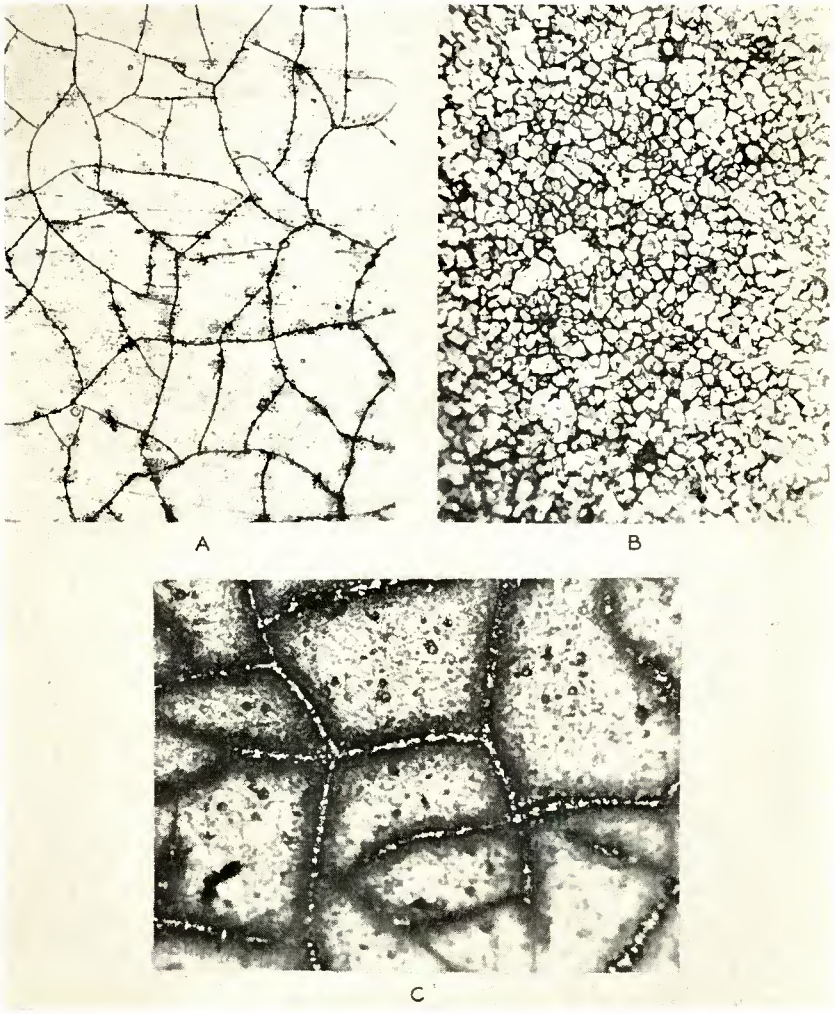

Fig. 2—Surface of a chromium-plated strip (400×) (a) after etching in HCl, (b) after firing in dry hydrogen, (c) after firing in air.

kept low in seals to copper-plated or copper-clad Kovar, particularly since the stress necessary to deform the copper layer comes principally from the Kovar, the material with the highest value of Young's modulus, rather than from the glass.

In the direction perpendicular to the copper layer, however, the change in thermal-expansion coefficient is larger. Table I shows transverse thermal-expansion coefficients for Kovar plated with various thicknesses of copper. When the values shown in Table I were calculated, it was assumed that stresses in the copper are continuously relieved; if the copper layer supports stress, smaller values than those given are obtained. The effect of copper on the transverse thermal-expansion coefficient of Kovar is an important consideration in the design of high-conductivity seals. Results obtained with some typical seals using copper-plated Kovar and a suitable glass are discussed below.

Table I—Computed Transverse Thermal-Expansion Coefficient for Copper-Plated Kovar.

Relative Amount of Copper*	Expansion Coefficient (parts per degree centigrade) Sheet	Wire
0.00	50×10^{-7}	50×10^{-7}
0.01	53.3×10^{-7}	53.3×10^{-7}
0.02	56.5×10^{-7}	56.4×10^{-7}
0.05	65.7×10^{-7}	65.3×10^{-7}
0.10	80.0×10^{-7}	78.7×10^{-7}
0.15	93.1×10^{-7}	90.2×10^{-7}

* Thickness of plating/thickness of kovar (flat sheet).
Thickness of plating/radius of kovar wire (wire).

"Outside" Cylindrical Seals

In a seal made to the outside surface of a copper-plated Kovar cylinder, as shown in Figure 3, the difference in contraction between the glass and metal on cooling is large in the radial direction but small axially and tangentially. The layer of copper plating on the Kovar cylinder produces radial tension at the glass-metal interface. For a seal such as that shown in Figure 3, maximum radial tension is observed at the inner seal edge.

In seals made to the outside surface of 2-inch-diameter Kovar cylinders having 0.030-inch wall thickness, copper plating up to 0.0015-inch thickness did not introduce dangerous strains. The seals were resistant to thermal shock and could be subjected to a boiling-water-to-liquid-air temperature cycle in either direction without breakage.

Similar seals made to Kovar cylinders clad with 0.0035-inch-thick copper either broke spontaneously or fractured under slight thermal shock. The fractures generally originated at the inner edge of the seal and ran at a slight angle to the Kovar cylinder through the glass wall.

"In-and-Out" Butt Seals

Figure 4 shows a butt seal made to a 2-inch-diameter Kovar cylinder having 0.030-inch wall thickness. The ends of the cylinder were rounded and polished. Thickness of the copper plating was varied from 0.0003 to 0.003 inch. After annealing, all seals of this type showed a high concentration of strain in the glass near the rounded end of the cylinder. This strain is caused primarily by the high transverse thermal expansion of the plated Kovar. None of the seals were resistant to thermal shock. Similar seals made with 0.030-inch Kovar clad with 3.5 mils of copper broke spontaneously after annealing. The fractures

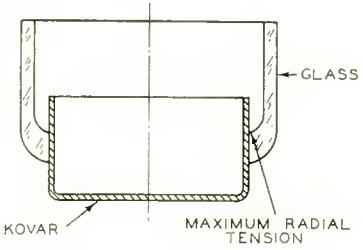

Fig. 3—Glass-to-metal seal made to the outside surface of a copper-plated Kovar cylinder.

generally passed tangent to the end of the Kovar cylinder, as shown by the dotted lines in Figure 4, with the origin probably at the tangent point.

Flange Seals

In the flange seal shown in Figure 5, the high transverse thermal expansion of the copper-plated Kovar produces no glass strain. Two-inch-diameter seals made to Kovar having 0.020-inch wall thickness and clad on either side with 0.0035-inch-thick copper showed moderate glass strain after annealing. The strain consisted of uniform compression parallel to the glass-metal interface. These seals withstood repeated thermal shock in the form of liquid-air-to-boiling-water temperature cycling. This design is the most satisfactory for heavily plated or clad material.

Residual strain in the flange seals is affected by thermal treatment at temperatures below the strain point of the glass. After the seals

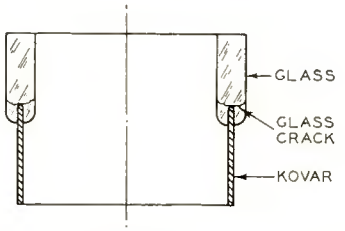

Fig. 4—Butt seal made to a Kovar cylinder two inches in diameter.

were warmed from liquid-air to room temperature, residual strain became uniform tension somewhat less in magnitude than the compression strain originally present. This behavior indicates that there is plastic deformation of the copper.

Effect of Chromium Plating

Flange seals were made to Kovar having 0.030-inch wall thickness and plated with 0.001 inch of chromium to determine the effect of thick chromium plating. Residual strain in this seal after annealing was three to four times that observed in a similar seal made with 0.001 inch of copper plating. Temperature cycles, such as cooling to liquid-air temperature and warming, had no permanent effect on residual strain for the seal to heavy chromium plating. The absence of plastic flow of the chromium, and its low thermal expansion, reduces the effect on transverse expansion of plating on strip and wire. Heavy chromium alone might be a desirable high-conductivity plating for alloys used in seals to soft glasses as the thermal expansion of chromium is close to that of these sealing alloys.

Measurement of Seal Heating

Measurements of seal heating were made to compare the conductivity of seals using copper-plated Kovar with that of seals using Kovar plated with both copper and chromium. The test apparatus could measure values of radio-frequency (r-f) current up to 27 amperes

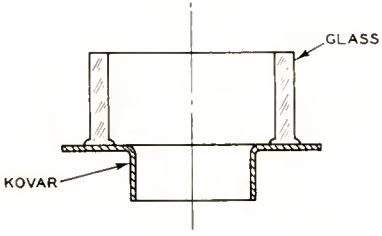

Fig. 5—Flange seal made between Kovar cup and glass cylinder.

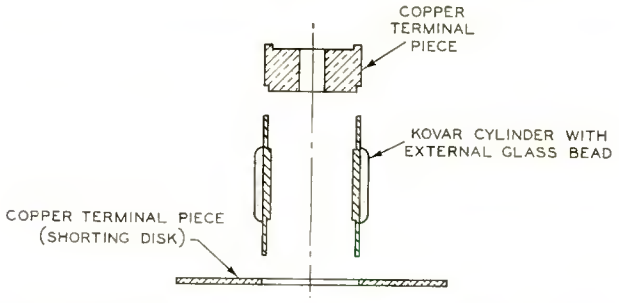

Fig. 6—Kovar test-cylinder used for measurement of seal heating.

per inch of seal circumference through a 1-inch-diameter seal at 120 megacycles. Current flow was in the same direction as in a power-tube seal. Temperature rise of the seal was measured and values for different seals were compared. In this equipment, a maximum rise of 40 degrees centigrade was obtained for seals having the highest conductivity, and a rise of 500 degrees centigrade was obtained for an unplated Kovar seal.

The Kovar test cylinder used for these measurements was assembled as shown in Figure 6. An external bead of Corning 7052 glass having a thickness of 1/16 inch was formed over a length of ⅝ inch at the center of the electro-plated Kovar cylinder. The cylinder was incorporated in a coaxial line as a continuous part of the center conductor to provide high r-f heating current. The line, shorted at each end by a copper disk, was a little less than ½ wave length. Exposed metal of the Kovar seal was copper plated, and the entire line, except for the glass seal, had copper surfaces. The shorted line is a high-Q cavity which, when excited in its fundamental mode, has high voltage at the center and high current at each end. The seal was placed at one end of the line, as shown in Figure 7, where the current across its surface is a maximum and the electric field at its surface is a minimum.

The line had a characteristic impedance of 63.5 ohms. The inner

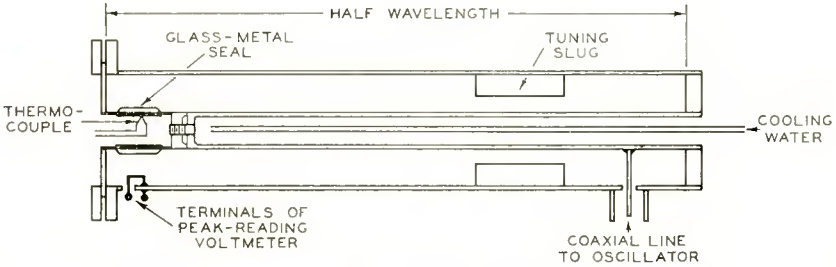

Fig. 7—Coaxial line used for testing seal heating.

diameter of the outer conductor was 2⅞ inches, and the outer diameter of the inner conductor was 1 inch. The line could be tuned by moving a slug along one half of the line. The slug had the effect of throwing the harmonic frequencies out of resonance. At resonance of the fundamental frequency, the harmonic voltages included in the test measurements were negligible.

The r-f power source was a 120-megacycle oscillator having a maximum power input of one kilowatt. Magnetic coupling between the oscillator and the resonant line was obtained through the use of two wire loops connected by a short length of coaxial line. Shielding was fairly complete, with no observed external coupling into the peak-reading voltmeter used to measure coaxial-line current. A maximum voltage of 6000 volts on the coaxial line could be obtained.

The current in the coaxial line was measured with a monitoring loop of wire inserted through the outer conductor just above the glass seal. Three independent calibrations of loop voltage in terms of seal current were made:

1. A direct calculation based upon the magnetic field through the loop in terms of the coaxial-line current.

2. Measurment of the voltage maximum at the center of the line with a second voltmeter, and substitution in the relation $I = E/Z$, where I is the maximum current, E the maximum voltage, and Z the characteristic impedance.

3. Measurement of power loss in the seal in terms of the rise in the temperature of water circulated inside the seal. Because the thermal conductivity of copper is known, the root-mean-square current can be obtained by calculation directly from the measurement of power loss.

The use of these three methods resulted in calibration constants for seal current in terms of the loop-voltmeter reading which agreed to within ± 10 per cent.

The ends of the Kovar test cylinder were made as thin as possible (0.005 inch) in order to reduce heat losses due to thermal conduction away from the seal. The terminal pieces and all other parts of the coaxial line were water-cooled to maintain a constant temperature. Cooling of the seal by conduction and convection is a constant factor, and it was assumed that temperature rise was the same function of power loss for all the seals. Actual cooling of a power-tube seal is more efficient than that achieved in the test method. The higher temperature rise obtained by thermal isolation, however, was preferred in order to attain higher values of seal temperature than would otherwise have been possible.

Table II gives average values of seal heating in terms of the r-f current at 120 megacycles required to produce a rise in seal temperature of 40 degrees centigrade. These values of current correspond to constant power input to the seal; the currents squared give the relative conductivity of the seals. Data could be repeated to ± 5 per cent on individual seals. There was a maximum variation of ± 15 per cent, however, between samples of the same plating thickness, probably due to accidental differences in dimensions of the Kovar parts, the glass beads, or the plating.

Table II—R-F Heating of Seals Made to Plated and Unplated Kovar.

Plating Thickness (inches)			Current for 40°C Rise in Seal Temperature (amperes per inch)
Copper	Chromium	Gold	
0.002	0.00002	None	24.5
0.002	0.00015	None	21.1
0.0015	None	None	24.3
0.0012	0.0001	None	26.1
0.0008	0.0001	None	22.9
0.0004	0.0001	None	17.1
None	0.0001	0.002	24.9
	No Plating		4.3

Table II shows that at 120 megacycles the conductivity of seals using Kovar plated with chromium and copper is not a function of the thickness of chromium. The currents measured for seals having 0.00002- and 0.00015-inch chromium thickness were about the same, within the limits of experimental error. The same values of current were also obtained for seals to copper-plated Kovar having no chromium plating. The gold-chromium seals have about the same conductivity as the copper-chromium seals, as would be expected because the direct-current conductivity of gold and copper is about the same.

The r-f current required to raise the temperature of these high-conductivity seals 40 degrees centigrade, therefore, is approximately 23 to 25 amperes per inch of seal circumference at 120 megacycles. The average value required to produce a similar temperature rise in unplated-Kovar seals is only 4.3 amperes per inch. The plated Kovar seals have a current-carrying capacity more than five times that of unplated Kovar at 120 megacycles, and a conductivity more than 25 times that of Kovar.

ON EXTENDING THE OPERATING VOLTAGE RANGE OF ELECTRON-TUBE HEATERS*

By

Jerome Kurshan

Research Department, RCA Laboratories Division,
Princeton, N. J.

Summary—*A preliminary survey has been conducted of means for increasing to ± 20 per cent the permissible supply-voltage variation for the heaters of radio receiving tubes with indirectly heated cathodes. The present tolerance is ± 10 per cent, corresponding to a cathode temperature change of ± 4 per cent, which may be considered a practical maximum with existing oxide cathode materials. The allowable voltage variation, ΔV, consistent with this temperature limitation, increases with the temperature exponent of resistance of the heater material. Even with an arbitrarily high temperature exponent of resistance, however, $\Delta V_{max} = \pm 16$ per cent, corresponding to constant current, is a fundamental physical limit.*

I. General Considerations

PRESENT-DAY vacuum tubes have some inherent voltage compensation which is incidental to their normal operation. The metals used for cathode heaters are tungsten and tungsten-molybdenum alloys which have positive temperature coefficients of resistivity which are large compared with most other nonmagnetic elements. Consequently, a temperature rise causes a resistance increase and thus curtails the power input change. In typical tubes, the fractional resistance change is about four-tenths the fractional voltage change and, as a result, temperature changes are reduced by about two-tenths of the value for a constant resistance. This is discussed in section III.

Another inherent factor making for temperature stability is the fact that radiated power is proportional to the fourth power of the absolute temperature. Consequently, if the cathode loses heat primarily by radiation, fractional changes in temperature are only one quarter of the fractional changes in power. Power losses by conduction, however, are proportional to the temperature differences, and the temperature changes of a conduction-cooled cathode will be greater than those of a pure radiator for the same changes in power input. Most receiving tube cathodes are predominantly radiation cooled but par-

* Decimal Classification: R 138.

ticular types, for example the cathodes of "lighthouse" and cathode-ray tubes, have considerable heat losses by conduction and so are somewhat poorer in their ability to tolerate low and high heater voltage.

In general, it can be said that the average 6.3-volt receiving tube (with radiation-cooled cathode) may be operated satisfactorily with heater voltages ranging from 5.7 to 6.9 volts. This is a deviation of approximately ± 10 per cent from the average value.[1] Because the attendant resistance change is about ± 4.2 per cent, the current spread is reduced to ± 5.8 per cent and the heater power spread is ± 15.8 per cent.[2] If the resistance remained constant, the corresponding values would be ± 10 per cent and ± 20 per cent, respectively. From the fourth-power radiation law, the cathode temperature spread would then be ± 4.0 per cent, or ± 40 degrees for a cathode normally at 1000 degrees Kelvin. It is the purpose of this paper to discuss various possible means of holding cathode temperature within these limits with larger variations in heater voltage than can now be tolerated. Devices which are circuit elements for use with tubes are included for comparison. The ballast phenomenon will be treated first since it embodies some basic limitations of tube heaters.

II. Ballast Tube

The gas-filled ballast resistance tube[3] is useful in stabilizing the input current to a low-voltage, high-current load, the biggest drawback being limited life compared to electron tubes. The ballast resistor usually takes the form of an iron wire mounted in a glass envelope filled with hydrogen at a pressure of about 10 millimeters of mercury. The theory of such a system predicts that the current will be nearly constant over a wide range of voltages.

Commercially available units are rated to have a current spread confined to ± 5 per cent for a voltage change of ± 50 per cent. The actual ballast voltage must be chosen high enough so that this range will absorb the difference between a line-voltage change of ± 20 per cent and the allowable heater voltage change of ± 8.6 per cent which corresponds to ± 5 per cent change in current. A simple calculation shows that the average ballast resistor voltage (or power) will be 38 per cent of the average value for the heater.

---

[1] This conforms with the design center system. See "Tube Ratings and Their Significance," *RCA Tube Handbook, Series HB-3*, RCA Victor Division, Harrison, N. J.

[2] Average of 8 types of tungsten heater tubes. See also C. E. Haller, "Filament and Heater Characteristics," *Electronics*, Vol. 17, pp. 126-131, 354-356, July, 1944.

[3] S. G. Taylor, "Ballast Tubes as Automatic Voltage Regulators," *Electronics*, Vol. 15, pp. 26-30, January, 1942.

The factors dictating the choice of materials for a ballast resistor will now be considered in order to determine whether simpler construction or lower power loss than the above can be achieved. It has been shown[4-7] that a necessary condition for ballast action is

$$n > w, \tag{1}$$

where

$$w = \frac{T}{W}\frac{dW}{dT}, \tag{2}$$

and

$$n = \frac{T}{R}\frac{dR}{dT}. \tag{3}$$

Here W is the power dissipated by the resistor, R is the resistance, and T is the absolute temperature. It is seen that w is primarily a function of the operating conditions (i.e., the way in which heat is lost), while n is a property of the material used.

The quantity n is called the "temperature exponent of resistance." This is the quantity tabulated by Jones and Langmuir[8] for tungsten. If, over a limited range, $R = cT^n$, where c is some constant, n is the quantity just defined. In a similar manner, w may be called the "temperature exponent of power dissipation." For a black body radiator, $W = k_1 eT^4$ and $w = 4$, since k_1 and e are constants. For a metal, however, e is approximately proportional to T and $w = 5$. Since n must be greater than w, the problem of good ballast action is that of achieving a sufficiently large n, or a sufficiently small w. Even iron, which assumes one of the largest values of n known, shows a maximum of $n = 2.3$ at 970° K, and tungsten, which can be used at very high temperatures has $n < 1.3$ at all temperatures above 273° K. It is thus apparent on considering the condition of Equation (1), that radiation cooling is inadequate for a ballast resistor unless one can find metals with a value of n about twice that of iron.

---

[4] H. A. Jones, "The Ballast Resistor in Practice," *GE Review*, Vol. 28, pp. 329-335, May, 1925.

[5] H. A. Jones, "Theory and Design of Ballast Resistors," *GE Review*, Vol. 28, pp. 650-659, September, 1925.

[6] H. Busch, "Über die Erwärmung von Drähten in Verdünnten Gasen Durch Elektrischen Strom," *Annalen der Physik*, IV, Vol. 64, pp. 401-450, 1921.

[7] F. Ollendorf, *Die Grundlagen Der Hoch-Frequenz-Technik*, pp. 108-111, Julius Springer, Berlin, 1926.

[8] H. A. Jones and I. Langmuir, "The Characteristics of Tungsten Filaments as Functions of Temperature, Part 11," *GE Review*, Vol. 30, p. 354, July, 1927.

Suppose, on the other hand, there could be constructed a resistance completely cooled by conduction to a sink at temperature T_0, without having the cooling medium short out the electrical resistance. Then

$$W = k_a (T - T_0),$$

and for constant heat conductivity,

$$w = 1/[1 - T_0/T]. \tag{5}$$

Note that w is infinite at $T = T_0$, but drops to 2 at $T = 2T_0$.

The use of a gas-filled tube[5,6] lowers the value of w by what is largely thermal conduction, effected without danger of electrical conduction. Hydrogen and helium may be used, the former working better and reaching its optimum cooling effect at a pressure of 10 millimeters.

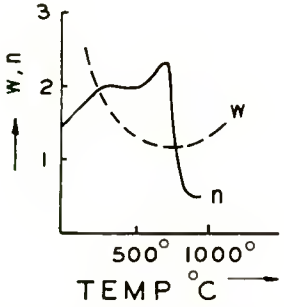

Fig. 1—Functions governing the ballast action of an iron wire in hydrogen at low pressure (after Busch).

The value for w is then 2 at 550° K (277° C), decreasing continuously and reaching 1.3 at 1400° K (1127° C). From 570° K to 1070° K (277° C to 797° C), the w is less than the n for iron, making possible the commercial ballast tube. These values are shown graphically for iron in Figure 1 and are plotted for iron, nickel, silver, platinum, and tungsten in the paper by Jones.[4]

Of course, the discovery of a material with a value of n greater than w over a larger temperature range than exhibited by iron will lead to a better ballast resistor even if the maximum value of n is not increased. In fact, iron is now used in preference to nickel, which, over a narrow range of temperatures, has a greater n than the maximum for iron. However, a metal with still greater n must be found before a vacuum ballast will be feasible.

It is difficult to find resistivity data on many metals and alloys for

temperatures above 100° C.[9] The behavior of the ferromagnetic elements (cobalt also exhibits a large value of n) suggests that better ballast resistor materials might be found among the many magnetic alloys now known, probably when operated in the vicinity of their Curie temperatures. It may be concluded that simpler construction (e.g., elimination of gas cooling), or at least lower power loss in the ballast resistor, awaits the discovery of such better materials.

III. Heater Material

As mentioned in section I, standard tubes have a certain amount of inherent stabilization due to the fact that heater resistance increases with voltage. A very satisfactory solution of the present problem would result if this effect could be sufficiently enhanced by the development of a heater with a higher temperature exponent of resistivity. No additional components would be required and all the power would be delivered to the cathode; the stabilization should be such that the residual variations of heater power would be tolerable. It is immediately apparent, however, that such a solution is impossible. This follows from the analysis of ballast resistors given in the references[4-7]. The references cited show that the resistance of a wire may increase very rapidly with voltage because of the attendant temperature rise, that the dynamic resistance may even become infinite resulting in a constant current device, but that, because of the instability which results in the ballast action, the dynamic resistance never becomes negative to give a falling current characteristic. This means that the greatest stability a heater can provide is to keep the current constant with rising voltage. Under such conditions, and assuming radiation cooling with a constant emissivity,[10] it is clear that

$$\frac{dW}{W} = \frac{dV}{V} = \frac{4\,dT_c}{T_c}$$

where W is power input, V is voltage and T_c is cathode temperature in degrees Kelvin. A voltage variation of ± 20 per cent with a constant-

[9] Additional references will be found in section III, but none of those reveals a better ballast resistor material. There is also an extensive bibliography in Landolt-Börnstein which has not been completely investigated in this preliminary work: Landolt-Börnstein, *Physikalisch-Chemische Tabellen*, 5th, Suppl. 2, part 3, pp. 2005-2010, 1936.

[10] In contrast with pure metals, an oxide cathode on a nickel base has an emissivity that is constant with temperature. See G. E. Moore and H. W. Allison, "Spectral and Total Emissivities of Oxide-Coated Cathodes," *Jour. Appl. Phys.*, Vol. 12, pp. 431-435, May, 1941.

current heater thus means a spread of at least ± 50° for a cathode at 1000° K. Nevertheless, significant improvement in performance may be achieved by increasing the temperature exponent of resistance of the heater. The relationships involved will now be treated in some detail in order to determine what resistance characteristics the heater wire should have for a given result.

Consider the effect of a heater voltage rise on the temperature of a cathode where all the heat losses are by radiation to surroundings at much lower temperature. Assume that under normal operating conditions, the cathode is at 1000° K and the heater wire is at 1400° K.

Let W be power input; V, heater voltage; T_h, heater temperature: T_c, cathode temperature; and R, heater resistance. Then

$$W = \frac{V^2}{R}.$$

For a first order approximation the differentials may be used,

whence
$$\frac{dW}{W} = \frac{2dV}{V} - \frac{dR}{R}. \tag{6}$$

W may be related to the temperature of the cathode coating by the radiation law, giving

$$W = k_1 T_c^4,$$

$$\frac{dW}{W} = 4\frac{dT_c}{T_c}. \tag{7}$$

Using n as defined in Equation (3),

$$\frac{dR}{R} = n\frac{dT_h}{T_h}. \tag{8}$$

To determine the relation between dT_h and dT_c, one must assume a mechanism for the heat transfer between coated heater and cathode. If this is entirely by radiation with constant emissivity,

$$W = k_2 (T_h^4 - T_c^4),$$

and by differentiating and then substituting from Equation (7), it is found that

$$\frac{dT_h}{T_h} = \frac{dT_c}{T_c}. \tag{9}$$

Other reasonable assumptions for radiative transfer give substantially the same result. Substituting Equations (7), (8), and (9) into Equation (6) leads to the relations

$$\frac{dV}{V} = \left(2 + \frac{n}{2}\right)\frac{dT_c}{T_c} \tag{10}$$

and

$$\frac{dR}{R} = \frac{2n}{4+n}\frac{dV}{V}. \tag{11}$$

On the other hand, if the heat transfer from heater to cathode is primarily by conduction (across the insulation coating),

$$W = k_3 (T_h - T_c),$$

and again differentiating and using Equation (7),

$$\frac{d\,T_h}{T_h} = \frac{d\,T_c}{T_c}\left(4 - \frac{3\,T_c}{T_h}\right). \tag{12}$$

Now, substituting Equations (7), (8), and (12) into Equation (6) gives

$$\frac{dV}{V} = \left(2 + 2n - \frac{3n\,T_c}{2\,T_h}\right)\frac{d\,T_c}{T_c}, \tag{13}$$

and

$$\frac{dR}{R} = \left[2 - \frac{4}{2 + 2n - \dfrac{3n\,T_c}{2\,T_h}}\right]\frac{dV}{V}. \tag{14}$$

Using Jones' and Langmuir's value of $n = 1.182$ for tungsten at 1400° K, Equation (11) gives $dR/R = 0.45\ dV/V$ for radiative transfer; Equation (14) gives $dR/R = 0.71\ dV/V$ for conductive transfer. Measurements made on a number of tungsten heater tubes give 0.42 for this factor, indicating that radiation probably accounts for most of the heat transfer.

To see how much the resistance increment reduces the temperature change of the heater, this last value for dR/R may be substituted in Equation (6), at the same time replacing dW/W by its value from Equation (7). This gives

$$\frac{dT_c}{\quad} = \tfrac{1}{2}\,(1 - 0.21)\,\frac{dV}{V}, \qquad (15)$$

where the second term in the parenthesis arises from the resistance change and is the basis for the statement made in section I that temperature changes are reduced about two tenths in practice because the resistance increases with temperature.

Equation (10) is useful in determining the temperature exponent of resistance (n) necessary for a given performance. For example, if a material with $n = 3.0$ is made available, $2 + n/2 = 3.5$. In order to limit dT_c/T_c to $\pm$ 4.0 per cent, $|dV/V| \leq 15$ per cent. This hypothetical material, then, would have an operating range 50 per cent greater than that of tungsten. It should be noted that ballast action (constant current) will start at a value of $n = 4$ (for a heater material with radiation cooling and constant emissivity). For such values the tacit assumption of a heater with a uniform temperature distribution is no longer valid and the analysis breaks down. With n's greater than this, one cannot, however, exceed the $\pm$ 16 per cent voltage tolerance, as discussed earlier.

The tube industry considers only tungsten and its alloys with molybdenum as being suitable for coated heaters, but a review of other materials will be instructive. One might start by examining the elements, because a higher temperature exponent of resistance n is desired and the alloying of metals generally causes a decrease in n. A first selection may be made according to melting points. With present-day techniques, the heater is fired at 1800° C in processing the insulation coating, and reaches 1600° C in breaking down the cathode coating. High melting point, however, is not enough, since many of the metals which remain solid have insufficient tensile strength at these temperatures. In addition to high n, a large value for the actual resistivity at the operating temperature is also a desirable heater property since it is often a serious problem to keep the total resistance of the heater sufficiently high.

As noted in section II, it is difficult to find reliable published data on resistivity of metals at elevated temperatures, particularly above 1100° C. The exceptions include tungsten, platinum, palladium, tanta-

lum, zirconium, niobium, and tungsten–molybdenum alloys.[8, 11-15]

The pertinent data found in these sources have been assembled in Table 1.

Table 1

Element	Symbol	Melt'g Pt. 0c	Resistivity μ ohm —cms	Resistivity Temp. °C	Temp. Variation* Coeff., α Per °C	Temp. Variation* Expon. n	Temp. Variation* Temp. °C
Tungsten	W	3370	5.00	0	0.0047	1.275	0
			37.19	1123	0.0063	1.182	1123
Molybdenum	Mo	2620	5.14	0	0.0048	1.32	0
Vanadium	V	1715					
Platinum	Pt	1773	9.83	0	0.0039	1.06	0-100
			45.8	1100	0.0027	0.79	1100
Iridium	Ir	2454	5.3	0	0.0039		0-100
Osmium	Os	2700?	9.5	0	0.0042		0-100
Rhodium	Rh	1985	4.3	0	0.0044		0-100
Ruthenium	Ru	>2450	14.4	18			
Boron	B	2300					
Carbon	C	>3500	3500	0	—0.0005		
Thorium	Th	1845	18	20	0.0021		20-1800
Titanium	Ti	1800	Data conflicting				
Zirconium	Zr	1860	39	0	0.0045		0-100
Tantalum	Ta	2850	47	0	0.0035		0-100
Niobium	Nb	2500				0.735	1510-2240
Rhenium	Re	3000?					
Ytterbium	Yb	1800					

* See section II of text for definitions

Elements with a melting point above 1600° C have been chosen and are listed in several groups. Although the platinum metals look most promising because of their chemical inertness, there is no indication from the data on platinum and palladium (melting point 1554° C and so not listed) that a large value of n is to be expected. The elements of the next group are usually rejected because of their chemi-

[11] R. F. Vines, *The Platinum Metals and Their Alloys*, International Nickel Company, N. Y., 1941.

[12] L. Malter and D. B. Langmuir, "Resistance, Emissivities, and Melting Point of Tantalum," *Phys. Rev.*, Vol. 55, pp. 743-747, April 15, 1939.

[13] D. B. Alnutt and C. L. Scheer, "Zirconium Metal, Its Manufacture, Fabrication and Properties," *Transactions of the Electrochemical Society*, Vol. 88, pp. 357-360, 1945.

[14] C. K. Grant and A. L. Reimann, "Some High Temperature Properties of Niobium," *Phil. Mag.*, Vol. 22, pp. 34-38, January, 1936.

[15] P. N. Bossart, "Spectral Emissivities, Resistivity and Thermal Expansion of Tungsten-Molybdenum Alloys," *Jour. Appl. Phys.*, Vol. 7, pp. 50-54, January, 1936.

cal activity, which would cause reduction of the alumina insulating coating.

If a material is available as wire, its resistance behavior for heater use can be determined by simple experiment. The wire is mounted in a vacuum and heated to about 1100° C by an electric current. A voltage-current characteristic is then taken and compared with similar data for other materials. Actual temperatures need not be measured accurately since it is the voltage-current behavior that ultimately determines the material's usefulness as a wide-voltage range heater.

IV. Arbitrary Combinations of Heater and Stabilizing Resistance

In the preceding two sections, the physical characteristics of the ballast tube and of the heater were considered separately. It is interesting to know what performance can be achieved in general by using two series elements of arbitrary current-voltage relationship.

At the outset it may be said that there is no advantage in a dynamic negative resistance for the stabilizing element. If one were used, the heater would have to exhibit positive resistance for stability. Since a rise in line voltage (and hence in current) would reduce the voltage drop on the negative resistance, the heater would experience a greater voltage change than if it had been connected directly across the line. A bridge circuit using thermistor[16] (or thyrite) elements will, however, stabilize the heater. Such a circuit will be considered later.

It is possible to give a general treatment[17] of the circuit consisting of two arbitrary elements connected in series. The graphical representation of Figure 2 is helpful. The logarithm of the voltage V is plotted against the logarithm of the current I. An arbitrary operating point has been chosen at a line voltage V_{l0} of 1. Line voltages of 0.8 and 1.2 ($V_{l0} \pm 20$ per cent) have also been indicated since these are the extremes for which stabilization is desired. Loci of constant power are straight lines with a slope of —1. Normal heater power, W_{h0}, has been arbitrarily chosen as 1. Lines are also drawn for 1.16 W_{h0} and 0.84 W_{h0}, since these are the limits already proposed for an oxide-coated cathode. Loci of constant resistance are straight lines with a slope of +1. In the case of a non-ohmic relation between current and voltage, if V increases with I (positive dynamic resistance), the slope will be positive, while if V decreases, the characteristic will have a

[16] J. A. Becker, C. B. Green, and G. L. Pearson, "Properties and Uses of Thermistors," *Bell Sys. Tech. Jour.*, Vol. 26, pp. 170-212, January, 1947.

[17] The method of analysis employed was suggested by I. Wolff, of RCA Laboratories Division, Princeton, N. J.

negative slope. In general, the slope gives the ratio of the dynamic resistance R_d to static resistance R_0 at any point. This can be shown as follows:

By definition $$R_d = \frac{dV}{dI},$$

and $$R_0 = \frac{V}{I}.$$

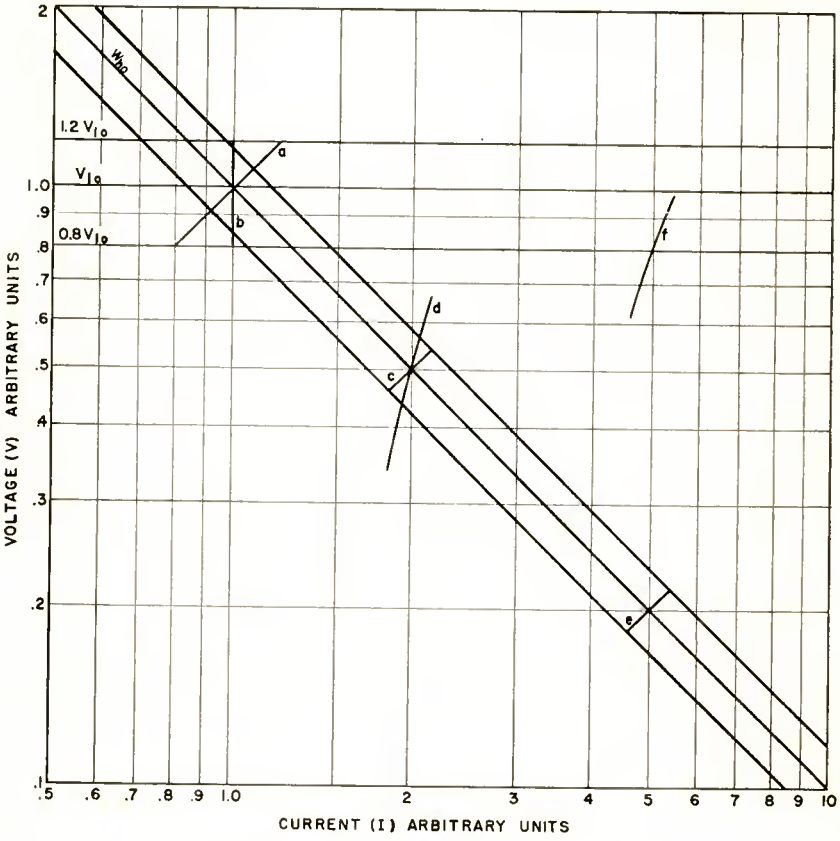

Fig. 2—Graphical stabilization of positive resistance.

$$\frac{d \log V}{d \log I} = \frac{I\, d \log V}{dI} = \frac{I\, dV}{V\, dI} = \frac{R_d}{R_0}.$$

It can be seen from curve *a* of Figure 2 that a simple ohmic resistance is inadequate for the heater since the curve of slope +1

exceeds the power limits when it is extended to the line-voltage limits. Similarly, curve *b* shows that even a single element with infinite dynamic resistance would be insufficient. It is apparent, then, that if an element with positive dynamic resistance is used for the heater, it must be connected in series with a control unit having a higher ratio of dynamic-to-static resistance so that a greater fraction of the line voltage changes appears across the control than across the heater.

Curve *c* of Figure 2 is the characteristic of an ohmic-resistance heater chosen so that half the line voltage (0.5 volt) appears across it at the operating point. The curve is drawn between the allowable power extremes. Curve *d* is the characteristic that the series control element must have for acceptable operation if the line voltage varies between its allowable extremes. It is seen that the dynamic-to-static resistance ratio is greater for the control element than for the heater. Curves *e* and *f* are similar characteristics where the normal voltage drop (and hence the dissipation) is greater for the control element. The required slope of the control element has been reduced.

If the heater characteristic is redrawn with a greater slope, it is found that the control characteristic must also be steeper. This will be verified in later analysis, but before judging this apparent anomaly, it should be noted that the required current extremes are reduced for the greater heater slope. This is an important consideration if an iron–hydrogen ballast tube is used for the control resistance. Also, although a heater characteristic with a steeper slope is more nearly self-stabilizing, its final stabilization may be more difficult since the control element must have a steeper logarithmic characteristic than the heater. In the limiting case, a heater with infinite dynamic resistance cannot be stabilized at all.

The value of a current-controlled negative dynamic resistance heater can be determined with the help of these curves. Such a heater may not need a series control element to limit the power variation, but it will need it to achieve stable operation.[18] The total series resistance must be positive, which means that the current will increase with the line voltage and that the voltage drop across the negative dynamic resistance of the heater will decrease. In Figure 3, curve *a* represents such a negative resistance, and the characteristic must be traversed from left to right as the line voltage increases. Curve *b* in the same figure represents an ohmic (positive) resistance drawn through the same operating point, while curves *d* and *e* are the characteristics of the control elements required to stabilize the respective heaters. It is

---

[18] E. W. Herold, "Negative Resistance and Devices for Obtaining It," *Proc. IRE*, Vol. 23, pp. 1201-1223, October, 1935.

seen that curve *e* is steeper than curve *d*, but curve *d* covers a wider current range. This appears to be generally true. The limiting case is the convergence of curves *a* and *b* to a horizontal line *c*, which requires the intermediate stabilizer characteristic *f*. As one departs from the horizontal curve *c*, the stabilizer for a positive heater resistance becomes steeper and shorter. The converse is true for a negative heater resistance.

Since all of these control elements dissipate the same power at the operating point, it will be of interest to find out which characteristic is easier to realize. The answer cannot be given categorically, but it

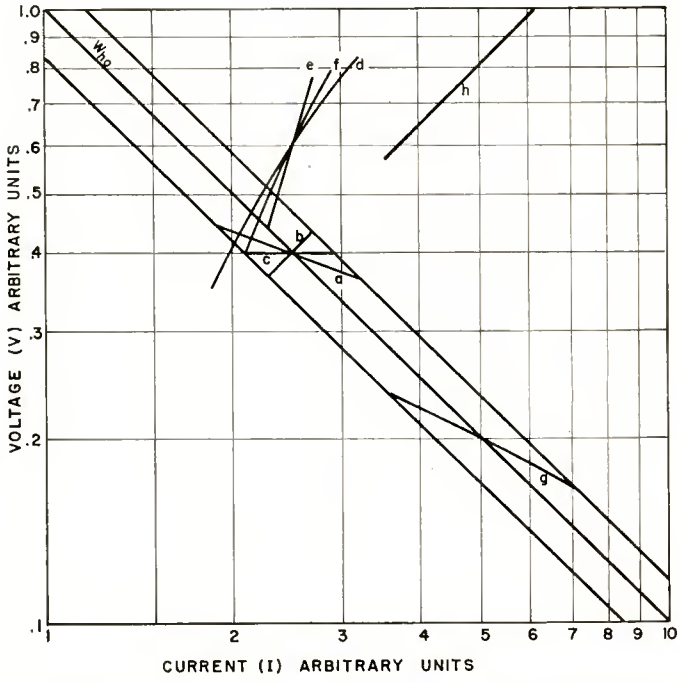

Fig. 3—Relation between heater and control at constant power.

may be said that all these stabilizers are of the ballast type—that is, large dynamic-to-static resistance ratios. In general, these are suitable for operation over a restricted current range and do not sustain their desired characteristics over large current ranges. For example, even a tungsten heater, for which there is less current variation than an ohmic resistance, exceeds the current variation limits of existing ballast tubes when the line voltage varies ± 20 per cent.

An ohmic resistance will not stabilize *any* assumed heater characteristic at the operating point shown in Figure 3. However, an ohmic

resistance can adequately stabilize a suitable negative resistance characteristic if the stabilizer dissipation is at least 4 times the heater power, as shown by curves g and h of Figure 3. This factor is to be compared with 0.38 for the combination of a ballast tube and tungsten heater.

The most generally useful type of heater characteristic still appears to be a positive dynamic resistance, and a general analysis can be made for the case where this is in series with a control element, also with positive dynamic resistance. The parameters which will enter into the analysis are: ratios of dynamic-to-static resistance for each element, the tolerances on line voltage and heater power, and the ratio of control power to heater power. This analysis is carried out in the Appendix and yields the following results: The fractional deviation in current from the normal value is

$$\Delta I/I_0 = t_p/(1 + r_h),$$

where t_p is the fractional deviation in power allowed for the heater and r_h is the dynamic-to-static resistance ratio for the heater.

The ratio of control element power to heater power at normal line voltage is

$$p_0 = \frac{(t_{vl}/t_p)\ (1 + r_h) - r_h}{r_c - (t_{vl}/t_p)\ (1 + r_h)},$$

where t_{vl} is the fractional line voltage tolerance, and r_c is the dynamic-to-static resistance ratio of the control element.

In this study $t_{vl} = 0.2$ and $t_p = 0.16$, and so $t_{vl}/t_p = 1.25$.

In the expression for p_0, the numerator will always be positive; thus there is meaning only when r_c is sufficiently larger than r_h so that the denominator is positive. In this range p_0 will be a monotonically decreasing function of r_c. This is shown in Figure 4 for two types of heater—an ohmic resistance ($r_h = 1$), and tungsten ($r_h = 2$). Note that for the same p_0, a steeper control characteristic (greater r_c) is needed with a steeper heater characteristic (greater r_h) as already mentioned. This is also true for other values of r_h, since

$$\frac{\partial r_c}{\partial r_h} = \frac{(t_{vl} - t_p) + t_{vl}\, p_0}{t_p\, p_0},$$

which is positive for $t_{vl} > t_p$.

Although the analytic expression for p_0 as a function of r_c shows

$p_0 \rightarrow 0$ as $r_c \rightarrow \infty$, there is actually a nonzero lower limit to p_0. The discrepancy arises because the mathematical expressions used do not take into account the physically significant point where the heater voltage becomes equal to the line voltage. Thus, a lower limit on V_{co} (normal voltage of control element) is set by the condition that V_{co}

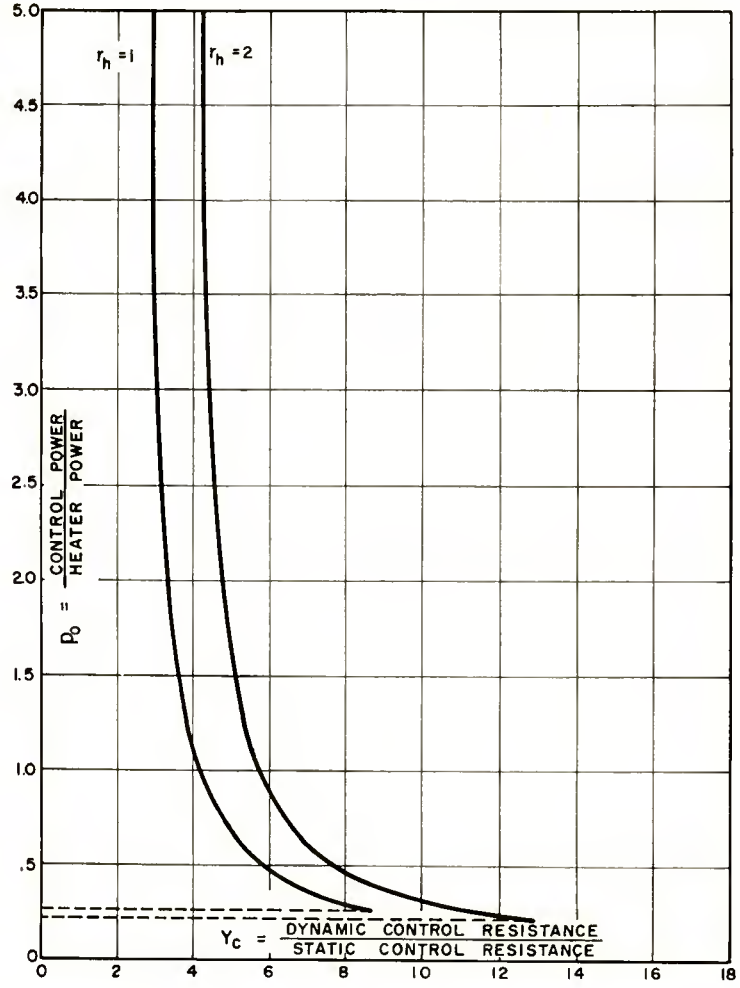

Fig. 4—Average power in control element.

must be at least as large as the change in V_{co} required when V decreases by the maximum amount. A minimum V_{co} means a minimum for $p_0 = V_{co}/_{ho}$, which may be called p_{0m}. It is shown in the Appendix that

$$p_{0m} = \frac{t_{vl} - t_{vh}}{1 - t_{vl}},$$

where t_{vh} is the fractional voltage change allowed for the heater and is given by

$$t_{vh} = t_p - (\Delta I/I_0)$$

$$= t_p r_h/(1 + r_h).$$

For a constant-resistance heater, $t_{vh} = t_p/2 = 0.08$ with the tolerances already specified, and $p_{0m} = 0.15$. A tungsten heater with $r_h = 2$ has $t_{vh} = 0.11$ and $p_{0m} = 0.11$. Thus, with present heaters, the power loss in the control must be at least 11 per cent of that in the heater at the normal operating point even if the control has the ideal characteristic of zero voltage drop at minimum line voltage. This may be compared with the value of 38 per cent found in section II for existing ballast tubes.

Bridge circuits with nonlinear elements have been reviewed by Kallman.[19] Any material with a decreasing resistance characteristic can be used; for example, thermistors, thyrite, and tube and contact rectifiers. In a rectifier power supply with a 0.1-megohm load, the output voltage change was reported as ± 0.5 per cent for an alternating-current line voltage change of 22 per cent, which is very good. The efficiency, however, is poor with a minimum wasted power of three times the useful power. Moreover, the normal operating point is at maximum voltage, not average voltage.

V. Alternate Heating Methods

It is possible that a different method of heating the cathode may be more readily controlled than a resistance heater. For example, the tube shown in Figure 5 can be made inherently self-stabilizing. K and P are the oxide-coated cathode and the plate of a conventional tube in which grids are not shown. F is a filament heated by the voltage E_f which is derived from the same line voltage as the voltage E_0 and hence the two voltages fluctuate in proportion.

If the electron emission from F is temperature-limited, the temperature of K will be stabilized because of the very great dependence of such emission on temperature. To understand this qualitatively, suppose E_0 were to increase. This by itself would tend to increase the

[19] H. E. Kallman, "Non-Linear Circuit Element Applications," *Electronics*, Vol. 19, pp. 130-136, August, 1946.

power input to cathode K. At the same time, however, E_f increases proportionately, raising the temperature of filament F and resulting in a larger emission current. Thus the plate resistance of the diode formed by F and K would drop relative to R and reduce the voltage appearing between F and K.

Analysis shows that if F is a tungsten filament and if R is chosen to have a voltage drop 20 per cent greater than the diode, stabilization will be perfect. That is, power input to the cathode will have a maximum or stationary value with respect to changes in supply voltage E_0. Unfortunately, perfect stabilization at one point does not necessarily mean wide operating range, and for change in E_0 greater than $\pm$ 3 per cent this device is no better than a conventional tungsten heater.

VI. Miscellaneous Devices

A few other devices[20] will be considered only briefly because their advantages and disadvantages are obvious.

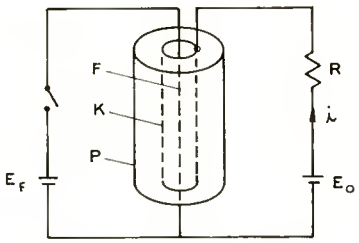

Fig. 5—Stabilized bombardment heater.

The most efficient way of controlling the cathode temperature is by keeping the average heater voltage, current or power constant without wasting power in an external load. The first might be achieved by interrupting the voltage regularly with a relay and varying the duty cycle as the supply voltage changes so that the average heater voltage is kept at the correct value. The heat capacity of the cathode assembly would keep its temperature substantially constant if the interruptions were rapid enough. The relay can be energized by the plate current in an emission-limited diode whose filament is connected in parallel with the other heaters (Figure 6).

A relay may also be used in a simple device to permit stepwise control of the heater voltage. The relay coil is connected in parallel with the supply voltage. The relay contacts are normally closed and

[20] The thermostatic switch and variable emissivity cathode coating were suggested by S. Umbriet of the RCA Victor Division, Harrison, N. J.

short a series resistor. If the supply voltage rises beyond a predetermined value, the series resistance will be thrown into the circuit. Consequently, the range of line voltages that the tube will stand will be effectively almost doubled.

To control the average heater power, a thermostatic switch may be incorporated in the tube either to open the heater circuit when the cathode is too hot or to short circuit part of the heater when the cathode is cool. This scheme has the merit of not wasting power at any voltage level, but is limited by the reliability of the contact and introduces a possible noise source into the tube. It would be necessary to protect the switch from the influence of anode heating in the tube. To stabilize the average heater current, one might devise a relay oscillator or thyratron circuit external to the tube which has the property of passing a constant average current independent of line voltage. The advantage would again be one of a saving in power compared with a voltage-dropping device.

A cathode coating that increases its emissivity with temperature

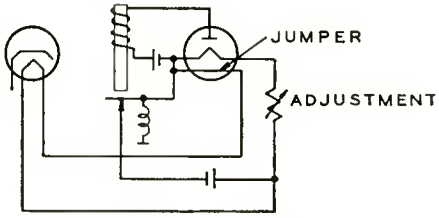

Fig. 6—Emission operated relay.

would reduce temperature changes by requiring a disproportionately large power increase to raise its temperature. Since, however, the power already varies as a large exponent of the temperature, the emissivity change would have to be relatively large. Although the process is essentially one of reducing the cathode efficiency, the over-all efficiency might be better than that obtained by using an external stabilizing device which absorbs extra power even on low-voltage operation.

An even more attractive solution would be a cathode coating capable of operation over a wider range of temperature. For example, a pure SrO coating could be run hotter than the usual BaO–SrO mixture. The net result of this and the preceding developments, however, might well be a cathode inherently very inefficient under all operating conditions.

Either alternating-current or direct-current voltages at high currents can readily be stabilized to a high degree, if the source is

alternating current, by using a diode-controlled regulator[21] employing a saturable core reactor. The unit necessarily employs heavy transformers and its use could be justified only where weight and space were secondary factors. There is also the simpler constant-voltage transformer which is now available in a form providing alternating-current plate and heater voltages directly. Although normally intended for ± 15 per cent voltage variation (with ± 1 per cent output regulation), this is not a basic limitation. The units require an extra weight and space allowance as well as special precautions against frequency variations such as normally occur in aircraft generators.

VII. Conclusions

Although vacuum-tube heaters may be operated with a voltage variation of ± 10 per cent, a range of approximately twice this value would be desirable. The series ballast tube exists as an attractive solution, but has a short life compared to an electron tube and on the average would dissipate a power equal to at least 38 per cent of that in the tube heater. It is possible that better ballast resistor materials may be discovered which would decrease this extra power dissipation. The several new magnetic alloys merit further investigation.

The discovery of a new heater material with a much larger temperature exponent of resistivity than tungsten would not completely solve the problem, but would extend the voltage range of operation. The platinum group and some other metals have some desirable heater properties but insufficient data are available.

A graphical representation shows that negative-resistance heaters are undesirable because of the excessive power dissipated in the series stabilizing element. A general analysis of two positive resistances in series explains their performance in terms of the ratio of dynamic-to-static resistance. This ratio for the stabilizer must always be greater than for the heater. With a tungsten heater, having a dynamic-to-static resistance ratio of 2, the average control power theoretically can be as low as 11 per cent of the average heater power for the tolerances already specified.

One solution to the problem might be a different method of heating the cathode. The suggested scheme, which uses electron bombardment, is self-stabilizing, but has a very limited operating voltage range.

A relay-operated switch in series with the heater supply and controlled by the temperature-limited emission from an auxiliary diode, is a simple device that could control the average heater voltage without

[21] T. Helterline, "Diode-Controlled Voltage Regulators," *Electronics*, Vol. 20, pp. 96-97, June, 1947.

any power loss in series or shunt circuit elements. Stepwise voltage control, via a relay which introduces series resistance at high supply voltage, would double the existing voltage range of tube heaters. These devices, however, do not provide "fail–safe" operation.

Improvements in the cathode coating would be desirable but may be considered a separate problem whose solution does not seem to be at hand. A thermal switch inside the tube is less desirable than a non-mechanical solution to the problem, but may be the only simple, low-cost, built-in means of solving the problem. Finally, standard electronic regulator circuits are likely either to be bulky or to consume excessive power, while standard constant-voltage transformers are frequency sensitive as well as bulky.

Appendix—General Analysis of Positive Resistance Heater and Series Control Resistance

In the following relations, the subscript "0" will denote values when the line voltage is normal; the subscript "2" will denote values for maximum line voltage.

V_l = line voltage

V_h = heater voltage

V_c = control element voltage

I = current.

Both resistances will be assumed linear over the restricted operating range, that is,

$$V_h = R_{h0} I_0 + R_{hd} (I - I_0),$$

and

$$V_c = R_{c0} I_0 + R_{cd} (I - I_0).$$

Thus, there can be defined what may be called static resistance (R_{h0} and R_{c0}) and dynamic resistance (R_{hd} and R_{cd}) for the heater and control element respectively. Symbols for their ratios are

$$R_{hd}/R_{h0} = r_h,$$
$$R_{cd}/R_{c0} = r_c.$$

It was shown in section IV that r_h and r_c are the slopes of log-log plots of the heater and control characteristics at the operating point.

Since the two elements are in series, they have the same current, I, and their powers W_h and W_c are proportional to their voltage drops.

The power ratio at the operating point can thus be defined as p_0, where $p_0 = V_{c0}/V_{h0} = R_{c0}/R_{h0}$.

There will be a certain fractional allowed variation in line voltage t_{vl}, and in heater power t_p. As these tolerances are utilized, the current in the system will vary. One can relate r_h to the required operating range of current, $\Delta I = I_2 - I_0$, by the geometric construction of Figure 7. Curve a is a selected linear portion of the heater characteristic near the normal operating point. Note that

$$\tan \theta = r_h,$$

and

$$I' - I_0 = t_p I_0.$$

From Figure 7

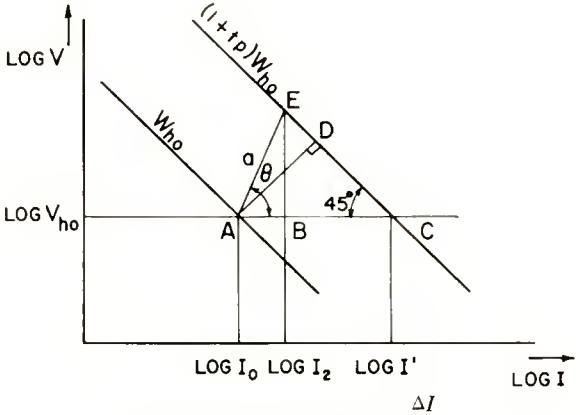

Fig. 7—Construction for $\frac{\Delta I}{I_0}$.

$$\overline{AD} = \overline{AC} \cos 45^\circ = \overline{AC}/\sqrt{2},$$

$$\overline{AE} = \overline{AC}/(\cos \theta + \sin \theta),$$

$$\overline{AB} = \overline{AC}/(1 + r_h),$$

$$1/(1 + r_h) = \overline{AB}/\overline{AC},$$

$$= \frac{\log\left(1 + \dfrac{I_2 - I_0}{I_0}\right)}{\log\left(1 + \dfrac{I' - I_0}{I_0}\right)}.$$

To simplify the last expression, use the relation

$$\log (1 + x) \approx x, \text{ for } x << 1.$$

$$(I_2 - I_0)/(I' - I_0) = 1/(1 + r_h),$$

or

$$\Delta I/I_0 = t_p/(1 + r_h). \tag{A-1}$$

The line-voltage tolerance may be expressed as

$$t_{vl} = (V_{l2} - V_{l0})/V_{l0}$$

$$= \frac{\Delta I\ (R_{hd} + R_{cd})}{I_0\ (R_{h0} + R_{c0})}.$$

Using Equation (A-1), $t_{vl}\ (1 + r_h)/t_p = (R_{hd} + R_{cd})/(R_{h0} + R_{c0})$.

This equation involves four resistance coefficients, but since it is linearly homogeneous in them, it can be reduced to three ratios of resistances. These ratios will be expressed $R_{hd}/R_{h0} = r_h$, $R_{cd}/R_{c0} = r_c$, and $R_{c0}/R_{h0} = p_0$. This gives

$$t_{vl}\ (1 + r_h)/t_p = (r_h + p_0 r_c)/(1 + p_0).$$

This can be solved for p_0:

$$p_0 = \frac{(t_{vl}/t_p)\ (1 + r_h) - r_h}{r_c - (t_{vl}/t_p)\ (1 + r_h)}.$$

The solution for r_c is

$$r_c = (t_{vl}/p_0 t_p)\ (1 + p_0)\ (1 + r_h) - (r_h/p_0);$$

that for r_h is

$$r_h = \frac{p_0 r_c - (t_{vl}/t_p)\ (1 + p_0)}{(t_{vl}/t_p)\ (1 + p_0) - 1}.$$

There is a minimum allowed value of p_0 which corresponds to the case where $V_c = 0$ at minimum line voltage. Call this minimum P_{0m}. It occurs when $\Delta V_c = -V_{c0}$.

$$\Delta V_l = \Delta V_h + \Delta V_c = \Delta V_h - V_{c0}.$$

Dividing through by

$$V_{l0} = V_{h0} + V_{c0}$$

gives

$$t_{vl} = \frac{-\Delta V_l}{V_{l0}} = \frac{-\Delta V_h + V_{c0}}{V_{h0} + V_{c0}}$$

$$= \frac{(-\Delta V_h/V_{h0}) + (V_{c0}/V_{h0})}{1 + (V_{c0}/V_{h0})}$$

$$= \frac{t_{vh} + p_{0m}}{1 + p_{0m}},$$

where $t_{vh} = -\Delta V_h/V_{h0}$ is the heater voltage tolerance. Solving for p_{0m},

$$p_{0m} = \frac{t_{vl} - t_{vh}}{1 - t_{vl}}.$$

ANALYSIS OF MICROWAVE ANTENNA SIDELOBES*

By

N. I. Korman, E. B. Herman, and J. R. Ford

Engineering Products Department, RCA Victor Division, Camden, N. J.

Summary—*A simple method is described, based on the theory of "paired echoes,"[1] whereby manufacturing tolerances can be described in terms of the side-lobe level for the majority of large microwave reflectors. It is also useful in predicting the radiation pattern of a given reflector whose mechanical variations from a perfect surface are known. Experimental evidence which agrees with the theory is presented.*

WHEN large microwave reflectors are to be produced in quantity, and the maximum side-lobe level is specified, a tolerance must be set on the errors in the reflecting surface. The main difficulty in setting a surface tolerance is that the distribution, as well as the magnitude of the surface errors, determines the side-lobe structure. While the side-lobe structure for a particular error distribution can be calculated in a straightforward manner by the use of the Fourier integral, it has been difficult, heretofore, to specify mechanical tolerances from purely theoretical considerations.

A statistical approach to the problem could be employed. The Fourier integral could be used to compute the side-lobe structure for a large number of possible error distributions having the same peak error. If it were found that the side-lobe ratio could then be correlated with the distributional probability, a surface tolerance could be set. This method, however, is somewhat involved and does not give a clear picture of side-lobe formation.

A simpler approach to the problem is to note that a sinusoidal distribution of phase error along a line source will generate two equal side lobes whose amplitude, in terms of the main lobe, is half the peak phase error expressed in radians. The side lobes, which are reproductions of the main lobe in miniature, are located symmetrically on either side of the main lobe at a distance of $n\lambda/l$ radians from it. Here, n is the number of cycles of error along the line source, λ is the radiated wave length, and l is the aperture or extent of the line source. Furthermore, except for second order terms, the process is linear so that the

* Decimal Classification: R326.8.

[1] H. A. Wheeler, "The Interpretation of Amplitude and Phase Distortion in Terms of Paired Echoes," *Proc. I.R.E.*, Vol. 27, pp. 359-385, June, 1939.

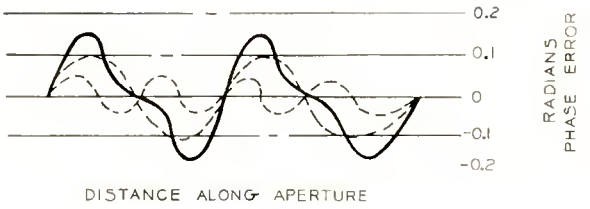

Fig. 1A—Phase-error distribution along a line source.

superposition theorem can be used. Hence, the side-lobe structure corresponding to any given phase-error distribution can be synthesized from the pairs of side lobes corresponding to the sinusoidal components of the phase-error distribution. A mathematical proof of these statements is contained in the appendix.

Figure 1 illustrates graphically the statements of the preceding paragraph. Figure 1(a) is the phase-error distribution along a line source. It consists of two sinusoidal waves, having 2 and 4 cycles of error across the aperture of 0.10 and 0.05 radians peak error, respectively. The resulting side-lobe pairs in the radiation pattern are given in Figure 1(b). In this example, an illumination pattern has been assumed which does not in itself cause appreciable side lobes.

The results of this approach have been particularly successful in their application to reflectors whose construction is of the bulkhead and truss-work type shown in Figure 2. In this method of fabrication, machined bulkheads or accurately formed and welded truss work are erected to support the reflecting surface at roughly equal intervals along the long dimension or major axis of, and perpendicular to, the reflector. These bulkheads are accurately held in position during fabrication by a steel fixture, while tubular cross supporting members are welded in place. When the truss work is removed from the fixture, stresses caused by welding are relieved. Most of the resulting strain error appears along the long dimension since the truss work is much less rigid in this direction. The reflecting surface, usually a mesh

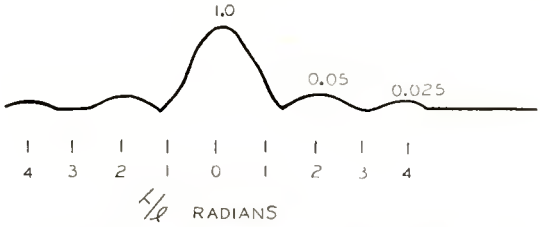

Fig. 1B—Resultant side-lobe distribution.

screen or parallel-spaced rods, is then spot welded or crimped to the supporting structure.

The pattern of the antenna in the plane of the major axis of the reflector can easily be found. This is true because the phase-error distribution along a line source having the same radiation pattern is approximately the same as the phase-error distribution along the major axis of the reflector. The phase-error distribution in radians along the major axis of the reflector can be calculated easily by multiplying the linear error, expressed in wave lengths, by $4\pi/\lambda$. The factor $4\pi/\lambda$ is used instead of $2\pi/\lambda$ because reflection doubles the effect of the linear error.

The pattern in the plane of the minor axis of the reflector generally has smaller side lobes than the pattern in the plane of the major axis.

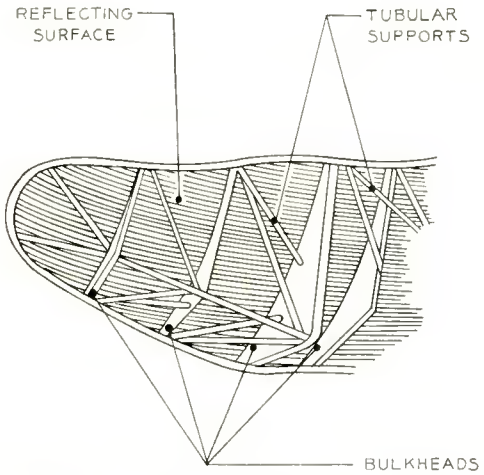

Fig. 2—Bulkhead and truss-work type antenna construction.

This can be understood by considering the phase-error distribution along a line-source equivalent for the minor axis. To find the phase errors of this line source, the phase errors of the reflector must be collapsed upon the minor axis by integration along paths perpendicular to the minor axis. Over any integration path, the phase error will generally fluctuate between positive and negative values so that integration has a smoothing effect which reduces the resultant phase errors and side lobes.

In principle, this same integration process must be used to find the equivalent line source for the major axis of the reflector. Practically, however, because of the method of constructing the bulkhead type of

reflector, the phase errors along lines perpendicular to the major axis tend to be constant. Therefore, the integration or averaging of the phase errors along paths perpendicular to the major axis does not appreciably change the phase errors along the major axis.

To set a surface tolerance on this type of reflector, a value must be determined for the probable ratio of the peak error to the largest sinusoidal component in the error distribution. Experience indicates that 2 is a reasonable value for this ratio, although additional experience may modify this estimate. This estimate is based on the observation that the phase-error distribution of a number of reflectors could be roughly approximated by two equal sinusoidal components. Since these sinusoidal components add constructively somewhere on the reflector, the largest sinusoidal component of error is usually half the peak value of the error. Therefore, if d is the peak-to-peak linear error, $2\pi d/\lambda$ is the peak phase error and the largest side lobe will have a peak value of $\pi d/2\lambda$.

The latter value can probably be regarded as the upper limit of the probable side-lobe ratio due to surface distortion in any microwave reflector. When the spectrum of the error distribution is about the same for all directions of travel across the reflecting surface, the side-lobe ratio will be considerably less than $\pi d/2\lambda$. The reduction from this figure will, in general, depend on the number of cycles of the predominate error component across the aperture. As we have seen, the preliminary integration that gives an equivalent line source has an averaging effect on the error. The higher the error frequency, the more the error is reduced. Even in large 15-foot reflectors, the largest sizeable error component usually has a frequency no higher than about 4 or 5 cycles across the aperture. The manufacturing process tends to act somewhat like a low-pass filter acting on a random error signal. As more experience is obtained, it will probably be found that $\pi d/2\lambda$ can be multiplied by a factor such as 2 or 3 to give a tolerance for the unrestricted error distribution.

Applications to Practical Antenna

There have been two immediate applications of the theory advanced in this paper: the first to production, and the second to development.

In the first application, it was determined from this theory that a certain L-band antenna reflector must be held to $\pm\frac{1}{8}''$ in order to assure that the maximum side-lobe level would be —23 decibels or less. The first reflector to be fabricated was measured and the results of this measurement are shown in Figure 3. This is a plot of the errors

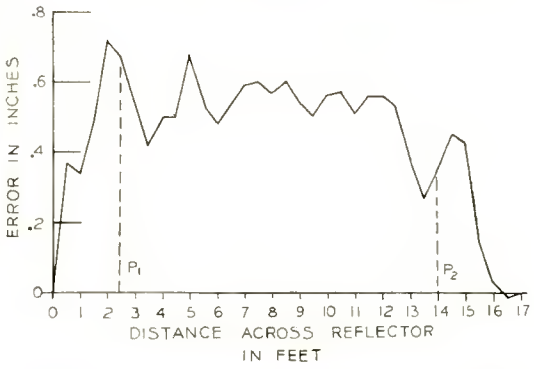

Fig. 3—Error plot of production antenna.

measured across the dish, assuming that the perfect parabola and the fabricated parabolic surface coincide at the tips of the reflector. Large deviations are seen to build up toward the center of the reflector with rapid variations near the tip sections.

Certain types of errors are considered removable. These are errors due to a constant displacement, a straight line or tilt error, and a parabolic or squared error. These all can be removed by repositioning the feed or focal point of the parabola.

Figure 4 shows the error function as curve A with all permissible error functions removed. What remains is the function which generates the error side lobes. It is this function in which we are most interested. Curve B of Figure 4 is a curve which has been synthesized of two sinusoids to approximate curve A.

The manner in which the error function is analyzed requires breaking up the function into its Fourier components. To do this exactly can be a very laborious task; however, it has been found empirically

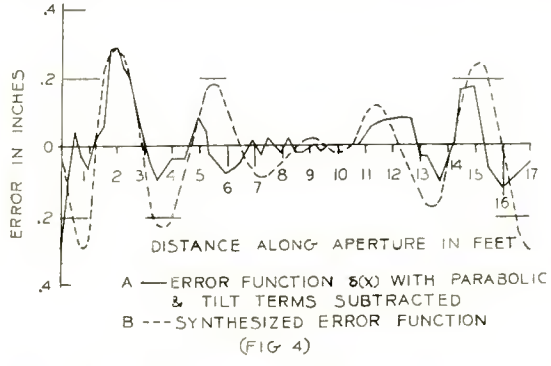

Fig. 4—Error function of production antenna.

that in most cases two sinusoidal components, which can be selected by careful inspection, are sufficient to give a good approximation of actual conditions.

Inspecting curve A, it can be seen that there are at least two major components beating together to cause addition at the tips and cancellation in the center of the reflector. From the general form of curve A, it appears that there is a four-cycle component and a five-cycle component; there may also be a three-cycle component present, which, for the moment, we shall consider to be negligible. Curve B, then, is what would result if we added a four- and a five-cycle component. Using these components, the type of pattern can be predicted.

The data we now have is as follows:

Peak to peak linear four-cycle error $(d) = 0.300$ inch,

Peak to peak linear five-cycle error $(d) = 0.300$ inch.

The number of cycles of error across the reflector are four and five respectively.

The error side lobe is then

$$\frac{\pi d}{2\lambda} = \frac{\pi(0.300)}{2 \times 9.1} = 0.052.$$

Thus, both the four- and five-cycle error side lobes are about 5 per cent. The five-cycle side lobe is located at an angle $\alpha = \frac{5\lambda}{l}(57.3) = 18$ degrees; the four-cycle side lobe is located at an angle of 14 degrees.

If this 5 per cent error side lobe were to be added to the side lobes of a perfect antenna, we could then predict the largest side lobe to be expected. The aperture illumination, when collapsed by integration to an equivalent line source, is cosine squared and is down 16 decibels at the edge.

According to Ramsey,* the side lobes, due to this illumination taper alone, are 2.5 per cent. If these are added to the 5.2 per cent side lobes of the error function, we now have a possible addition to give us 7.7 per cent, or —22.2-decibel side lobes.

Since the tip sections seem to contain a large portion of the error, it was of interest to find out what would happen if an absorbing material were used as a mask to reduce the illumination to a negligible

* J. F. Ramsay, "Fourier Transforms in Aerial Theory," *Marconi Review*, Vol. IX, pp. 139-145, October-December, 1946.

amount in these regions. This would, in effect, eliminate the errors in the tips but raise the edge illumination somewhat. If, in Figure 4, the error from 0 to 2.5 feet and from 15 to 17.5 feet were removed, then the maximum error component would have an amplitude of .100 inch and would give rise to 1.7 per cent side lobes. Due to the higher edge illumination, the perfect reflector side lobes are now, by Ramsey, 4.1 per cent, and when added to the error side lobes could produce a maximum side lobes of 5.8 per cent, or about —25 decibels. The angular displacements of the side lobes would be nearly the same.

Now, examining actual patterns made under the two conditions discussed, we see in Figure 5 the results of masked and unmasked

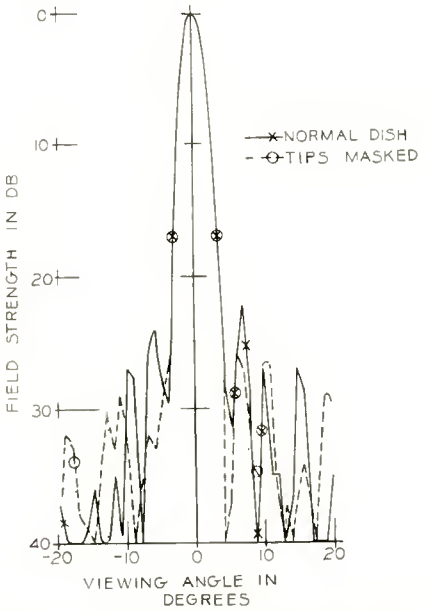

Fig. 5—Measured patterns of production antenna.

errors in the tips. The curve marked "normal dish" shows that the maximum side lobe of —22.2 decibels was realized for the reflector, and when the tips were masked the maximum side lobe promptly dropped to —26 decibels, slightly less than predicted.

It is also noted that the error lobes also appear at somewhat different angles from predicted values. While there are error lobes at the predicted 14 and 18 degrees, there are also error lobes at 7 and 10 degrees. This indicates that components are present which were not included in the synthesis of the error function. This points out the

difficulty of exact construction of an antenna pattern; however, it is to be noted that the maximum side lobes were predicted in each case. It was found that the maximum levels could be predicted with ease, but frequently the positions would be in error, since the frequency of the error was approximated. It is felt that this is not a serious limitation of the method since in most instances the requirements specify the maximum level of the side lobes, but do not place restrictions on side-lobe structure.

A second application of this theory was made in the development of an X-band model of an antenna. Here it was desired to know if it was possible, through positioning of the feed, to attain a —26-decibel maximum side-lobe level. The procedure is roughly the same. The error plot and error function are shown in Figure 6. By inspection it is seen that the maximum error amplitude gives an error side lobe

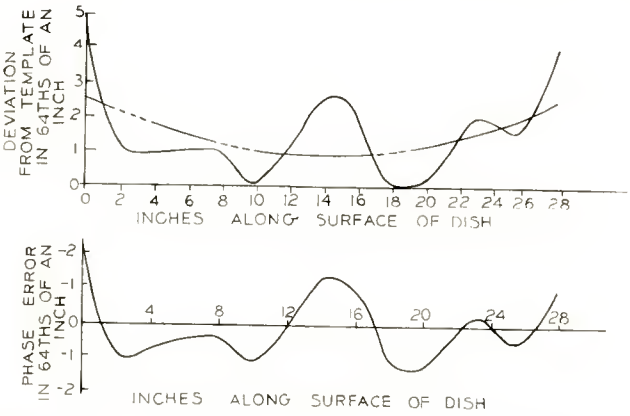

Fig. 6—Error plot and error function of X-band dish.

of 5.9 per cent, or about −24.7 decibels. The main frequency components of the error are three and four cycles, and therefore the angles of the error side lobe should be 7 and 10 degrees. From this, it is immediately evident that a —26-decibel maximum side-lobe level is out of the question.

Carrying the analysis further, Figure 7 shows a pattern of a perfect antenna having the illumination used. The maximum side lobes are about —32 decibels.

In Figure 8, the perfect dish pattern is shown along with the error side lobes, and finally the two are added together to give the pattern to be expected with a reflector having the given error function. In Figure 9, a measured pattern is compared with a calculated pattern

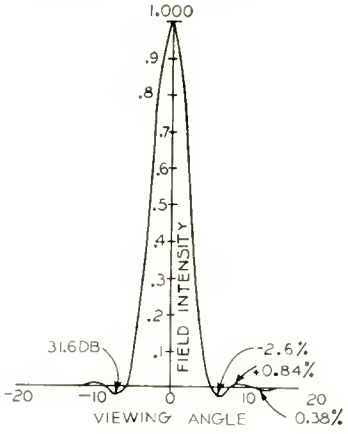

Fig. 7—Theoretical pattern for illumination of perfect cosine-squared X-band dish.

and good agreement is shown between the two. In this case the surface of the antenna was relatively simple and easy to measure. This made it possible to obtain good agreement between the measured and the calculated patterns.

It must be remembered that for most applications, the exact nature of the side-lobe structure is unnecessary, and only the maximum level need be considered. In most all cases to date where the theory has been applied, the maximum side-lobe level has been predicted with success.

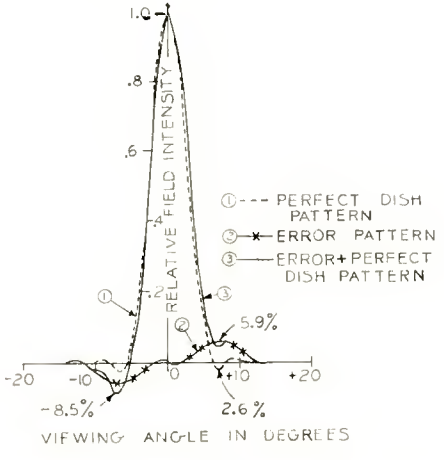

Fig. 8—Theoretical pattern of X-band dish of Figure 6.

Appendix—Derivation of the Relation Between the Sinusoidal Error Component and the Resulting Side-Lobe Pairs

Let x = distance measured along a line source,

$I(x)$ = nominal current density distribution along the line source,

a = peak phase error in an actual distribution in radians,

$F(\theta)$ = radiation pattern,

$F_0(\theta)$ = radiation pattern for an antenna without phase errors,

θ = radiation angle measured with respect to a normal to the line source,

λ = wave length of the radiation,

l = aperture or length of the line source.

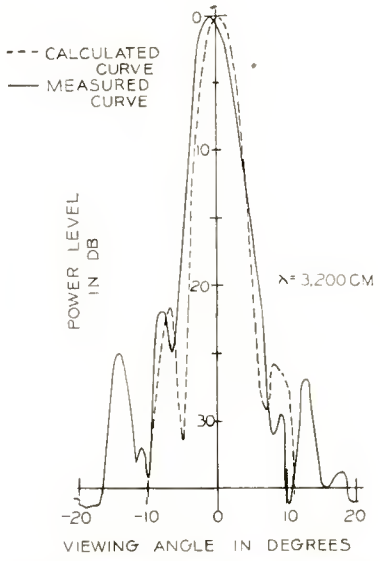

Fig. 9—Measured pattern of X-band dish of Figure 6.

It is well known that the radiation and the current distribution are related by the expression

$$F_0(\theta) = \int_{-\infty}^{\infty} I(x)\, e^{j\frac{2\pi x \sin\theta}{\lambda}}\, dx.$$

Suppose a sinusoidal distribution of phase error is assumed to exist along the line source. The error can then be written as

$$a \cos\left(\frac{2\pi m x}{l} + \phi\right),$$

where $\frac{m}{l}$ = space frequency of the error in cycles across the aperture,

ϕ = constant controlling the position of a maximum error relative to the center of the line source.

Then the radiation pattern is

$$F(\theta) = \int_{-\infty}^{\infty} I(x)\, e^{j\, a \cos\left(\frac{2\pi m x}{l} + \phi\right)} e^{j\frac{2\pi x}{\lambda}\sin\theta}\, dx. \qquad (1)$$

For a reasonably good reflector, a will be small so that Equation (1) can be written

$$F(\theta) \cong \int_{-\infty}^{\infty} \left[1 + j\, a \cos\left(\frac{2\pi m x}{l} + \phi\right)\right] I(x)\, e^{j\frac{2\pi x}{\lambda}\sin\theta}\, dx. \qquad (2)$$

The first term in this integral is the nominal pattern designated by $F_0(\theta)$ or $F_0(\sin\theta)$. Expressing the cosine term exponentially, Equation (2) becomes

$$F(\theta) \cong F_0(\sin\theta) + je^{j\phi}\frac{a}{2}\int_{-\infty}^{\infty} I(x)\, e^{j\left(\sin\theta + \frac{m\lambda}{l}\right)\frac{2\pi x}{\lambda}}\, dx$$

$$+ je^{-j\phi}\frac{a}{2}\int_{-\infty}^{\infty} I(x)\, e^{j\left(\sin\theta - \frac{m\lambda}{l}\right)\frac{2\pi x}{\lambda}}\, dx.$$

Now let $\sin\theta_1 = \sin\theta + \frac{m\lambda}{l}$, $\sin\theta_2 = \sin\theta - \frac{m\lambda}{l}$. Then

$$F(\theta) = F_0(\sin\theta) + j\, e^{j\phi}\frac{a}{2}F_0(\sin\theta_1) + j\, e^{-j\phi}\frac{a}{2}F_0(\sin\theta_2).$$

The beam width of most microwave antennas is small enough that throughout the angular range needed to obtain a radiation pattern, the sine equals the angle. Hence

$$F(\theta) \cong F_0(\theta) + j\, e^{j\phi} \frac{a}{2} F_0\left(\theta + \frac{m\lambda}{l}\right) + j\, e^{-j\phi} \frac{a}{2} F_0\left(\theta - \frac{m\lambda}{l}\right) \quad (3)$$

Equation (3) is equivalent to the statement contained in the third paragraph of this paper. A similar result occurs if the amplitude $I(x)$ is assumed to have a sinusoidal component, so that the actual illumination can be written as[2]

$$I(x)\left[1 + b\cos\left(\frac{2\pi n x}{l} + \rho\right)\right],$$

where b, n and ρ are analogous to a, m and ϕ above.

It can easily be demonstrated that the relation between the sinusoidal components and the side-lobe pairs is linear. Suppose the error is the sum of q sinusoidal components

$$\sum_{p=1}^{p=q} a_p \cos\left(\frac{2\pi m_p}{l} + \phi_p\right),$$

and that the error is small, then

$$F(\theta) = \int_{-\infty}^{+\infty} I(x)\, e^{j \sum_{p=1}^{p=q} a_p \cos\left(\frac{2\pi m_p}{l} + \phi_p\right)} e^{j\frac{2\pi x}{\lambda}\sin\theta}\, dx$$

$$\cong \int_{-\infty}^{\infty} I(x)\left[1 + j \sum_{p=1}^{p=q} a_p \cos\left(\frac{2\pi m_p}{l} + \phi_p\right)\right] e^{j\frac{2\pi x}{\lambda}\sin\theta}\, dx. \quad (4)$$

Here, again, the first term is the nominal pattern $F_0(\theta)$ and each of the remaining q terms corresponds to the second term in Equation (2), and so describes one side-lobe pair.

---

[2] J. Brown, "The Effect of a Periodic Variation in the Field Intensity across a Radiating Aperture," *Proc. Inst. Elec. Eng.* (Brit.), Vol. 97, Pt. III, pp. 419-424, 1950.

A NOTE ON THE DESIGN OF CONSTANT-RESISTANCE CATHODE-RAY DEFLECTION CIRCUITS*

By

Richard C. Webb†

Absent on leave from Research Department, RCA Laboratories Division, Princeton, N. J.

Summary—*A new horizontal-deflection circuit has recently been introduced which is particularly useful with small television pickup tubes such as the Vidicon. Several hundred feet of transmission line may be interposed between the amplifier tubes and deflection coil since the coil is built into a network which appears as a pure resistance matching the line impedance. Although the efficiency of the system is low, and varies in inverse proportion to the deflection ampere-turns required, it is characterized by a remarkable freedom from transient disturbance to low-level video circuits, and the scanning linearity can readily be set to a precision of one per cent or better.*

Introduction

THE introduction of the small, new, photoconductive television camera tube known as the Vidicon[1] brought about a demand for a simple horizontal-deflection circuit that will permit a horizontal-deflection coil to operate at the end of several hundred feet of transmission line without introducing serious transient disturbances into the video circuit, either in the transmission path or by proximity to the low-level amplifier stages near the pickup tube. A. W. Vance[2] has suggested a circuit that very adequately fulfills these requirements. This circuit is now being widely used in the industrial television systems that employ the Vidicon tube.[3] The purpose of these notes is to set forth the design considerations of this constant-resistance deflection system, as it is called, so that the method can be extended to other fields.

The circuit is shown in Figure 1. Many basic electrical engineering text books have shown and analyzed this parallel connection of capaci-

* Decimal Classification: R583.13.

† Institute of Industrial Research, University of Denver, Denver, Col.

[1] P. K. Weimer, S. V. Forgue, and R. R. Goodrich, "The Vidicon—Photoconductive Camera Tube," *Electronics*, Vol. 23, p. 70, May, 1950.

[2] A. W. Vance, "Cathode-Ray Deflection Circuit," U. S. Patent No. 2,559,525, issued July 3, 1951.

[3] R. C. Webb and J. M. Morgan, "Simplified Television for Industry," *Electronics*, Vol. 23, pp. 70-73, June, 1950.

tance and inductance with series resistance in each arm. It is well known, moreover, that such a circuit is anti-resonant at all frequencies when the unique condition is satisfied that the two resistance elements are equal and related to the reactive elements as follows:

$$R_1 = R_2 = \sqrt{\frac{L}{C}}. \tag{1}$$

In this case the impedance of the series-parallel assembly is found to be,

$$Z = \sqrt{\frac{L}{C}} + j\,0 \text{ ohms}. \tag{2}$$

Furthermore, it is known that critical damping is reached in a resonant circuit when the total resistance in the loop becomes

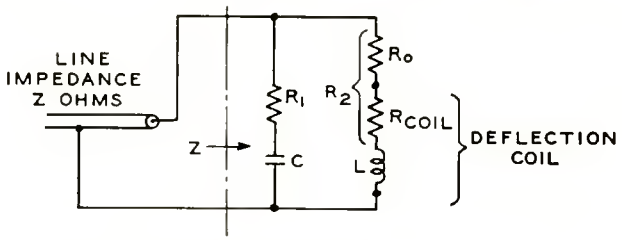

Fig. 1—Constant resistance deflection circuit.

$$R_{\text{total}} = 2\sqrt{\frac{L}{C}}, \tag{3}$$

hence, this circuit is seen to be completely aperiodic or fully damped when so proportioned. Thus, it is capable of terminating a transmission line properly as a pure resistance load.

In order to obtain linear deflection of a cathode-ray device which may employ the inductive element of this network as its deflection coil, it is only necessary to pass a saw-tooth current wave form through the arm containing the coil. The voltage wave form that must be impressed upon the whole network in order to secure the desired internal current wave as shown in Figure 2(b) is the sum of the voltage known to exist across the inductance when a linear saw-tooth of current is flowing in it as shown in Figure 2(c) and the voltage across the resistance element as shown in Figure 2(d). Thus the composite driving voltage, as illustrated in Figure 2(e), is comprised

of both pulse and saw-tooth components. When it is applied to the circuit, the ideal current saw-tooth is forced to flow in the deflection coil. This abrupt wave form is readily synthesized in electronic circuits and can be amplified, attenuated, and transmitted like any other video signal since its ultimate termination is in a pure resistance load. It should be noted, however, that the accuracy of the scanning linearity is directly related to the precision with which the required wave form is synthesized.

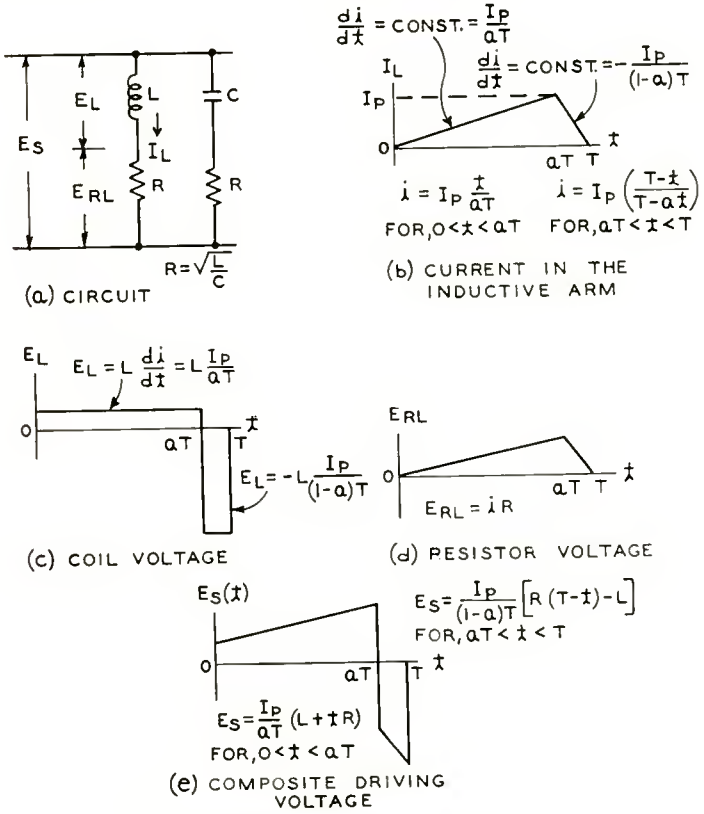

Fig. 2—Synthesis of driving voltage.

Equation (1) gives the basic law relating the element values to be employed with the system, and it will be assumed throughout this discussion that the constants are proportioned so that Equation (1) holds. There are two logical ways that one might approach the design of this type of deflection circuit. In the first case one might be given the value of the impedance of a certain transmission line over which the deflection wave form is to be passed; hence, the network must be

built to match the line impedance, R. In the second case it might be necessary to make use of a certain deflection coil L; thus, the best impedance level R at which to build the network must be determined. It is evident that there is no limit to the values that will satisfy Equation (1). There are definite limits, however, to practical values of L and C. We shall define the optimum design of the circuit as that which will permit maximum deflection ampere-turns to be developed for a minimum driving power. All cases of which the writer knows that were designed in accordance with this latter criterion have led to quite reasonable values for L and C.

Figure 2(b) indicates that the required current in the inductance rises from zero to its maximum value I_p in the horizontal scanning interval which is taken to be a fraction a of the entire period T. During the retrace interval, $(1-a)\ T$, the current falls from I_p back to zero. Within the first interval the value of the current at any instant is given by

$$i = I_p \frac{t}{aT}, \tag{4}$$

and in the second interval,

$$i = I_p \left(\frac{T-t}{T-aT} \right). \tag{5}$$

Furthermore, the slope of the function in the first interval is

$$\frac{di}{dt} = \frac{I_p}{aT} = \text{constant}, \tag{6}$$

and in the second interval,

$$\frac{di}{dt} = -\frac{I_p}{(1-a)\,T} = \text{constant}. \tag{7}$$

Figure 2(a) indicates the voltage drops across the inductance E_L and across the series resistor E_{RL} as required to permit the desired saw-tooth current wave to flow in the inductance. The voltage to be applied to the entire system, E_s, is of course the sum of the drops.

During the scanning interval the voltage across the inductor as shown in Figure 2(c) is

$$E_L = L\frac{di}{dt} = L\frac{I_p}{aT}, \tag{8}$$

and during the retrace time the voltage becomes

$$E_L = -L\frac{I_p}{(1-a)T}. \tag{9}$$

The drop across the resistor in the inductive branch at any time in the entire period as indicated in Figure 2(d) is given by

$$E_{RL} = i\,R. \tag{10}$$

Thus, the required signal voltage, E_s, in each interval becomes the sum of E_L and E_{RL} as indicated in Figure 2(e). Thus

$$E_{s_1} = L\frac{I_p}{aT} + i\,R$$

$$= \frac{I_p}{aT}(L + tR), \text{ for } 0 < t < aT, \tag{11}$$

and $$E_{s_2} = -L\frac{I_p}{(1-a)T} + i\,R$$

$$= -\frac{I_p}{(1-a)T}|L - (T-t)R|, \quad \text{for} \quad aT < t < T. \tag{12}$$

The instantaneous power applied to the system during the first interval is

$$P_i|_1 = \frac{E_{s_1}^2}{R} = \frac{\left[\frac{I_p}{aT}(L + tR)\right]^2}{R}. \tag{13}$$

The average power applied during the first interval is

$$P_{\text{AVG.}}|_1 = \frac{1}{aT}\int_0^{aT}\frac{E_{s_1}^2}{R}\,dt$$

$$= I_p^2 R \left[\frac{\left(\frac{L}{R}\right)^2}{a^2 T^2} + \frac{\left(\frac{L}{R}\right)}{aT} + \frac{1}{3} \right]. \tag{14}$$

The average power applied during the second interval is

$$P_{\text{AVG.}}|_2 = \frac{1}{(1-a)\,T} \int_{aT}^{T} \frac{E_{s_2}^2}{R}\, dt$$

$$= I_p^2 R \left[\left(\frac{L}{R}\right)^2 \frac{1}{(1-a)^2 T^2} - \left(\frac{L}{R}\right) \frac{1}{(1-a)\,T} + \frac{1}{3} \right]. \tag{15}$$

The average power over the cycle is the sum

$$P_T = \frac{P_{\text{AVG.}}|_1\,(aT) + P_{\text{AVG.}}|_2\,(1-a)\,T}{T}$$

$$= I_p^2 R \left[\left(\frac{L}{R}\right)^2 \frac{1}{a(1-a)\,T^2} + \frac{1}{3} \right]. \tag{16}$$

We know that the peak deflection is proportional to the peak ampere-turns in the deflection coil, so that

$$\text{deflection} = k\,N\,I_p,$$

or

$$\text{deflection} = k\,\sqrt{L}\,I_p, \tag{17}$$

where k is the deflection coil constant.

Denoting by ψ the ratio of deflection to the power required to produce it, we have

$$\psi = \frac{k}{\sqrt{L}\,I_p} \frac{\left(\frac{L}{R}\right)}{\left(\frac{L}{R}\right)^2 \frac{1}{a(1-a)\,T^2} + \frac{1}{3}}. \tag{18}$$

The first factor in this equation indicates that the deflection efficiency

is proportional to the quality of the yoke, as denoted by its deflection factor k, and is *inversely* proportional to the number of ampere-turns required. The second factor is a function of the L/R ratio which, for a given television system (a and T fixed), can be maximized by choice of an optimum L/R ratio. Denoting the parametric factor by m,

$$m = \frac{1}{a(1-a)T^2}.$$

The second factor in Equation (18) can be maximized as follows:

$$f\left(\frac{L}{R}\right) = \frac{\left(\frac{L}{R}\right)}{m\left(\frac{L}{R}\right)^2 + \frac{1}{3}}, \tag{19}$$

which has as its derivative

$$f'\left(\frac{L}{R}\right) = \frac{\left[m\left(\frac{L}{R}\right)^2 + \frac{1}{3}\right] - \left(\frac{L}{R}\right)\left[2m\left(\frac{L}{R}\right)\right]}{\left[m\left(\frac{L}{R}\right)^2 + \frac{1}{3}\right]^2}. \tag{20}$$

Equating this to zero,

$$m\left(\frac{L}{R}\right)^2_{\text{OPT.}} = \frac{1}{3},$$

and we obtain

$$\left(\frac{L}{R}\right)_{\text{OPT.}} = \sqrt{\frac{1}{3m}} = T\sqrt{\frac{a(1-a)}{3}}. \tag{21}$$

Thus, Equation (21) gives the optimum ratio of L to R that will maximize the value of the second factor in Equation (18), and hence, it can be used as the design equation. Figure 3 shows how the value of the second term of Equation (18) varies near its maximum and hence, is useful in estimating the performance of a circuit which for

some reason or another can not be proportioned to the optimum value. In this curve, the parameters $a = .85$ and $T = 1/15{,}750$ have been used since these are typical constants for the standard monochrome television system.

As an example of the use of the equations, assume that it is desired to transmit horizontal deflection current to a small tube such as a Vidicon over a length of 52-ohm transmission line for a standard 525-line television system permitting a 15 per cent retrace time. Then $T = 1/15{,}750$ and $a = .85$. From Equation (21), we have

$$\left(\frac{L}{R}\right)_{\text{OPT.}} = 1.31 \times 10^{-5}.$$

With R fixed at 52 ohms, the optimum coil inductance becomes

$$L = 0.667 \times 10^{-3} \text{ henry}.$$

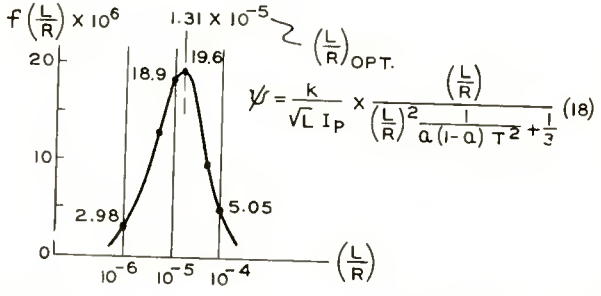

Fig. 3—Evaluation of the second factor in the equation for deflection efficiency, Equation (18), for 15 per cent flyback time, $a = .85$, with $T = 1/15{,}750$.

The value of the capacitance from Equation (1) then becomes

$$C = 0.247 \times 10^{-6} \text{ farad}.$$

It is then experimentally determined that a peak current of 0.2 ampere is required in the prescribed coil in order to secure the necessary amount of deflection. The power that must be supplied to the circuit is found from Equation (16);

$$P_T = 1.39 \text{ watts}.$$

The peak-to-peak line voltage can then be determined by adding the peak coil and resistor voltages giving

$$E_{s(\text{peak to peak})} = 26.88 \text{ volts.}$$

Another example illustrates how rapidly the power requirements go up as the ampere-turns are increased to obtain deflection for a larger tube such as an image orthicon. Assume that a 1.45-millihenry deflection coil is given which requires a peak current of 1.2 amperes to produce the desired amount of deflection. In this case, the optimum impedance level for the circuit is sought. It will be assumed, as before, that $a = .85$ and $T = 1/15{,}750$. It has already been shown that for these values the optimum L/R ratio is 1.31×10^{-5}; hence, the impedance level should be

$$R = 110 \text{ ohms.}$$

Equation (1) gives the value of the capacitor as

$$C = .12 \times 10^{-6} \text{ farad.}$$

The power required according to Equation (16) is

$$P_T = 106 \text{ watts.}$$

The peak-to-peak driving voltage is found, as before, by adding the peak coil and resistor voltages:

$$E_{s(\text{peak to peak})} = 347 \text{ volts.}$$

LOW-NOISE TRAVELING-WAVE AMPLIFIER*

By

R. W. Peter

Research Department, RCA Laboratories Division,
Princeton, N. J.

Summary—As a result of theoretical and experimental studies, an experimental small-signal microwave amplifier of the traveling-wave tube type has been developed which is outstanding not only with respect to gain and band width, but which competes with the best crystal-mixer amplifiers with respect to noise factor. The optimum performance obtained with a 500-volt S-band traveling-wave amplifier with wide frequency band is 8.5 decibels noise factor, at 15 decibels gain.

A short account is given of the design considerations for the gun and circuit of broad-band, low-noise, traveling-wave amplifiers. In particular, the theory of the "three-region" low-noise gun, which is the essential factor in this amplifier, is given in detail. Measurements are presented which show the dependence of the noise factor upon various parameters.

Introduction

IN HIS TWO papers covering the earliest investigation on traveling-wave amplifiers, R. Kompfner[1,2] reported very low measured noise factors: 11.0 decibels for an 1800-volt tube with 11.5 decibels gain. For a long time thereafter, no duplication of these early low noise factors was reported. Typical traveling-wave amplifiers showed characteristics similar to those reported by Rogers[3] and Robinson:[4] 17-20 decibel noise factor at 25 decibels gain.

A noise factor of 16 decibels measured at RCA Laboratories on a 1250-volt dispersive-helix tube with 28 decibels gain was considered an accomplishment at the beginning of 1949.

The key to a better understanding of the problems involved in attaining low noise factors was contained in the application, by Pierce,[†,5] of the beam noise model of Rack[6] and Llewellyn and Peterson[7,8] to the computation of the noise factor of traveling-wave tubes. Pierce considered a gun consisting of a single anode followed by a

---

* Decimal Classification: R339.2.

[1] R. Kompfner, "The Traveling-Wave Valve," *Wireless World*, Vol. 52, pp. 369-372, November, 1946.

[2] R. Kompfner, "The Traveling-Wave Tube as Amplifier at Microwaves," *Proc. I.R.E.*, Vol. 35, pp. 124-127, February, 1947.

[3] D. C. Rogers, "Traveling-Wave Amplifier for Six to Eight Centimeters," *Electrical Communication*, Vol. 26, pp. 114-152, June, 1949.

[4] F. N. H. Robinson, "Traveling-Wave Tubes with Dispersive Helices," *Wireless Eng.*, Vol. 28, p. 110, April, 1951.

drift space. Using the same model, we investigated the beam noise produced by a gun with two and with three anodes (or "regions"). At the same time, experiments were carried out with three- and four-anode guns to study the effect of various electrode potentials on the noise factor.

This early work culminated in a 10.5-decibel noise factor traveling-wave tube.** Its theoretical part, included in an early report,[9] is reproduced in the present paper.

Further theoretical and experimental studies led to an 8.5-decibel noise factor S-band traveling-wave amplifier.‡,[10] Noise factors lower than 8 decibels have been measured with narrow-band filter-type circuits.‡ The latter work will be discussed in a forthcoming paper.

Other independent approaches to the same problem have been made by Robinson and Kompfner,[11] who describe an 11-decibel noise factor tube and by Watkins,[12] who measured a 10-decibel noise factor on an S-band traveling-wave amplifier.

Watkins' low-noise gun consists of constant-potential drift tubes and short accelerating or decelerating gaps. His "single-" and "double-velocity-jump" guns will be compared with the "three-region" gun used in our tubes. It will be seen that not only is the three-region gun more flexible as regards control of electrical drift angle, but that in addition, the theory indicates that a somewhat greater noise reduction can be expected from it.

---

† Paper presented at the I.R.E. Electron Devices Conference at Princeton, June, 1949.

[5] J. R. Pierce, *Traveling-Wave Tubes*, D. Van Nostrand Co., Inc., New York, N. Y., 1950.

[6] A. J. Rack, "Effect of Space Charge and Transit Time on the Shot Noise in Diodes," *Bell. Sys. Tech. Jour.*, Vol. 17, pp. 592-619, October, 1938.

[7] F. B. Llewellyn and L. C. Peterson, "Vacuum Tube Networks," *Proc. I.R.E.*, Vol. 32, pp. 144-166, March, 1944.

[8] L. C. Peterson, "Space-Charge and Transit-Time Effects on Signal and Noise in Microwave Tetrodes," *Proc. I.R.E.*, Vol. 35, pp. 1264-1272, November, 1947.

** Reported at the I.R.E. Electron Devices Conference, University of New Hampshire, June, 1951.

[9] First Quarterly Report, Signal Corps Contract No. DA36-039-sc-5548, RCA Laboratories Division, August 20, 1951.

‡ Reported at the I.R.E. Conference on Electron Tube Research, Ottawa, Canada, June, 1952.

[10] Fourth Quarterly Report, Signal Corps Contract No. DA-36-039-sc-5548, RCA Laboratories Division, April 30, 1952.

[11] F. N. H. Robinson and R. Kompfner, "Noise in Traveling-Wave Tubes," *Proc. I.R.E.*, Vol. 39, pp. 918-926, August, 1951.

[12] D. A. Watkins, "Noise Reduction in Beam-Type Amplifiers," *Proc. I.R.E.*, Vol. 40, pp. 65-70, January, 1952.

Theoretical and Design Considerations

Theoretical Basis

In the model of Rack,[6] Llewellyn and Peterson,[7,8] which was used by Pierce to compute the noise factor of a traveling-wave tube, it is assumed that the electron beam leaves the potential minimum in front of the cathode perfectly "smooth", i.e., without current fluctuations but with random velocity. Furthermore, the actual multivalued initial velocity fluctuation across the beam is replaced by a single-valued velocity with the same root-mean-square value. The beam, therefore, can be thought of as emerging velocity modulated from the space-charge cloud in front of the cathode. The accelerated, and later drifting, electrons will bunch and debunch periodically along the beam, in accordance with klystron theory.[13,14]

Some justification for the applicability of this model was later obtained from results of noise measurements with a cavity probe sliding along the beam. Such studies were made by Cutler and Quate,[15] L. D. Smullin,[16] and by the author.[10] As predicted by the model, a standing-wavelike pattern of the noise current versus drift length was found. The maximum value of the noise current agreed closely with the theory. The noise minimum, however, instead of being zero was found to be finite. Several theories have been proposed to account for this finite minimum noise. They indicate that several causes may be responsible simultaneously, but little is known about their individual weights.

Assuming that the simplified model holds, the noise factor of a traveling-wave tube has been obtained by different workers in similar form:[5,12,17]

$$F = 1 + \frac{1}{2}(4 - \pi)\frac{T_c}{T}\frac{r}{C} f(QC, d, \delta z), \qquad (1)$$

where T_c = cathode temperature in degrees Kelvin,

[13] W. C. Hahn, "Small Signal Theory of Velocity-Modulated Electron Beams," *G. E. Rev.*, Vol. 42, pp. 258-270, June, 1939.

[14] S. Ramo, "Space Charge and Field Waves in an Electron Beam," *Phys. Rev.*, Vol. 56, pp. 276-283, August, 1939.

[15] C. C. Cutler and C. F. Quate, "Experimental Verification of Space-Charge and Transit-Time Reduction of Noise in Electron Beams," *Phys. Rev.*, Vol. 80, pp. 875-878, December 1, 1950.

[16] L. D. Smullin and H. A. Haus, Quarterly Progress Report, Contract No. DA36-039-sc-100, MIT, Research Laboratory of Electronics, January 15, 1952; p. 36.

[17] L. D. Smullin, "Shot Noise in Beam Type Traveling-Wave Amplifiers," PR-No. 142, Research Laboratory of Electronics, MIT, October 24, 1949.

T = room temperature in degrees Kelvin,

C = gain parameter,

$$r \equiv \overline{v_m^2}/\overline{v_a^2}, \tag{2}$$

and v_m and v_a are respectively the amplitudes of the maximum velocity fluctuation in the beam and of the initial fluctuation at the cathode. r will be referred to as the noise-reduction factor of the gun. Pierce's[5] notation is used as far as possible throughout this paper. (See in particular his Chapter X.)

Watkins[12] has evaluated the function

$$f = |(\delta_2 + \delta_3)\cos \delta z - (\delta_2\delta_3 - 4QC)(4QC)^{-1/2}\sin \delta z|^2 \tag{3}$$

for practical values of the space-charge factor, QC, the attenuation factor, d, and the distance δz (in plasma wave lengths) from a noise-current minimum to the beginning of the helix. His curves show that f increases with the circuit-loss parameter d, but is little affected by increased space charge, QC.

The two important factors which can be varied to make the noise factor small are the gain parameter, C, given by the ratio of the circuit and beam impedances, and the noise-reduction factor, r, of the gun.

This paper deals mainly with the method used to improve the noise-reduction factor of the electron gun. The circuit is a standard helix optimized in its impedance with respect to frequency. The effect of increased circuit impedance, e.g., as obtained in filter helices, on the noise factor will be discussed in a forthcoming paper.

In the following section, the noise-reduction factor is computed for the three-region low-noise gun which is used in the tubes with lowest noise factor.

The Three-Region Gun

Based upon the above simplified beam-noise model, the objective was to find the arrangement of accelerating or decelerating electrodes which would minimize the velocity (or density) fluctuations in the electron beam. The sketch in Figure 2 shows in principle what is referred to as a three-region gun. We intend to compute the noise-reduction factor, $r = \overline{v_d^2}/\overline{v_a^2}$, at point d for this arrangement under the assumptions that the one-dimensional Llewellyn–Peterson equations hold and that the current fluctuations at d are zero.

The one-dimensional theory gives useful answers if the beam diameter is large compared with the electronic wave length in the beam. This condition is approximately fulfilled in the low-voltage

regions *a-b* and *b-c*. It does not hold exactly in the space *c-d*, which turns out to be the main accelerating region. However, since *c-d* represents a very small transit angle, the one-dimensional model can be used for an approximate study in this region too.

For a "general-drift region" with a transit angle $\theta > 3\pi$ and with the electrodes n and $(n-1)$ short-circuited for alternating current, the Llewellyn-Peterson equations reduce to†

$$\begin{aligned} q_n &= E^* q_{n-1} + F^* v_{n-1}, \\ v_n &= H^* q_{n-1} + G^* v_{n-1}, \end{aligned} \tag{4}$$

or, in matrix form,

$$\begin{pmatrix} q \\ v \end{pmatrix} = (\mathrm{M}_n) \begin{pmatrix} q_{n-1} \\ v_{n-1} \end{pmatrix}, \tag{5}$$

$$(M_n) \equiv \begin{pmatrix} E^* & F^* \\ H^* & G^* \end{pmatrix} = \begin{bmatrix} 1 - \zeta_n \left(1 + \dfrac{u_{n-1}}{u_n} \right) & j\, G_n' \\ \dfrac{j}{G_n'} \zeta_n (1 - \zeta_n) & \dfrac{u_{n-1}}{u_n} - \zeta_n \left(1 - \dfrac{u_{n-1}}{u_n} \right) \end{bmatrix}, \tag{6}$$

$$G_n' \equiv \theta_n I_D / u_n. \tag{7}$$

Multiplying the matrices of the different drift regions yields, for the three-region gun,

$$\begin{pmatrix} q_d \\ v_d \end{pmatrix} = (M_b)\,(M_c)\,(M_d) \begin{pmatrix} q_a \\ v_a \end{pmatrix}. \tag{8}$$

This operation will be carried out step by step. Assuming space-charge-limited emission with $q_a \equiv 0$, the noise current and velocity fluctuations at the first anode, *b*, become a function of the initial velocity fluctuation only:

$$\begin{aligned} q_b &= j\, G_b' v_a \exp.\ (-j\theta_b), \\ v_b &= -\, v_a \exp.\ (-j\theta_b). \end{aligned} \tag{9}$$

Similarly, one obtains for the two-region gun, *a-c*, in Figure 1,

† The notation is that of Reference 7.

$$q_c = j\, G_b'\, \bar{A}\, v_a,$$
$$v_c = -\bar{B}\, v_a, \tag{10}$$

with

$$\bar{A} = 1 - \zeta_c \left(1 + \frac{u_b}{u_c}\right) - \frac{\theta_c}{\theta_b}\frac{u_b}{u_c}, \tag{11}$$

$$\bar{B} = \frac{\theta_b}{\theta_c}\left(1 + \frac{u_b}{u_c}\right)\left(1 + \frac{u_c}{u_b}\right)\zeta_c\,(1 - \zeta_c) + \frac{u_b}{u_c} - \zeta_c\left(1 + \frac{u_b}{u_c}\right). \tag{12}$$

The common phase angle exp. $(-j\theta_b - j\theta_c)$ is omitted.

Figure 1 shows the noise-reduction factor,

$$r = |v_c/v_a|^2 = |\bar{B}|^2, \tag{13}$$

and the relative drift-region length, l_c/l_b, as functions of the relative voltage, V_c/V_b, for the special case $q_c = 0$.

It can be seen, furthermore, that in this case the direct current, I_D, is always less than the maximum current that can pass through the region *b-c*, i.e.,

$$I_D/I_{\max} = \frac{(l_c/l_b)^2}{(1 + \sqrt{V_c/V_b})^3} < 1. \tag{14}$$

The best noise reduction obtainable from a two-region gun under this condition is about $r = 0.5$.

For the three-region gun, finally, Equation (4) yields

$$q_d = \bar{C}\, q_c + j\, G_d'\, v_c,$$
$$v_d = (j\, \bar{D}/G_d')\, q_c + \bar{E}\, v_c, \tag{15}$$

where

$$\bar{C} = 1 - \zeta_d\,(1 + u_c/u_d), \tag{16}$$

$$\bar{D} = (1 + u_c/u_d)^2\, \zeta_d\,(1 - \zeta_d), \tag{17}$$

$$\bar{E} = u_c/u_d - \zeta_d\,(1 + u_c/u_d). \tag{18}$$

The noise-reduction factor will be computed for the special case $q_d = 0$,

for which

$$\bar{B}/\bar{A} = \bar{C}\, u_a\theta_b/u_b\theta_a, \tag{19}$$

and

$$r \equiv |v_d/v_a|^2 = |\bar{B}\ (\bar{D}/\bar{C} + \bar{E})\,|^2. \tag{20}$$

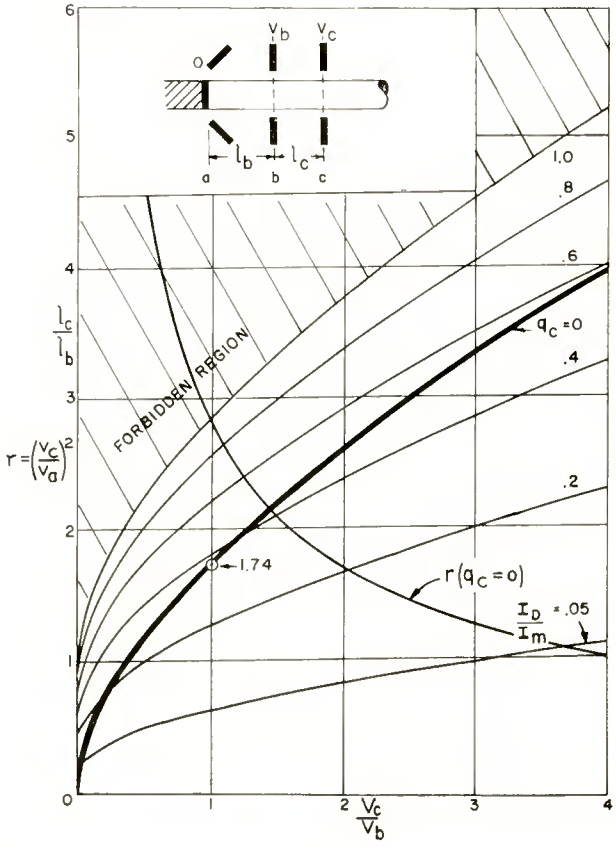

Fig. 1—Two-region gun: Relative drift-region length, l_c/l_b, as a function of the relative voltage, V_c/V_b, for the case $q_c = 0$; for several values of current saturation I_D/I_m.
Noise-reduction factor $r = |v_c/v_a|^2$ for $q_c = 0$.

This transforms into

$$r = \left| \bar{B}\, \frac{u_c/u_d}{1 - \zeta_d\ (1 + u_c/u_d)} \right|^2. \tag{21}$$

In Appendix I, r is evaluated as a function of the three design parameters

$$l_c/l_b, \quad V_c/V_b = (u_c/u_b)^2, \quad V_d/V_b = (u_d/u_b)^2. \tag{22}$$

rV_d/V_b is plotted in Figure 2 for $u_d/u_b = 20$. It is seen that the shorter the second drift region, l_c, with respect to the first diode space, l_b, the better the noise reduction. Relative optima occur under the condition

$$l_d = 0 \quad \text{or} \quad q_d = 0 = q_c. \tag{23}$$

The theoretically optimum case $l_c/l_b = 0$, with $r\ V_d/V_b = 1$, cannot be attained in practice. It is not possible to reduce electrode spacings below a minimum, $l_{\min}$, which is about one beam diameter. There exists, therefore, the limiting condition

$$l_b \geqq l_{\min} \leqq l_c. \tag{24}$$

Any decrease of l_c/l_b below unity results in an increase of l_b, which means an increase of V_b with the current $I_0 \propto V_b^{3/2}/l_b^2$ held constant.

Therefore, r will be larger by a factor $(l_b/l_c)^{3/4}$ than the value of Figure 2 for $l_c/l_b < 1$, i.e., the optimum noise reduction is found under the condition

$$l_c/l_b = 1, \quad V_c/V_b = 0.38, \quad \text{with} \quad r\ V_d/V_b = 2.05.$$

The case of a drift space with equal electrode potentials is less favorable:

$$V_c/V_b = 1, \quad l_c/l_b = 1.7, \quad \text{with} \quad r\ V_d/V_b = 2.7.$$

These two cases of three-region guns with infinitely extended beam are shown in Figure 3a as dashed lines.

Comparison with "Multivelocity-Jump" Guns

Watkins[12] considered low-noise guns consisting of a succession of colinear constant-potential drift tubes separated by short accelerating or decelerating gaps. For a beam in a cylindrical drift tube of length L, the matrix of Equation (6) becomes

$$(M_n) = \begin{pmatrix} \cos\phi & j\,G_n \sin\phi \\ j \sin\phi/G_n & \cos\phi \end{pmatrix}, \tag{25}$$

where

$$G_n \equiv \frac{\omega}{\omega_{pn}} \frac{I_D}{u_n}, \tag{26}$$

$\omega_p \equiv p\,\omega_{p\infty}$ = actual plasma frequency of finite beam,

$\omega_{p\infty}$ = plasma frequency of extended beam,

p = plasma frequency reduction factor.

G_n represents a sort of admittance for the beam surrounded by a cylin-

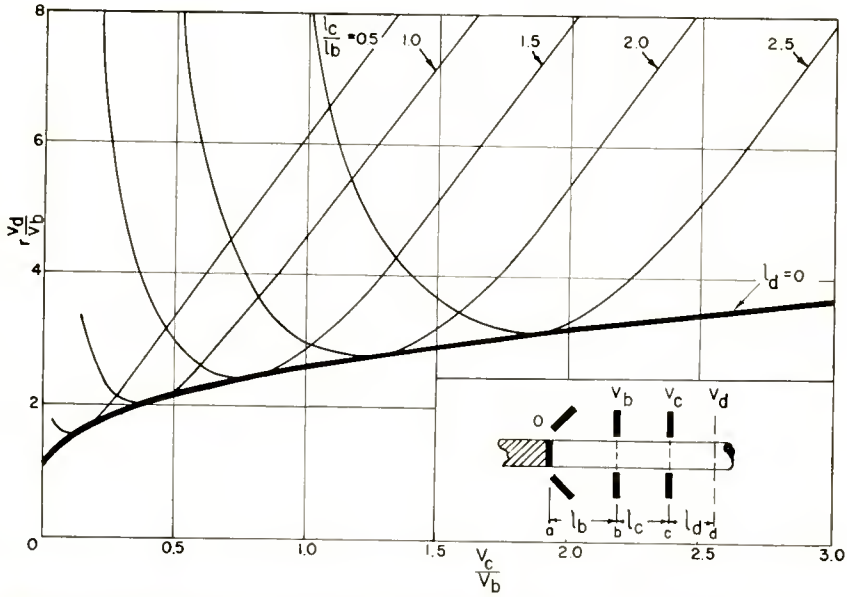

Fig. 2—Three region gun: Noise-reduction factor $r = |v_d/v_a|^2$ as a function of the relative voltage, V_c/V_b, for the case $q_d = 0$; for several relative drift-space lengths, l_c/l_d.
Relative optima are obtained for $l_d = 0$.

drical metal boundary, as does G_n' for the infinite beam crossing the space between two plane-parallel electrodes.

The drift-gap arrangement analogous to the three-region gun with $V_b = V_c$ is shown in Figure 3a. It may be called a "single-velocity-jump" gun. Its noise-reduction factor,

$$r = (1 + 2p^2)\ V_1/V_2, \tag{27}$$

is plotted for several beam diameters at 3000 megacycles operating frequency. It is assumed that the diameter of the cylindrical shield

is at least twice the beam diameter, so that the influence of the shield on the plasma frequency, ω_p, or on p is negligible.

Comparison between the noise-reduction factor of the plane-parallel-electrode three-region gun with radially extended beam and $V_b = V_c$, and the single-jump gun with $2s = \infty$ (Figure 3a) shows that there is practically no difference. Reduction of the beam diameter, however, results in some reduction of r. For example, at $V_1 = 20$ volts, $r = 0.12$ for the extended beam and $r = 0.091$ for a 0.025-inch diameter beam.

Watkins[12] proposed to cascade accelerating and decelerating gaps with intermediate drift tubes. For comparison, the noise reduction factor of a "double-velocity-jump" gun,

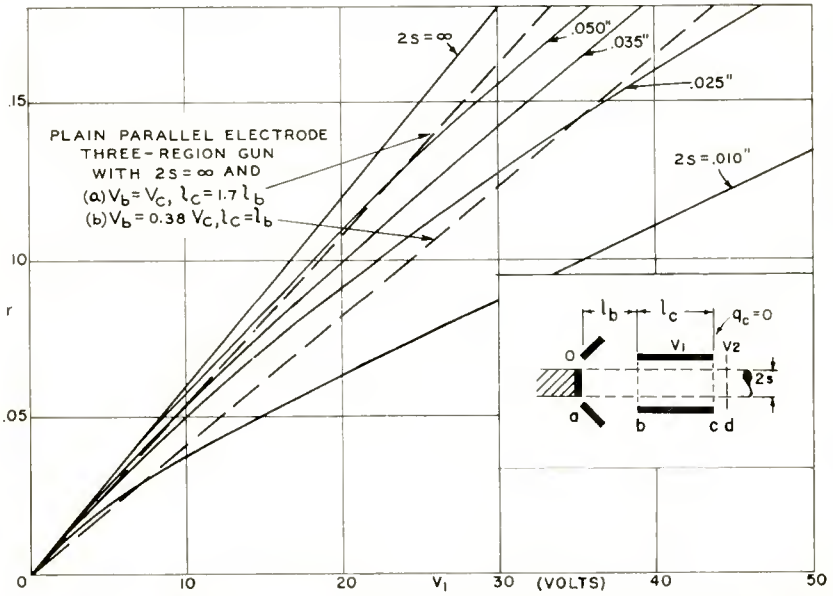

Fig. 3a—Single-jump gun with parallel electron flow: Noise-reduction factor $r = |v_d/v_a|^2$ versus first drift-tube potential V_1, for several beam diameters 2s, frequency $f = 3000$ megacycles and $V_2 = 500$ volts. The factor r is also plotted for a three-region gun (a) with $l_c = l_b$ and (b) with $V_c = V_b$ assuming infinitely extended beam.

$$r = |v_f/v_a|^2 = (1 + 2p^2)\left(\frac{V_2}{V_1}\right)^{1/2}\left(\frac{p_2}{p_1}\right)^2\left(\frac{V_2}{V_3}\right), \qquad (28)$$

is plotted in Figure 4 as a function of the two drift-tube voltages for different beam diameters. It is seen that this type of gun does not give a better noise reduction than a single-jump gun with small beam diameter (e.g., 0.010 inch) unless a very small voltage V_2 is used. Experimentally it seems improbable that $V_2 < 30$ volts can be realized.

Further cascading of gaps and drift spaces, resulting in multi-velocity-jump guns, indicates increasingly better noise reduction when computed for the simplified model where the periodic noise-current minima in the beam go to zero. In the actual beam, however, this condition is not fulfilled; the noise current minima along the beam are finite instead of zero. This seems to indicate the presence of two or more pairs of electron waves which are:

(a) uncorrelated and have the same propagation constants, or
(b) correlated and have different propagation constants, or
(c) uncorrelated and have different propagation constants.

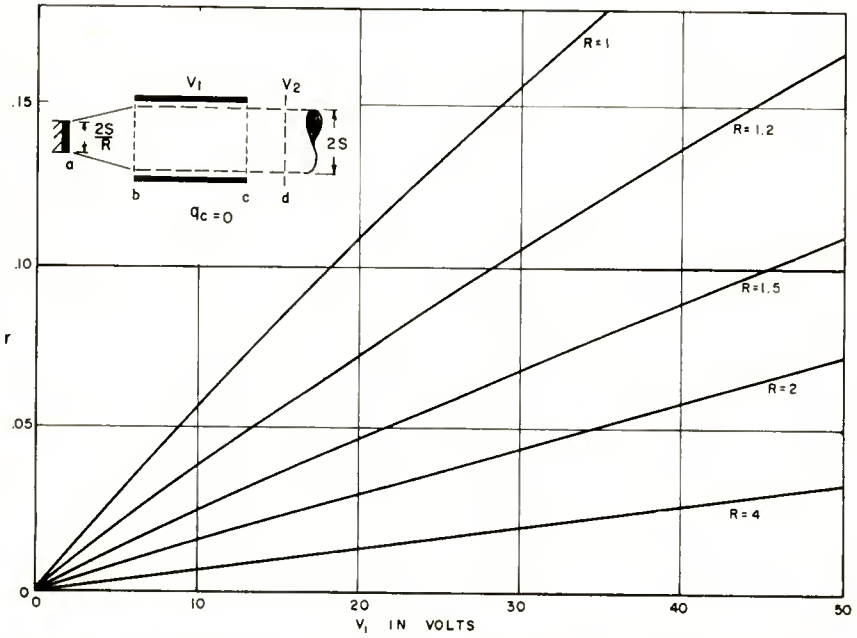

Fig. 3b—Single-jump gun with divergent electron flow: Noise-reduction factor $r = |v_d/v_o|^2$ versus first drift-tube potential V_1, for various beam diameter to cathode diameter ratios $R = 2s/2s_o$ where $2s = .050$ inch, $f = 3000$ megacycles and $V_2 = 500$ volts.

It can be shown that in any of these cases there is only a limited noise reduction possible with schemes of the multiple-velocity-jump type. Experimentally, it has been found that the three-region gun is equally or more effective in noise reduction than either a double-jump or a triple-jump gun. This may indicate that a three-region gun is able to provide the maximum possible noise reduction for beams with the noise minima presently obtainable under best conditions. If it should be possible in the future to design beams with a higher ratio

between maximum- and minimum-noise current, multiple-jump guns may become practical.

Design of a Three-Region Gun

The theoretical gun study indicated that:

1. The first anode, *b*, should be at as low a potential as possible, i.e., it should be located as close to the cathode as is practical, the desideratum being maximum perveance.
2. The second anode, *c*, should be spaced 1 to 1.7 times the cathode–anode distance, l_a, away from the first anode.
3. The third anode should be at helix potential and close to the second anode.

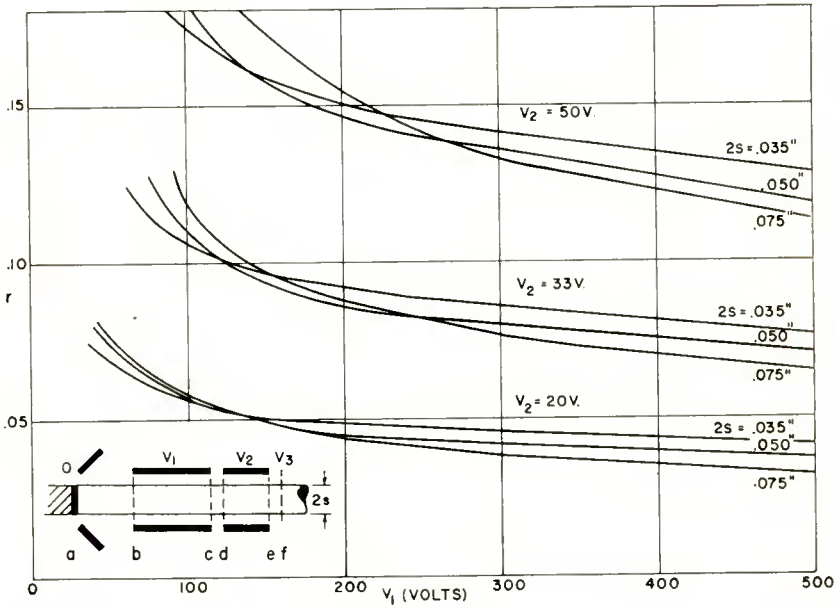

Fig. 4—Double-jump gun with parallel electron flow: Noise-reduction factor $r = |v_1/v_a|^2$ versus first and second drift-tube potentials for various beam diameters, $f = 3000$ megacycles and $V_3 = 500$ volts.

To satisfy the first condition and, in addition, to make the beam-current control independent of the first-anode voltage, a rather unconventional gun was designed (Figure 5) in which the cathode protrudes into the space between a negative shield and the anode. The direct-current potential distribution through the gun for optimum noise reduction is shown in Figure 6. By varying the shield potential, the perveance of the gun with, e.g., a .025-inch cathode, can be continuously changed from 0 to 2.5×10^{-6} $A/V^{3/2}$, as seen from the measured curves

in Figure 7. For larger cathode areas the perveance is proportionally higher.

At higher shield potentials than those corresponding to parallel flow, the beam diverges from the cathode. Its maximum diameter, however, is limited by the axial magnetic field.

Empirically, it was found that a distance ratio $l_c/l_b = 2$ was preferable to a smaller value. The same holds for l_d/l_b. The reason for this

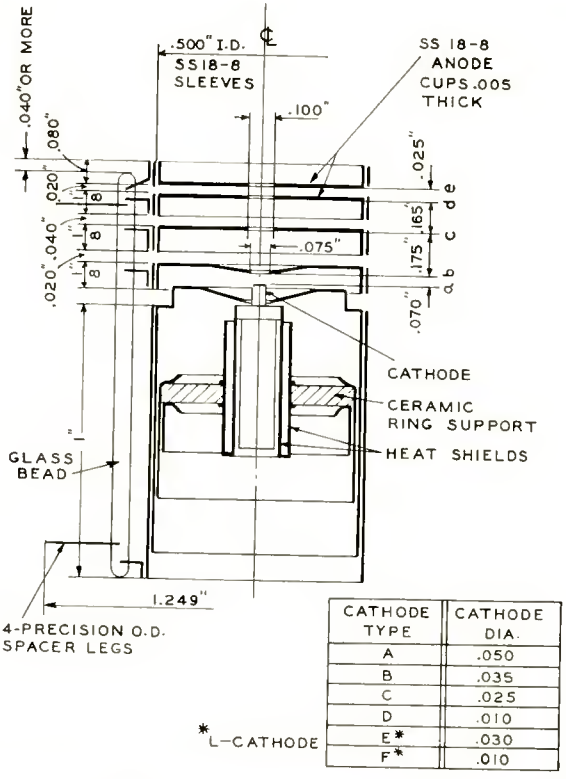

CATHODE TYPE	CATHODE DIA.
A	.050
B	.035
C	.025
D	.010
E*	.030
F*	.010

Fig. 5—Three-region low-noise gun construction: The most important feature of this gun is its protruding cathode which allows perveance variation of 0 to 2.5 $\times$ 10^{-6} $A/V^{3/2}$ (see Figure 7).

may be the reduction of the nonuniformity across the gradient field *c-d-e*. For the same reason, all the anode apertures were made large compared with the beam diameter.

Divergent Electron Flow

The shape of the beam in the three-region gun has been computed for the conditions present at optimum noise reduction (see Figure 7)

for the case in which the gun is immersed in a parallel magnetic field of 500 gausses. The result is drawn to scale in Figure 6. The beam diverges from the cathode to a maximum diameter of about 1½ times the cathode diameter $2s_0$, then oscillates around an average diameter $2s$, such that the expansion ratio $R = s/s_0 = 1.2$.

Unpublished studies of C. F. Quate,* H. E. Rowe,* and S. Bloom**

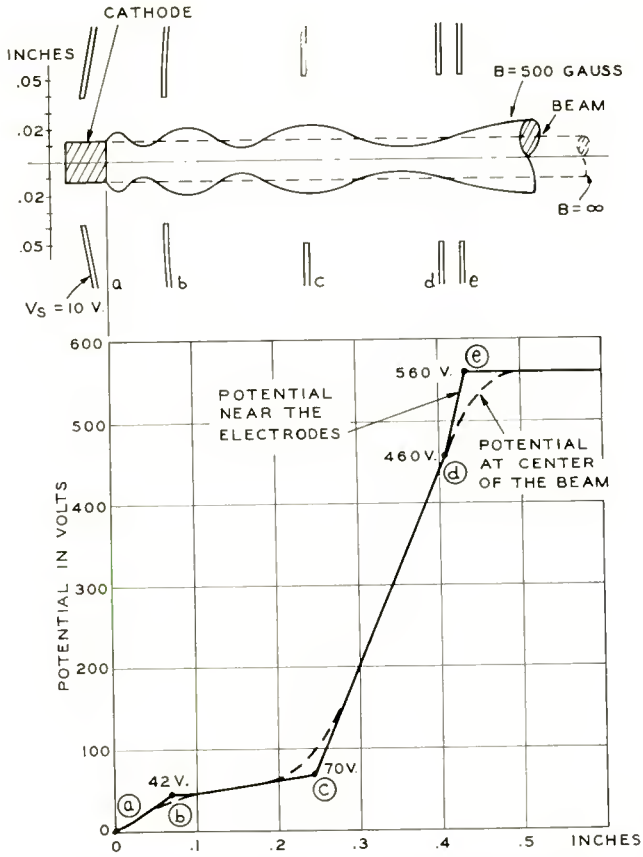

Fig. 6—Potential distribution along the axes of the gun of Figure 5 under operating conditions for lowest noise factor.

indicate that expanding the beam between cathode and anode reduces the noise fluctuations in the beam over that obtained with parallel electron flow.

The three-region gun model investigated by Bloom approximates

* Papers presented at the I.R.E. Conference on Electron Tube Research, Ottawa, Canada, June, 1952.

** RCA Laboratories Division, Princeton, N. J.

the actual electron flow by considering a divergent flow in the first region, *a-b*. The noise-reduction factor in the case of a final beam diameter of .050 inch is plotted in Figure 3b. The manner of deriving this result is outlined in Appendix II.

Comparison of Figures 3a and 3b shows that an expansion of $R = 1.2$ reduces the noise in a beam of final diameter .050 inch, with $V_1 = 40$ volts, from .20 to .137 (or 1.6 decibels).

There is experimental evidence that additional noise reduction may be actually obtained from the gun of Figure 5.

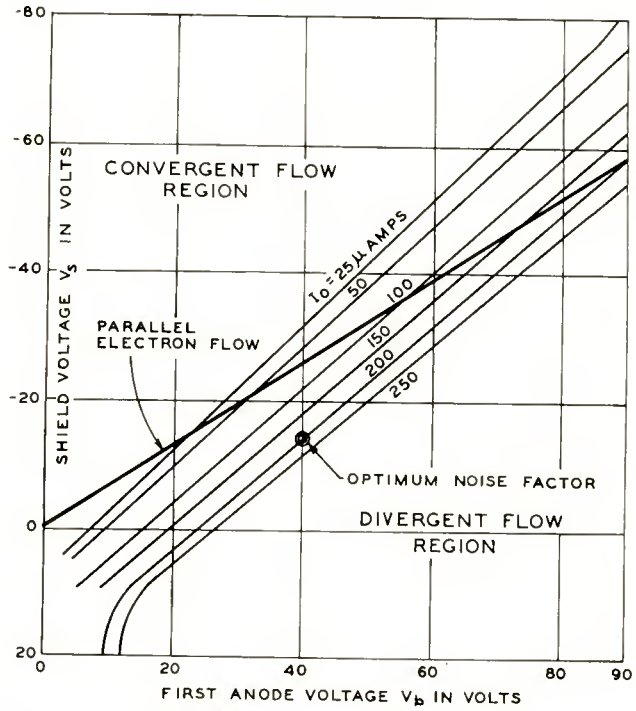

Fig. 7—Beam current obtained from the gun of Figure 5 as a function of first-anode potential, V_b, and shield potential, $-V_s$. Under optimum operating conditions, the gun produces a divergent-flow beam.

The Circuit

The principal idea in designing the helix circuit was to obtain maximum gain from the amplifier in the neighborhood of the operating frequency of 3000 megacycles. Use of Pierce's data[5] yields the following optimum helix design specifications:

[5] J. R. Pierce, *op. cit.*, p. 29, Figure 3.6.

$b/a = 0.6$		$\gamma a = 1.75$		$f = 3000$ megacycles	
#	2a (inches)	Outside diameter (inches)	Wire diameter (inches)	V_0 (volts)	Turns per inch in quartz envelope
I	.080	.085	.005	335	72
II	.103	.110	.007	560	56
III	.138	.150	.012	1000	—

For all measurements quoted in this paper, a 9½-inch long helix #II was used (Figure 8). It was made of silver-plated tungsten wire and supported in a precision quartz tubing. The optimum positioning

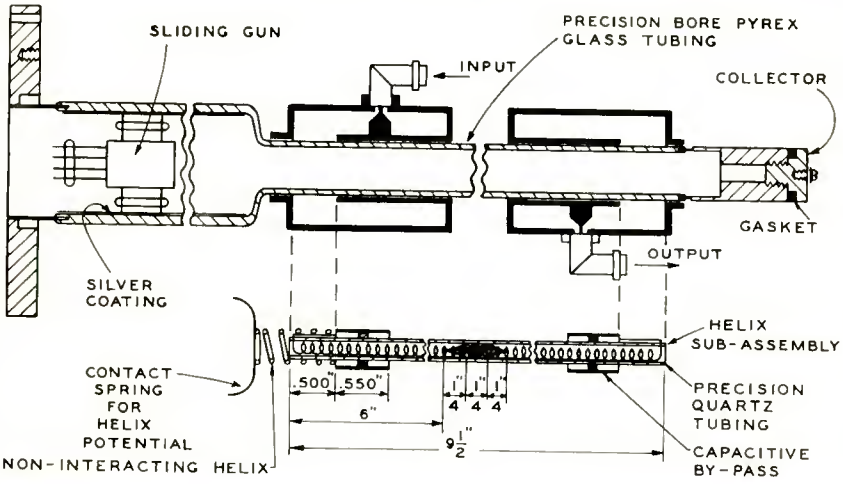

Fig. 8—Demountable traveling-wave amplifier tube: The helix assembly is shown outside of the precision glass envelope. The gun can be moved in the precision bulb under operation.

of the ¾-inch long attenuator from the standpoints of noise factor and gain was found to be 6 inches from the beginning of the helix. It consisted of a tapered aquadag strip painted on a dielectric film spread between the turns of the helix. From the specifications, one computes[5] for this helix: $\gamma a = 1.8$, $N = 53$, $K_x = 130$ ohms, $Q_x = 5$, $d = 0.1$.

The wide-band matching transformer developed to connect the helix with the coaxial input and output lines is shown in Figure 8. It consists of a coaxial cavity with a capacitive gap into which the helix antenna is introduced. The antenna is folded back and connected to

[5] J. R. Pierce, *op. cit.*, p. 252.

a capacitive bypass sleeve. This arrangement reduces the total circuit length to the active helix length. The direct-current potential is applied through a noninteracting choke helix.

Experimental Results

The following experiments were made with the demountable traveling-wave tube of Figure 8. The tube was continuously pumped and the gun could be adjusted in axial position with respect to the helix.

The net gain of the amplifier as a function of beam current did not vary much when different cathode diameters were tested. The most successful experiments were made with 0.025-inch diameter cathodes. The net gain which was measured for the gun type C of Figure 5 immersed in a 600-gauss focusing field is

$$G \doteq 5 \times (I_0{}^{\mu A})^{1/3} - 16.5 \text{ decibels.} \tag{29}$$

This expression holds for currents I_0 between 35 and 350 microamperes. The distributed loss was 7.5 decibels, the center loss 18.5 decibels, adding up to a total cold insertion loss of 26 decibels. The theoretical gain[5] agrees well with Equation (29).

In the following figures, the dependence of the measured noise factor of this tube upon various parameters is shown. The measurements were made with a gas-discharge noise source using the method described earlier.[18] The relative average error of measurement is smaller than ± 0.1 decibel, the absolute calibration is estimated to be within ± 0.5 decibel. In Figures 9 and 10, the noise factor, F, is plotted for two types of guns (Figure 5): type C with a 0.025-inch diameter oxide cathode ($T_c = 840°C$), and type E with a 0.030-inch diameter L-cathode ($T_c = 1140°C$).** Figure 9 shows how F varies with the first-anode potential, V_b, the current being held constant by suitably changing the shield voltage, $-V_s$. V_c is adjusted for lowest noise factor while the drift length, l_0, between anode e and helix is kept constant. Empirically, the relationship

$$V_b \times V_c \doteq V_{bc}{}^2 \tag{30}$$

was found to hold closely. V_{bc} represents the case for which $V_b = V_c$. Computation of the noise components v and q for this case, under the

[18] R. W. Peter, "Direct Reading Noise-Factor Measuring Systems," *RCA Review*, Vol. 12, p. 269, June, 1951.

** Actually, this cathode was of the "impregnated" variety wherein the Barium alloy is mixed and sintered together with the tungsten powder. This cathode was supplied by Philips Laboratories.

assumption of parallel flow at an average diameter of 0.030 inch [Equation (10)], yields $q = 0$ in the region between c and e (Figure 6) in agreement with theory.

Figure 10a indicates the effect of changing the transit angle between b and c by varying the voltage V_c. In Figure 10b, the gun position was varied to change the drift length l_0. The plasma wave length, λ_p, for the beam obtained with type-C gun (see Figure 5), with an assumed average diameter of 0.030 inch, is computed to be 11.5 inches, in agreement with the measured value of $\lambda_p/4 = 2\frac{3}{4}$ inches. The optimum drift length, $l_0 = 2.0$ inches, corresponding to a distance of about $\lambda_p/6$ from the $q = 0$ point (between c and e), does not, however, seem to agree with theory[12] which predicts a much larger angle. For $T_c/T = 3.8$, $C = .018$, $f = 0.32$,[12] the noise factor [Equation (1)] becomes $F = 29r$.

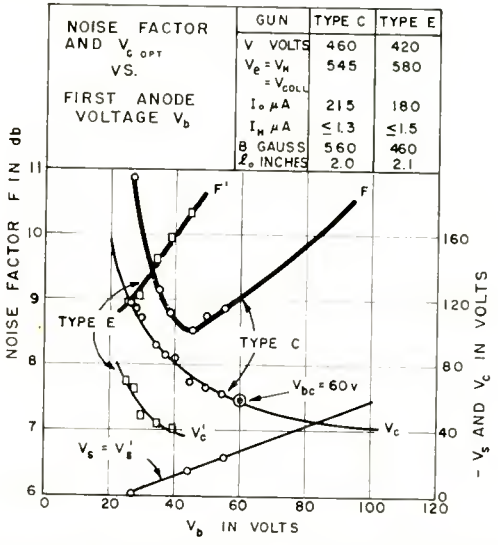

Fig. 9—Noise factors measured with a type C and a type E gun (Figure 5) as a function of the first-anode potential, V_b. The current is kept constant by varying the shield potential, $-V_s$. V_c is adjusted for lowest noise factor.

For an average beam diameter $2s = .030$ inch, $V_1 = 45$ volts and $V_2 = 545$ volts, and Figure 3a yields $r = 0.175$ and $F = 7.8$ decibels. Taking account of the beam expansion of $R = 1.2$ by using the same reduction as obtained for $2s = 0.50$ inch (Figure 3b), one would get $r = .12$ and $F = 6.5$ decibels. The difference between the actual measured lowest noise factor of $F = 8.5$ decibels and the theoretical figures must be attributed to some of the three causes discussed in the comparison with multivelocity-jump guns.

In all measurements of Figures 9 and 10, the gain stays practically constant with constant beam current. The intercepted current is always considerably below 1 per cent, of which the major part is believed to be collected at the end of the helix. It was observed, furthermore, that the optimum drift length, l_0, varies with the magnetic focusing field. Referring to the "gun-type E" curve in Figure 10b, it was found that the

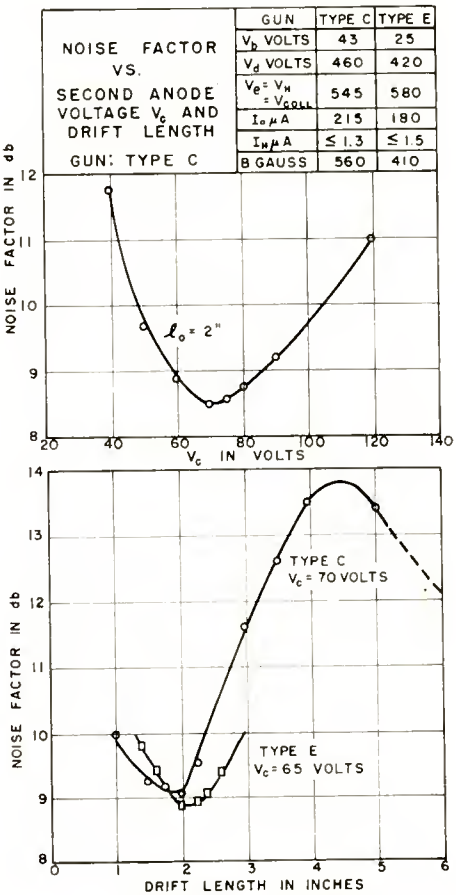

Fig. 10—Noise factor measured with types C and E guns: (a) versus second-anode potential, V_c, at fixed gun position; (b) versus the drift length between last anode and helix beginning.

noise-factor minimum occurred at $l_0 = 2.2$ inches for 340 gausses, but at $l_0 = 1.75$ inches for 480 gausses. This effect is to be expected as the plasma wave length becomes shorter if the beam diameter is reduced at constant current.

The measurements of Figures 11 and 12 were made on an earlier

sealed-off tube. Figure 11 shows that the noise factor decreases if the circuit impedance, and therefore C, is increased by moving the beam closer to the helix, in accordance with Equation (1). Figure 12 gives a quantitative picture of the "noise-factor band width" of a broad-band traveling-wave amplifier. F is below 10 decibels over a 400-megacycle frequency band.

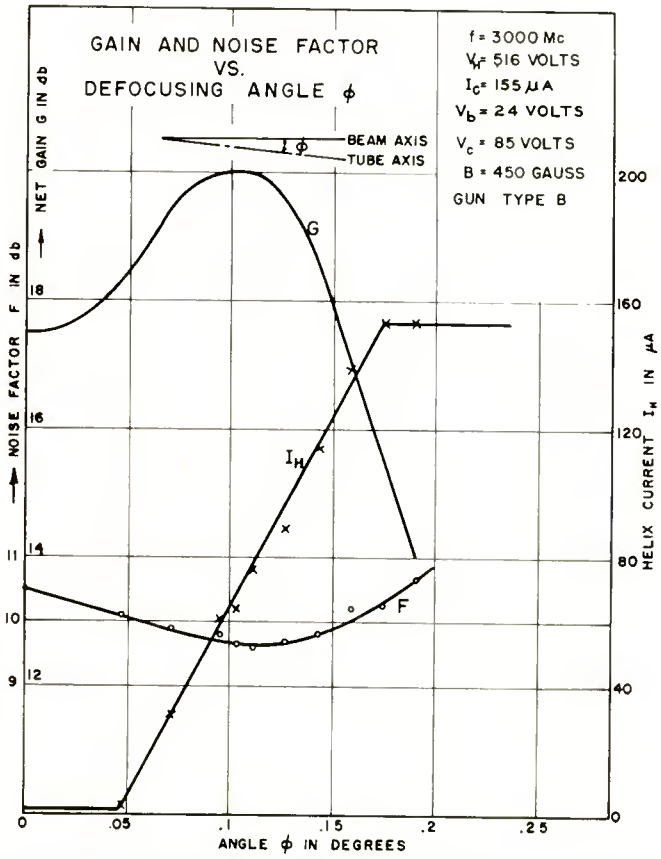

Fig. 11—Noise factor, gain, and helix current as a function of the angle between beam and helix axis.

The importance of a high-perveance gun with divergent flow was apparent when comparative measurements were made on the standard-construction parallel-flow gun of Figure 13 which has the same main dimensions as gun type B of Figure 5. The best noise factors measured with the parallel-flow gun were about 2 decibels higher than the corresponding ones with the divergent-flow gun.

Of a more speculative nature are the results given in Figure 14,

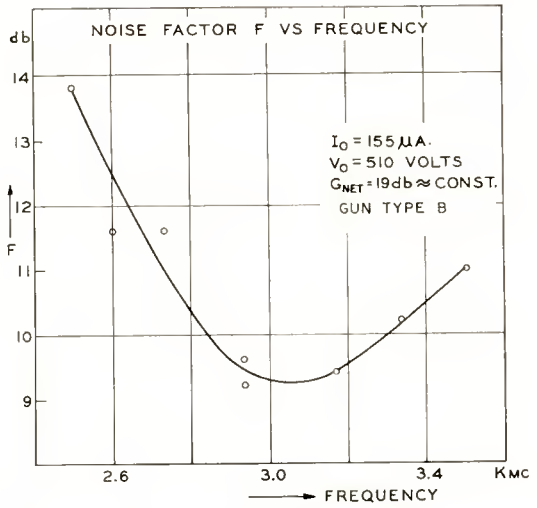

Fig. 12—Noise factor of a broad-band traveling-wave amplifier versus frequency.

wherein are plotted the lowest noise factors observed with approximately the same helix circuit but with different types of guns (Figure 5). The trend strongly indicates the desirability of a point cathode, in agreement with theory (Figures 3a and 3b). In the first experiment

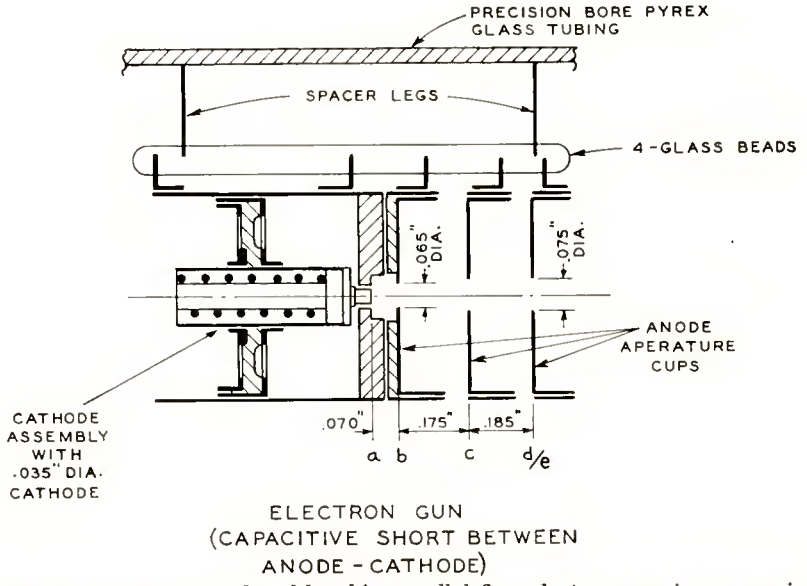

Fig. 13—The beam produced by this parallel-flow electron gun is more noisy than that of gun type B in Figure 5 although both have the same main dimensions.

with a 0.010-inch cathode, oxide coating was used. This is not, however, a sufficiently uniform emitter to insure space-charge-limited emission over the whole surface at current densities in excess of 0.5 ampere per square centimeter. One should not, therefore, expect a better result than that obtained.

It is somewhat surprising to find that the L-cathode point falls on the oxide-cathode line, as its higher operating temperature would lead one to expect a larger noise factor. One may conclude that its greater surface smoothness and uniformity of emission is responsible for this. In this connection, it should be stressed that all quoted experimental

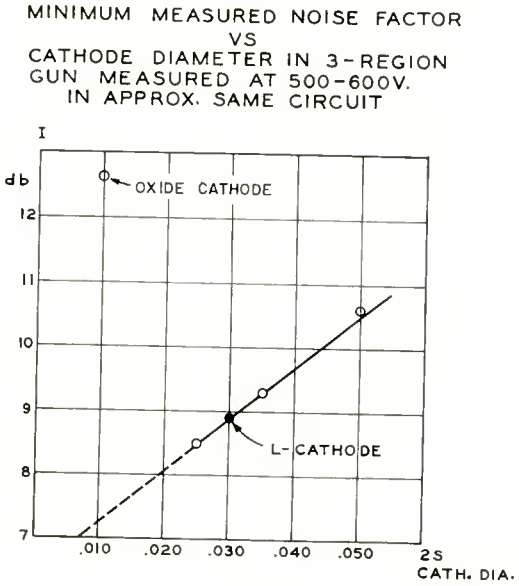

Fig. 14—Lowest noise factors measured with about identical circuits and guns but different cathode diameters.

results were obtained with painted smooth-surface oxide cathodes which were well activated. This is an important point, since the noise factor is very dependent upon the cathode surface quality.

Acknowledgment

The author wishes to thank J. A. Ruetz for his great help in much of the experimental work, and K. R. DeRemer and M. Heald for their contributions in evaluating and computing some of the theoretical results and curves.

Some of the work presented here was done under a Signal Corps contract.

Appendix I

To express Equation (21) as a function of the three variables (22) only, the dependence of ζ_d upon those variables must first be obtained.

The ratio of the transit angle through an arbitrary region in the gun, θ_n, to that through the space-charge-limited first region, θ_b, is[7]

$$\frac{\theta_n}{\theta_b} = \frac{2}{3-\zeta_n}\,\frac{l_n}{l_b}\,\frac{u_b}{u_{n-1}+u_n}. \tag{I-1}$$

Substituting (I-1) into (19) transforms the right side of the equation into

$$\frac{u_d}{u_b}\left(\frac{u_c}{u_b}+\frac{u_d}{u_b}\right)^{-1/2}\zeta_d^{\,-1/2}\left(1-\zeta_d\left(1+\frac{u_c}{u_d}\right)\right), \tag{I-2}$$

and the left side into

$$\frac{(l_b/l_c)\,(1+u_c/u_b)^2\,(\zeta_c/2)\,(3-\zeta_c)\,(1-\zeta_c)+(1+u_c/u_b)^{-1}}{(1+u_b/u_c)^{-1}-\zeta_c-2\,(l_c/l_b)\,(3-\zeta_c)^{-1}\,(1+u_c/u_b)^{-2}}, \tag{I-3}$$

where ζ_c is given by[7]

$$(3/4)\,(3-\zeta_c)\,\zeta_c = I_D/I_m = (l_c/l_b)^2\,(1+u_c/u_b)^{-3}. \tag{I-4}$$

By equating (I-2) and (I-3) one finds ζ_d in the form

$$\zeta_d = (1+u_d/u_c)^{-2}\{1+u_d/u_c+S^2/2-|S|\,(1+u_d/u_c+S^2/4)^{1/2}\}, \tag{I-5}$$

with

$$S = (\bar{B}/\bar{A})\,(u_b/u_d)\,(u_c/u_b+u_d/u_b)^{1/2}. \tag{I-6}$$

Introducing (I-5) into (21) makes r a function solely of the three parameters (22).

[7] L. C. Peterson, *op. cit.*, p. 148.

Appendix II — Evaluation of Noise-Reduction Factor for Divergent-Flow Gun

In a manner similar to that employed by Quate,* Bloom treated the problem of noise propagation in a divergent electron beam by means of a spherical diode mode. Depending on whether the radius s_0 of the cathode is less, equal to, or larger than the anode radius s, divergent, parallel, or convergent flow is present. This model is one-dimensional if uniform excitation over the cathode surface is assumed.

Writing the velocity as

$$v = v_0(r) + v_1(r)\, e^{j\omega t - j\omega \int dr/v_0}, \tag{II-1}$$

and calling, for convenience, $\psi = v_0(r)\, v_1(r)$ where v_0 and v_1 represent the direct current and alternating current velocity, one obtains from the divergence, continuity, and force equations

$$\frac{d^2\psi}{dr^2} + \frac{2}{r}\frac{d\psi}{dr} + \frac{\eta I_0'}{4\pi\epsilon_0 r^2 v_0^3(r)}\psi = 0, \tag{II-2}$$

where I_0' is the total diode current.

Making use of the expression of Langmuir and Compton[19] for $v_0(r)$ in the space-charge-limited spherical diode, Equation (II-2) can be solved by a series method. Since the alternating-current density is related to ψ by

$$q_1 = -\frac{j\omega\epsilon_0}{\eta}\frac{d\psi}{dr}, \tag{II-3}$$

the knowledge of $\psi(R)$ gives the complete solution, where $R = s/s_0$. For a conical beam of semi angle θ, the alternating velocity and current at the anode, b, become

$$\begin{aligned} v_b &= -\frac{\phi(R)}{\alpha^{2/3}(R)}\, v_a, \\ q_b &= \frac{j\omega\epsilon_0}{\eta r_0}\left(\frac{9\eta I_0}{8\pi\epsilon_0 \sin^2\theta/2}\right)^{1/3}\frac{d\phi}{dR}\, v_a, \end{aligned} \tag{II-4}$$

* Paper presented at the I.R.E. Conference on Electron Tube Research, Ottawa, Canada, June 1952.

[19] I. Langmuir and K. T. Compton, "Electrical Discharges in Gases, Part II—Fundamental Phenomena in Electrical Discharges," *Rev. Mod. Phys.*, Vol. 3, pp. 191-257, April, 1931.

where I_0 is the total direct current, $\alpha(R)$ is known, and $\phi(R)$ is proportional to $\psi(R)$.

Equations (II-4) replace in general Equation (9), and become equivalent in the special case $R = 1$. After passing through a drift tube and a velocity jump at the $q_c = 0$ point (Figure 3b), the beam has a noise-reduction factor of

$$\gamma \equiv \left| \frac{v_d}{v_a} \right|^2 = \frac{\phi^2}{\alpha^{4/3}} + \frac{9}{2} p^2 R^2 \alpha^{2/3} \left(\frac{d\phi}{dR} \right)^2. \qquad \text{(II-5)}$$

This is plotted in Figure 3b.

TRANSISTOR OSCILLATORS*

By

Edwin A. Oser†, Richard O. Enders‡, and
Raymond P. Moore, Jr.‡

Summary—*The basic oscillators which utilize current-multiplication transistors are described, and their mode of operation is discussed. A fundamental mathematical criterion for oscillation in these circuits is presented, and the physical significance of current feedback is explained as it applies to their operation. The generation of sinusoidal voltages by tuned-circuit, crystal-controlled, and phase-shift-type oscillators is discussed. In connection with these circuits, means are described for improving their high-frequency operation and for obtaining frequency multiplication. Basic relaxation oscillators are presented. These oscillators may be arranged to be free running or triggered. Their operation is explained by means of the voltage and current wave forms developed at the transistor electrodes. By combining the features of the sine-wave oscillator with those of the relaxation oscillator, self-quenching oscillation, or stabilized frequency division may be obtained.*

Introduction

THIS paper discusses the phenomenon of oscillation which may be associated with a number of crystalline devices, in particular the transistor which is presently the foremost among these devices.

The utilization of solid-state elements as oscillators is not new. For a considerable time, oscillators using crystal rectifiers have been known.[1] These circuits make use of the negative resistance which some crystal rectifiers exhibit under certain operating conditions, particularly near breakdown. A current-multiplication transistor also exhibits negative resistance under certain conditions, and this phenomenon is primarily a function of its current gain, α. Most point-contact-type transistors (having rectifying electrodes), as well as certain other types of transistors, exhibit current gain in which the short-circuit collector current increments (Δi_c) are larger than the corresponding emitter current increments (Δi_e) (Figure 1):

---

* Decimal Classification: R282.12 × R355.911.

† Formerly, Patent Department, RCA Laboratories Division, Camden, N. J. Now with the Hughes Aircraft Company, Culver City, Cal.

‡ Engineering Products Department, RCA Victor Division, Camden, N. J.

[1] V. Gabel, "The Crystal as a Generator and Amplifier," *The Wireless World and Radio Review*, Vol. 15, pp. 2-5, October 1, 1924 and pp. 47-50, October 8, 1924. O. Lossev, "Oscillating Crystals," *The Wireless World and Radio Review*, Vol. 15, pp. 93-96, October 22, 1924. R. S. Ohl, U. S. patent 2,469,568 (filed March 2, 1945).

$$\left.\frac{\Delta i_c}{\Delta i_e}\right|_{E_{cb}} \equiv \alpha > 1.$$

The oscillators to be described here are based on the negative resistance characteristics of those transistors having current multiplication. Since a vacuum tube amplifier does not have a current gain exceeding unity (except for those operated so as to have secondary electron multiplication), this unique characteristic of a transistor permits the design of many unusual circuits.

Transistor oscillators[2] having an external feed-back path providing voltage feedback were described in the literature shortly after the transistor[3] was first disclosed. However, it is not with respect to this type of operation that the transistor exhibits its most unique and useful mode of operation. Rather, due to the negative resistance exhibited by the current multiplication transistor, various oscillators can be designed which do not require voltage feedback.

L–C Sine-Wave Oscillators

Figure 1 shows a conventional equivalent network[4] of a transistor (indicated by the dotted rectangle) and the associated external circuit

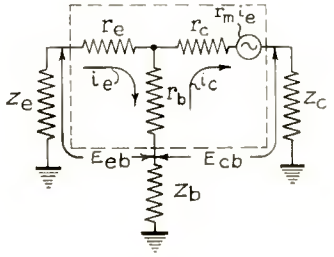

Fig. 1—Equivalent circuit diagram of a transistor.

[2] "The Eclipse of the Radio Tube," *Radio Craft*, Vol. 19, pp. 24-25, September, 1948. C. E. Atkins, "A Crystal that Amplifies," *Rad. and Tel. News*, Vol. 40, p. 39, October, 1948. R. M. Ryder and R. J. Kircher, "Some Circuit Aspects of the Transistor," *Bell Sys. Tech. Jour.*, Vol. 28, pp. 367-400, July, 1949; Figure 26(a). J. Bardeen and W. H. Brattain, U. S. Patents 2,524,035 and 2,586,597 (filed June 17, 1948); Figure 12. "Transistor Circuits," *Cornell-Dubilier Capacitor*, Vol. 15, pp. 3-7, February, 1950; Figure 5.

[3] J. Bardeen and W. H. Brattain "The Transistor, a Semi-Conductor Triode," W. H. Brattain and J. Bardeen, "Nature of the Forward Current in Germanium Point Contacts," and W. Shockley and G. L. Pearson, "Modulation of Conductance of Thin Films of Semi-Conductors by Surface Charges," *Phys. Rev.*, Vol. 74, pp. 230-233, July 15, 1948.

[4] W. M. Webster, E. Eberhard, and L. E. Barton, "Some Novel Circuits for the Three-Terminal Semi-Conductor Amplifier," *RCA Review*, Vol. 10, pp. 5-16, March, 1949; Figure 4.

elements (indicated as impedances). From this equivalent circuit, the following equation may be derived:

$$\frac{Z_c + r_c}{Z_b + r_b} = \frac{r_m - Z_e - r_e}{Z_c + r_c} - 1 + \frac{\Delta}{(Z_b + r_b)(Z_c + r_c)}, \qquad (1)$$

where Δ is the circuit determinant. The condition for oscillation is that $\Delta \leq 0$. Under this condition, Equation (1) may be rewritten as follows in order to clarify the role of the circuit elements:

$$\frac{Z_c + r_c}{Z_b + r_b} \leq \frac{r_m - Z_e - r_e}{Z_c + r_c} - 1. \qquad (2)$$

The symbols used in these equations are indicated in Figure 1. It will be assumed that r_c, r_b, r_e, and r_m are constant over the operating

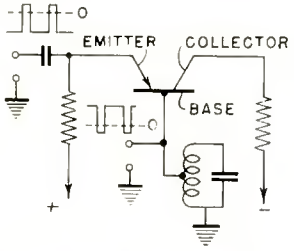

Fig. 2—Sine-wave oscillator (case A).

range to be considered. Accordingly, only the values of the external impedances Z_c, Z_b, and Z_e can be selected at will. Thus, oscillations may be produced by increasing the value of Z_b (case A), by decreasing the value of Z_e (case B), or by decreasing the value of Z_c (case C). By any of these three conditions, Equation (2) may be satisfied. Sine-wave oscillators[5] of the L–C type, corresponding to cases A, B, and C, are illustrated in connection with Figures 2, and 4 through 8.

A tuned circuit oscillator corresponding to case A is shown in Figure 2.[6] A grounded parallel resonant circuit is connected to the

[5] Webster, Eberhard, and Barton, *op. cit.*, Figure 10. "Transistor Beat-Frequency Oscillator and Amplifier," *Electronics*, Vol. 22, pp. 120, 122, November, 1949, and "Transistor et transistron," *La Technique Moderne*, Vol. 42, pp. 220-223, July 1 and 15, 1950, in Figure 7 show, however, a different sine-wave oscillator where a parallel resonant circuit is connected to the collector. H. Heins, "The Germanium Crystal Triode," *The Sylvania Technologist*, Vol. 3, pp. 13-18, January, 1950; Figure 9 (d).

[6] Webster, Eberhard and Barton, *op. cit.*, Figure 10. Ryder and Kircher, *op. cit.*, Figure 26(b). Frank W. Lehan, "Transistor Oscillator for Telemetering," *Electronics*, Vol. 22, pp. 90-91, August, 1949; Figures 2 (c) and 3. "Transistor Circuits," *Cornell-Dubilier Capacitor*, Vol. 15, pp. 3-7, February, 1950; Figure 6. E. Bohr and H. French, "Tubeless Oscillator Covers Audio to 2 Mc," *Radio-Electronics*, Vol. 22, p. 43, June, 1951.

base. In order to facilitate an adjustment of a portion of the total impedance of the resonant circuit to the impedance of the base, the base is connected to an intermediate point of the inductor. With this arrangement, the base impedance Z_b becomes a maximum at the resonant frequency of the tuned circuit. The collector is biased in the reverse direction and the emitter in the forward direction, both with respect to the base as indicated. Both the emitter and the collector may be connected directly to their voltage supplies, but in view of the limited current-carrying capabilities of some transistors, current limiting resistors may be necessary.

Figure 3 illustrates the resistance which appears looking into the base, R_b', as a function of the voltage between emitter and base, E_{eb}, in a regenerative amplifier. Between the ordinate axis ($E_{eb} = 0$) and the dotted line m ($E_{eb} = m$), the internal base resistance, R_b', is negative, and within this range of emitter voltage values, oscillation may take place; to the left of the ordinate axis and to the right of the line m, no oscillation is possible. Consequently, the emitter of the

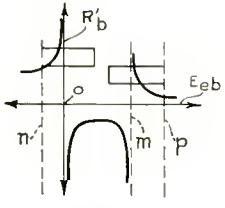

Fig. 3—Base resistance as a function of the emitter-to-base voltage.

circuit of Figure 2 could be biased to a value to the left of the ordinate axis, as shown by dotted line n, to prevent the circuit from oscillating. By applying a positive pulse to the emitter, the circuit will oscillate for the duration of the trigger pulse provided the pulse amplitude is sufficient to carry the voltage E_{eb} to the right of the ordinate axis as shown in Figure 3. The same result may be obtained by applying a negative trigger pulse to the base, as indicated in Figure 2. The circuit of Figure 2 may also be triggered into oscillation by the application of a negative trigger pulse to the collector. This has the same effect as a negative pulse applied to the base, since the collector current increases in response to the negative collector pulse. This results in a larger current through the base impedance which, in turn, drives the base voltage more negative.

The curves of Figure 3 also show that for higher positive values of E_{eb} the internal base resistance R_b' again becomes positive. Hence, by biasing the emitter to a value as shown by the dotted line p, the circuit of Figure 2 will also be normally quiescent. It may be triggered

by the application of a negative trigger pulse to the emitter or by the application to the base or collector of a positive trigger pulse of sufficient amplitude to carry E_{eb} to the left of the line m.

At frequencies of the order of a few hundred kilocycles, the transistor constants are no longer pure resistances, but exhibit reactive components of appreciable magnitude. Therefore, at these higher frequencies a phase shift is developed between the emitter and collector currents. When this phase shift becomes too large, the real component of the collector current which is returned to the emitter may no longer be of sufficient magnitude to sustain oscillation. In order to secure oscillatory operation at these higher frequencies, it will be found necessary to compensate for this phase shift. Perhaps one of the simplest means to this end is that shown in Figure 4, wherein shunt capacitances of a few micromicrofarads each are applied to both the emitter and collector electrodes. Either one of these shunt capacitors will provide a degree of compensation. In this particular oscillator, the maximum oscillation frequency may be increased by a factor of two over that which may be obtained without phase shift

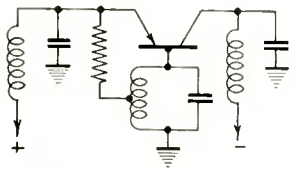

Fig. 4—Sine-wave oscillator suitable for high-frequency operation.

compensation. This manner of compensation is generally applicable to current-feedback oscillators. Regeneration in the circuit of Figure 4 is enhanced by the addition of voltage feedback through the emitter resistor which is tapped onto the oscillator tank circuit.

Oscillators of the type shown in Figure 2 may readily be modified to provide frequency multiplication. A parallel resonant circuit connected to the collector may be tuned to a harmonic of the frequency to which the parallel resonant base circuit is tuned. This arrangement is practical since the collector circuit impedance remains at a relatively low value at the fundamental frequency of oscillation. Such a circuit is shown in Figure 5.

The flexibility of the transistor operating under conditions of current feedback is further illustrated by reference to Figure 6. This circuit operates under the conditions of case B. Here the emitter impedance, Z_e, becomes a minimum at the resonant frequency of the series-tuned circuit. In order to satisfy the condition of Equation

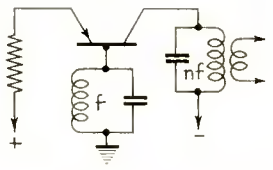

Fig. 5—Sine-wave oscillator arranged as frequency multiplier.

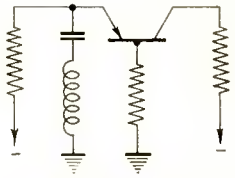

Fig. 6—Sine-wave oscillator (case B).

(2), a resistor is inserted between base and ground. The emitter requires a negative bias voltage in this case to maintain its potential slightly positive with respect to the base; in view of the collector current flowing through the base impedance, a relatively high negative voltage is developed at the base.

Figure 7 illustrates an oscillator which operates under the conditions of case C. The collector impedance, Z_c, is made a minimum at the resonant frequency of the series resonant collector circuit. The oscillator of Figure 8[7] has a series resonant circuit connected directly between emitter and collector and combines the features of cases B and C. A circuit combining the features of all three cases is also feasible.

For the oscillators of Figures 6, 7, and 8, the curves of Figure 3 still represent the internal base resistance, R_b'. These oscillators may again be biased to the left of the ordinate axis of Figure 3 and triggered by the application of a positive pulse to the emitter or by the application of negative pulses to the base or collector. Such a triggered circuit is shown in Figure 8. On the other hand, if the oscillator is biased to the right of line m of Figure 3, it may be triggered into oscillation by applying negative pulses to the emitter or positive pulses to the base or collector. The same result will be obtained by varying any of the external network resistances either mechanically or electronically to bring the circuit into or out of its oscillating range. Preferably, the emitter resistance should be varied since it provides the greatest control.

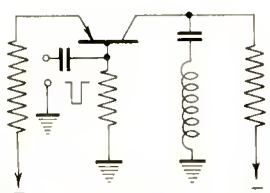

Fig. 7—Sine-wave oscillator (case C).

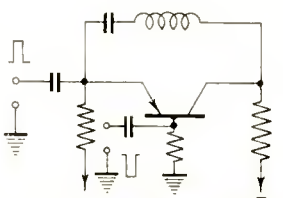

Fig. 8—Sine-wave oscillator (cases B and C).

[7] Ryder and Kircher, *op. cit.*, Figure 26(c).

Frequency stability with respect to variations in the supply voltage may be obtained by operating these circuits from a common bias source. This will be evident from an inspection of Figure 9, which indicates that frequency varies directly with emitter voltage, E_{eb}, and inversely with collector voltage, E_{cb}. These curves, centered at about 500 kilocycles, indicate a frequency change of the order of 10 per cent for changes of collector or emitter current of about 10 per cent. Hence, operation from a common bias source is desirable. On the other hand, the phenomenon indicated in Figure 9 may be used to advantage to obtain frequency modulation of these oscillators. This may be accomplished by varying either the bias voltages or the external resistances in such a manner as to cause variations in the effective emitter or collector voltages.

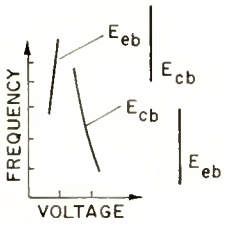

Fig. 9—Operating frequency of sine-wave oscillators as a function of the applied voltages.

The operation of these three types of L–C sine-wave oscillators may also be explained on the basis of the current multiplication of the transistor oscillator network. Reference is again made to the equivalent circuit (Figure 1). Anther form of Equation (1) is

$$\frac{Z_e + r_e}{Z_b + r_b} = \alpha - 1 + \frac{\Delta}{(Z_b + r_b)(Z_b + r_b + Z_c + r_c)},$$

where $$\alpha = \frac{r_m + Z_b + r_b}{Z_e + r_e + Z_b + r_b}.$$

As before, this equation may be more easily understood by rewriting it in the following way in accordance with the condition for oscillation:

$$\alpha \geq 1 + \frac{Z_e + r_e}{Z_b + r_b}. \qquad (3)$$

Consequently, this equation represents a necessary condition for oscilla-

tion. Since Z_e, r_e, Z_b, and r_b are all positive and finite, α must be greater than unity to satisfy Equation (3) and to cause oscillation. In the oscillator of Figure 2, the collector current, i_c, is fed back to the emitter at the resonant frequency of the base circuit; at other frequencies a portion of the collector current is returned to the base through the base impedance which now has a lower value, and hence oscillations cannot be maintained. As is shown in Figure 1, i_e and i_c flow in opposite directions through Z_b. With a series resonant circuit connected to the emitter (Figure 6) or to the collector (Figure 7), a low-impedance path is provided at the resonant frequency of the series resonant circuit between collector and emitter for feeding back a portion of the collector current sufficient to sustain oscillation. The relatively large external resistance in the base circuit prevents a substantial portion of the collector current from returning to the base. In the oscillator of Figure 8 there is, of course, a direct low-impedance path for i_c between collector and emitter.

The field of application for these tuned-circuit oscillators is generally not unlike that to which their vacuum tube counterpart is applied. Of course, these transistor oscillators must be utilized in accordance with their frequency range and power limitations.

Crystal-Controlled Oscillators

The transistor oscillator is readily adapted to crystal frequency control. There are, however, certain necessary operating conditions which must be recognized and taken into account. This oscillator type is especially valuable since the previously discussed oscillators tend to be frequency sensitive with respect to the applied voltages. The conventional vacuum tube crystal-controlled oscillator includes a piezoelectric crystal which has a very high Q at its resonant frequency. In order to effectively couple such a crystal to a transistor, a high impedance must be provided looking into the electrode to which the crystal is connected to preserve the Q of the crystal. Fortunately, by suitable choice of the operating conditions of a current multiplication transistor, a high impedance may be provided looking into any of its three electrodes.[8] Accordingly, the transistor provides a high degree of flexibility in the design of crystal-controlled oscillators.

The oscillators of Figures 10, 12, and 14 combine the features of the L–C sine-wave oscillators previously described with the high impedance of the electrode to which the crystal is connected. As illustrated in

[8] E. Eberhard and R. O. Endres, U. S. patent 2,570,436 (filed September 30, 1949).

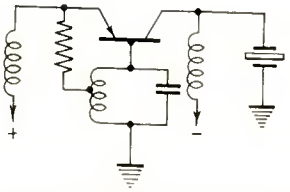

Fig. 10—Crystal controlled oscillator; crystal connected to the collector.

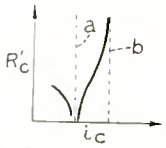

Fig. 11—Collector resistance as a function of the collector current.

Figure 10, the crystal may be connected between collector and ground. The resistance looking into the collector, R_c', shown as a function of i_c in Figure 11, indicates that R_c' approaches infinity when i_c approaches the dotted line b; in the neighborhood of the dotted line a, R_c' approaches zero. A parallel resonant circuit is coupled to the base, and a feed-back path, which may include a resistor, is provided between the emitter and the base resonant circuit.

The crystal may also be connected to the emitter as indicated in Figures 12 and 14. The resistance looking into the emitter, R_e', is shown in Figure 13 as a function of i_c. Near the dotted line c, R_e' approaches infinity. Figure 12 shows a parallel resonant circuit connected to the base, and in Figure 14, a series resonant circuit is connected to the collector. In the oscillator of Figure 14, a large resistor is connected to the base as a necessary condition for oscillation and to produce the high emitter impedance. In this oscillator the crystal and the series resonant circuit may also be exchanged. The feed-back principle by which these crystal-controlled oscillators operate will be evident from the preceding explanation of the L–C sine-wave oscillators.

In Figure 15, the crystal is connected to the base and is bypassed for direct current by a radio-frequency choke. In this oscillator circuit, use is made of the parallel resonance of the crystal. A series resonant circuit is connected between collector and ground and tuned approximately to the crystal frequency. It is also possible to connect the series resonant circuit between emitter and ground. Figure 16 shows that the resistance R_b' which appears looking into the base, approaches

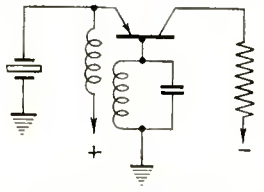

Fig. 12—Crystal-controlled oscillator; crystal connected to the emitter; parallel resonant circuit connected to the base.

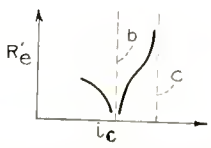

Fig. 13—Emitter resistance as a function of the collector current.

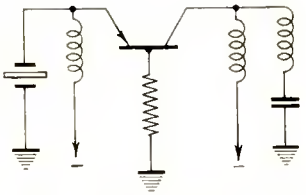

Fig. 14—Crystal-controlled oscillator; crystal connected to the emitter; series resonant circuit connected to the collector.

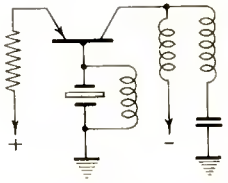

Fig. 15—Crystal-controlled oscillator; crystal connected to the base.

infinity as i_e approaches the dotted line b. In this manner R_b' can be made large enough to present only a small load to the crystal. Dotted lines b in Figures 11, 13, and 16 correspond to the same value of i_e for a given transistor. In the crystal-controlled oscillators discussed here, it should be pointed out that the resonant circuit may be replaced by a resistor. However, this modification will increase the harmonic content of the output signal, while the presence of the tuned circuit will tend to enforce oscillation at the desired frequency. Hence, in those circuits where a fixed frequency oscillation is demanded, the crystal-controlled oscillator should find wide applications.

Phase-Shift Sine-Wave Oscillators

A very satisfactory oscillator for use especially in the audio range, where fixed frequency operation is needed, is the phase-shift oscillator. This type of oscillator is desirable because it is able to generate a very pure sine wave and maintain its frequency relatively independent of supply-voltage variations.

A practical phase-shift oscillator is shown in Figure 17. Feedback is furnished by a resistance–capacitance network, which may be considered a band-elimination filter. At the predetermined frequency, the network exhibits a zero-degree phase shift and maximum attenuation.[9]

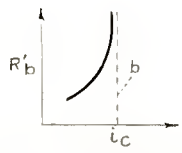

Fig. 16—Base resistance as a function of the collector current.

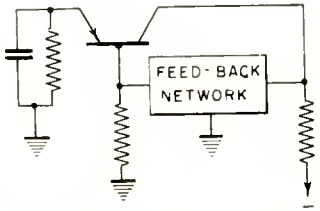

Fig. 17—Phase-shift or feed-back network oscillator.

[9] B. Chance, V. Hughes, E. F. MacNichols, Jr., D. Sayre and F. C. Williams, *Wave Forms*, M. I. T. Radiation Laboratory Series, 1949, pp. 110-122.

Regeneration is provided by the base resistor and is only effective at the operating frequency. At other frequencies, degeneration provided by the flow of collector current through the network into the base inhibits oscillation. Hence, for a current-multiplication transistor, oscillation will take place at the frequency for which the network provides maximum attenuation.

It is also feasible to replace the zero phase-shift network by a 180-degree phase-shift network in the oscillator of Figure 17. In that case, the circuit oscillates by virtue of voltage feedback between collector and base, which is of the correct phase to promote oscillation.[10]

Relaxation Oscillators

One of the fields of application of the transistor is the relaxation oscillator. The transistor exhibits some very attractive characteristics when operated in this type of circuit. At the present stage of development, most transistors are limited in power handling ability. Furthermore, the point-contact transistor has a high noise level; hence, the relaxation oscillator becomes especially important since, normally, neither of these limitations is important in this type of application.

One basic type of relaxation oscillator employs a resistance–capacitance time-constant network which has previously been described in the literature.[11] In this oscillator a capacitor is inserted between collector and ground or between emitter and ground. This capacitor is charged at a relatively slow rate from the collector or emitter voltage supply through a resistor. Ultimately, when the voltage across the capacitor has attained a certain value, the transistor reaches its regenerative region. When this occurs, the capacitor is discharged at a relatively rapid rate through the transistor, and during each oscillatory cycle a saw-tooth wave is developed.

These two circuits may be arranged so as to operate as frequency dividers, in which case they are biased to free-running operation, but are synchronized in time by externally applied voltage pulses. While these circuits will operate satisfactorily in applications where division ratios of three or four to one are required, they are not presently stable enough for reliable operation at higher division ratios. This is due primarily to the free-running frequency dependence on the bias voltage.

A self-quenching oscillator also requiring a current-multiplication

---

[10] A. J. Rack, U. S. patent 2,556,296 (filed April 26, 1949) illustrates in Figure 9 a related oscillator circuit.

[11] Webster, Eberhard and Barton, *op. cit.*, Figures 11-13. E. Eberhard, R. O. Endres and R. P. Moore, "Counter Circuits Using Transistors," *RCA Review*, Vol. 10, pp. 459-476, December, 1949; Figures 9(a) and (b).

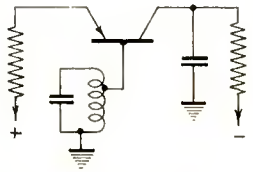

Fig. 18—Self-quenching oscillator or stabilized frequency divider.

transistor is illustrated in Figure 18. The capacitor connected between collector and ground is charged from the collector-voltage supply through the collector resistor; a parallel resonant circuit is connected to the base. The time constant of the R–C circuit connected to the collector should be larger than the period of the L–C circuit connected to the base.

The operation of this circuit may be more easily understood by reference to Figure 19, which shows the collector voltage wave, e_c, and base voltage wave, e_b. The collector circuit operates independently of the base circuit and produces the saw-tooth wave associated with the R–C relaxation oscillator. The operation of the base circuit, however, is quite dependent upon the amplitude of the voltage excursion of the collector. It is evident that without the collector capacitor the circuit will act as a sine-wave oscillator as previously described. However, in the circuit of Figure 18, as the collector capacitor charges in the negative direction, the transistor is carried into its regenerative region. At some point regeneration becomes sufficiently great to support oscillation in the base tank circuit once it has been initiated by a noise pulse or other voltage transient. The oscillation attains its peak ampli-

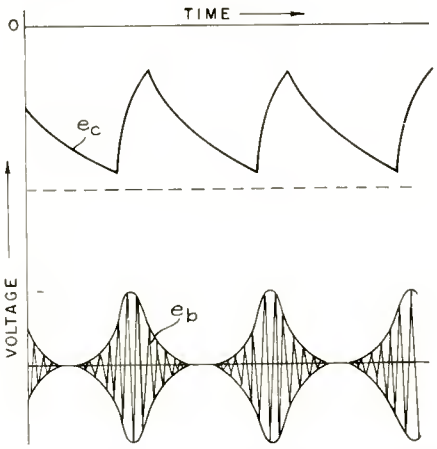

Fig. 19—Voltage waves of the circuit of Figure 18 operating as a self-quenching oscillator.

tude at the moment the collector capacitor starts to discharge. Thereafter, the oscillations are sustained by the energy stored in the tank circuit, and their duration becomes solely a function of the Q of the circuit and the load imposed by the circuit constants. Under proper conditions, the sine-wave oscillations may be made to be continuous but with varying amplitude. A second self-quenching oscillator, similar in operation, is obtained when the capacitor is connected to the emitter and charged from the emitter-voltage supply through a resistor.

The circuit of Figure 18 may also be operated so that the time

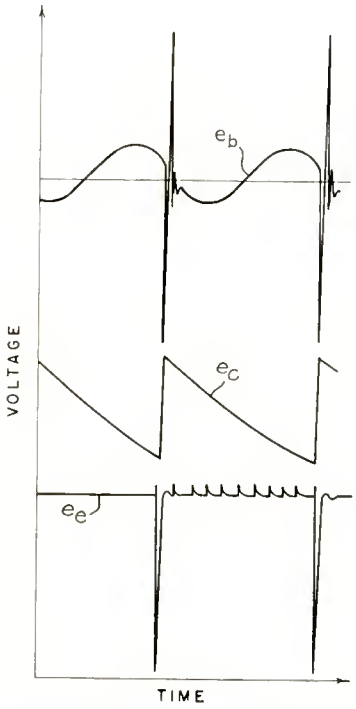

Fig. 20—Voltage waves of the curcuit of Figure 18 operating as a frequency divider.

constant of the R–C network connected to the collector is only slightly larger than the period of the L–C base circuit. Thus, during each charge and discharge cycle of the collector capacitor, there may be a few oscillations or possibly only one cycle of the sine wave developed across the parallel resonant base circuit. The voltages e_b, e_c, and e_e developed by such an R–C, L–C relaxation oscillator are illustrated in Figure 20.

When the circuit of Figure 18 is operated as described above, it is

biased in such a manner that a portion of the collector voltage cycle occurs in the regenerative or negative resistance region of the transistor. As the oscillator enters this region, the internal collector impedance suddenly becomes small. This, in turn, causes the rapid discharge of the collector capacitor in a positive direction as shown by the e_c curve of Figure 20. Due to the suddenly increased collector current at the instant of regeneration, e_b increases rapidly in the negative direction. At this instant a negative pulse is formed at the emitter as a result of the negative base voltage swing. When the circuit leaves the regenerative region, the collector current is substantially cut off. This abrupt change of the rate of flow of the collector current through the base inductance causes the base voltage to increase rapidly to a high positive value. The discharge of the collector capacitor carries the transistor outside of the regenerative region and the capacitor is again charged from the negative collector voltage supply. During the charging period of the capacitor, the sinusoidal wave developed across the base circuit continues until a swing of the base sine wave in a negative direction coincides with a high negative collector voltage so as to assist mutually in driving the transistor into the regenerative region again and to initiate the next cycle. If the base voltage is sufficiently large to determine primarily the free-running frequency of the oscillator, a greater change of the collector bias voltage can be tolerated before frequency instability occurs.

This suggests the desirability of utilizing such a circuit as a stabilized frequency divider where large division ratios are desired. Figure 20 indicates the presence of synchronizing trigger pulses applied to the emitter. Such a circuit has proved to be most valuable in providing division ratios of as high as 20 to 1 over a wide variation of emitter and collector bias voltages. It must be kept in mind that the repetition rate of the synchronizing trigger pulses should be substantially an integral multiple of the oscillator frequency.

As described elsewhere,[12] separate R–C networks may be connected to both emitter and collector and an L–C circuit may be coupled to the base. In that case, both the emitter and collector voltages assume the shape of a saw-tooth wave, and the circuit may be synchronized by the application of positive pulses to the emitter or negative pulses to the collector or base. This relaxation oscillator may be further modified by replacing the R–C emitter network by a resonant circuit connected to the emitter. The addition of such a timing circuit to the emitter enhances the stability of these oscillators.

A transistor R–L relaxation oscillator has previously been re-

[12] Eberhard, Endres, Moore, *op. cit.*, Figure 11.

ported.[13] Such an oscillator is illustrated in Figure 21 and has an inductor between base and ground. The period of oscillation is determined by the R–L time-constant circuit which includes the inductance of the base inductor and the resistance which appears looking into the base. The voltages e_b, e_e, and e_c, and the base current, i_b, are shown in Figure 22, which is plotted so that an increase of i_b corresponds to an increase of the net current flowing from ground through the inductor to the base.

When the relaxation oscillator reaches the regenerative region, a steadily increasing base current, i_b, will flow which, in turn, will cause the base voltage to go initially in a negative direction. The resulting larger emitter current will drive the emitter voltage, e_e, also in a negative direction; e_c goes in a positive direction due to the larger collector current. The base voltage, e_b, depends on the current through the base inductor and is proportional to the negative derivative of base current with respect to time $(-di_b/dt)$. Accordingly, as the

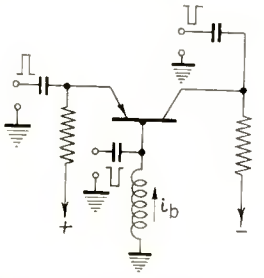

Fig. 21—Triggered relaxation oscillator of the R–L type.

value of the derivative decreases, e_b becomes less negative. Eventually, the base voltage becomes sufficiently positive to carry the circuit out of the regenerative region. This abrupt change of the base current derivative causes a positive voltage swing of e_b with a corresponding decrease of the emitter and collector currents. Consequently, e_e and e_c approach their positive and negative supply voltages respectively. Finally, e_b decays again exponentially at a rate determined by the R–L time constant, eventually driving the oscillator again into the regenerative region to initiate the next cycle of operation.

Synchronizing pulses of positive polarity may be applied to the emitter, or negative pulses may be impressed on base or collector, as shown in Figure 21. By appropriate choice of either the emitter or the collector voltage, the circuit of Figure 21, as well as the circuits of previously described oscillators, may be made to be normally quies-

[13] Eberhard, Endres and Moore, *op. cit.*, Figure 9(c).

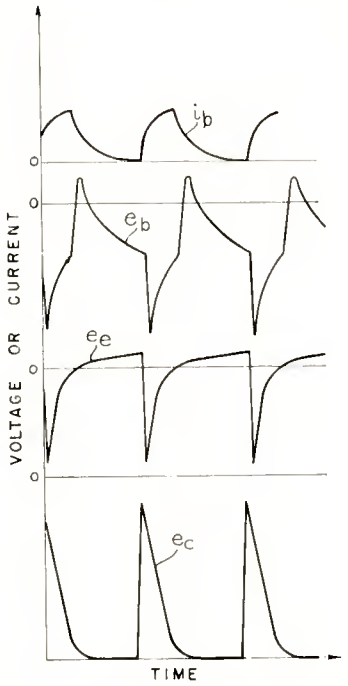

Fig. 22—Wave shapes of the relaxation oscillator of Figure 21.

cent and may be triggered into the regenerative region by applying trigger pulses. The circuit of Figure 21 may also be triggered by applying a sinusoidal wave to the emitter or base.

The R–L relaxation oscillator of Figure 21 will also function with a capacitor between collector and ground as shown in Figure 23. The time constants of the R–C and R–L networks are chosen so that e_c and e_b will go simultaneously in a negative direction during each cycle of operation so that the collector and base voltages drive the oscillator concomitantly into the regenerative region.

The operation of the oscillator of Figure 23 is essentially that described in connection with Figures 21 and 22. However, the collector voltage is a saw-tooth wave. When the oscillator enters the regenera-

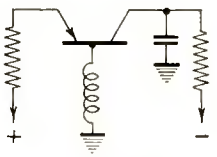

Fig. 23—Modified R–L relaxation oscillator.

tive region, the collector capacitor will be rapidly discharged to provide a large current through the base inductor. At this instant, a highly negative voltage pulse is developed at the base by the inductive "kick" of the base inductor. Subsequently, the base current will increase at successively slower rates in the manner described earlier. As the rising base voltage carries the operation of the unit into the low-current region, the base voltage increases sharply again to a highly positive value.

The oscillator of Figure 23 is quite stable and can tolerate a substantial variation of the supply voltages without changing its repetition frequency. The oscillator may again be triggered or synchronized or it may be used as a frequency divider as long as the frequency of the synchronizing pulses is approximately an integral multiple of the free-running frequency of the oscillator.

ACKNOWLEDGMENT

The experimental work on which this paper is based was carried out under the direction of Everett Eberhard. John V. Kane assisted in the development of the phase-shift sine-wave oscillator.

PARALLEL-TUNED CIRCUIT PERIODICALLY SWITCHED TO A DIRECT-CURRENT SOURCE*†

By

L. J. Giacoletto

Research Department, RCA Laboratories Division.
Princeton, N. J.

Summary—*A parallel-tuned circuit periodically connected to a source of linear direct-current energy (e.g., by means of an electron tube or switch) is fundamental to a large group of energy conversion circuits. This prototype circuit is examined analytically. Linear solutions can be employed if the operating period is analyzed in two parts consisting of the periods during which the switch is closed and open. The complete solution is then obtained by matching boundary conditions for the two sets of solutions. This complete solution embraces many voltage and current variations including sinusoidal, sawtooth, and more complex wave shapes depending upon circuit parameters and switch period. The general solution can be simplified by eliminating dissipative elements to permit a clear insight into the basic operation of the prototype circuit.*

A mechanically driven circuit was used to verify the analytic results. By varying the operating parameters, the entire gamut of wave shapes can be obtained. The agreement between theory and practice is very close.

The analytic results can be used to analyze sinusoidal and nonsinusoidal oscillators, class C amplifiers, and many pulsed circuits.

Introduction

IN A CONVENTIONAL electric oscillator circuit, direct-current energy is converted to oscillatory energy. A circuit that can be considered an idealized prototype of a large group of electric oscillator circuits is shown in Figure 1(a). Here, a parallel circuit composed of energy storage elements, L and C, and energy conversion elements, R_L and R_C, is periodically connected to a source of direct-current energy represented by a perfect battery of voltage V_B, in series with its internal resistance, R_B. The following assumptions and premises are used:

a) All circuit elements are linear and constant.

b) The energy source is linear, i.e., terminal voltage and load current are linearly related.

---

* Decimal Classification: R140.

† The material in this paper is included as a chapter and an appendix in the author's doctoral thesis, "Dynatron Oscillator Operation with Particular Emphasis to a New Saw-Tooth Current Oscillator" on file with the Graduate School, University of Michigan. Parts of this paper were presented orally at the March 1952 I.R.E. Convention.

c) The ideal switch is closed for a time t_p, after which it is open for a time $t_0 - t_p$, when it is again closed, and the operation is repeated cyclically [see Figure 1(b)].

d) The circuit has reached a steady-state condition.

e) The closing of the switch is chosen to coincide with $t = 0$.

Analysis

If one uses the usual current convention (reverse of electron flow), the nodal equation for the circuit of Figure 1(a) can be written

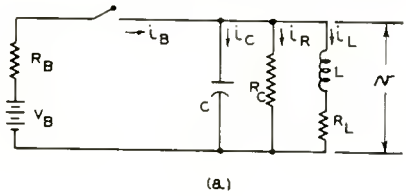

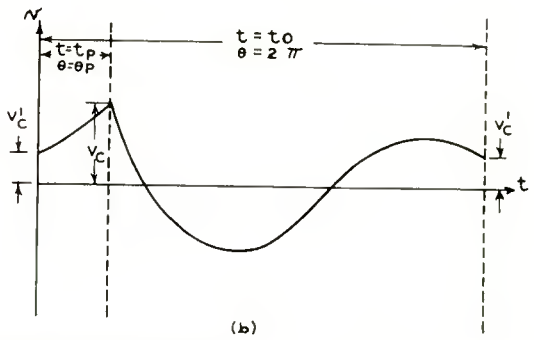

Fig. 1—Linear-power-transfer circuit. (a) Circuit. (b) Typical wave shape.

$$i_B = i_C + i_R + i_L. \tag{1}$$

$$i_B = C\frac{dv}{dt} + \frac{v}{R_C} + e^{-\frac{R_L}{L}t}\int \frac{v}{L} e^{\frac{R_L}{L}t}\, dt. \tag{2}$$

Differentiate once and replace the independent variable by

$\theta = 2\pi f_0 t = \dfrac{2\pi t}{t_0} = \omega_0 t$. Then

$$\frac{d^2 v}{d\theta^2} + \left[\frac{1}{\omega_0 C R_C} + \frac{R_L}{\omega_0 L}\right]\frac{dv}{d\theta} + \left[\frac{1}{\omega_0^2 LC} + \frac{R_L}{\omega_0^2 LC R_C}\right] v$$

$$= \frac{R_L}{\omega_0^2 LC} i_B + \frac{1}{\omega_0 C} \frac{d\, i_B}{d\, \theta}. \tag{3}$$

If one introduces the following supplementary quantities,

$$\omega_r^2 = \frac{1}{LC}, \tag{4}$$

$$\omega_0 C R_C = Q_C, \tag{5}$$

$$\frac{\omega_0 L}{R_L} = Q_L, \tag{6}$$

$$\omega_0 C \frac{R_C R_B}{R_C + R_B} = Q_C', \tag{7}$$

Equation (3) can be written

$$\frac{d^2\left(\frac{v}{V_B}\right)}{d\,\theta^2} + \left[\frac{1}{Q_C} + \frac{1}{Q_L}\right] \frac{d\left(\frac{v}{V_B}\right)}{d\,\theta} + \frac{\omega_r^2}{\omega_0^2}\left[1 + \frac{R_L}{R_C}\right] \frac{v}{V_B}$$

$$= \frac{\omega_r^2}{\omega_0^2} R_L \frac{i_B}{V_B} + \frac{1}{\omega_0 C} \frac{d\left(\frac{i_B}{V_B}\right)}{d\,\theta}. \tag{8}$$

From $\theta = 0$ to $\theta = \theta_p$,

$$i_B = \frac{V_B - v}{R_B}, \tag{9}$$

and from $\theta = \theta_p$ to $\theta = 2\pi$, $i_B = 0$. Therefore, the differential equations to be solved in these two time intervals are

$$\frac{d^2\left(\frac{v}{V_B}\right)}{d\,\theta^2} + \left[\frac{1}{Q_C'} + \frac{1}{Q_L}\right] \frac{d\left(\frac{v}{V_B}\right)}{d\,\theta} + \frac{\omega_r^2}{\omega_0^2}\left[1 + \frac{R_L}{R_C} + \frac{R_L}{R_B}\right] \frac{v}{V_B}$$

$$= \frac{\omega_r^2}{\omega_0^2} \frac{R_L}{R_B},$$

(valid from $\theta = 0$ to $\theta = \theta_p$), (10)

and

$$\frac{d^2\left(\frac{v}{V_B}\right)}{d\theta^2} + \left[\frac{1}{Q_C} + \frac{1}{Q_L}\right] \frac{d\left(\frac{v}{V_B}\right)}{d\theta} + \frac{\omega_r^2}{\omega_0^2}\left[1 + \frac{R_L}{R_C}\right] \frac{v}{V_B} = 0.$$

(valid from $\theta = \theta_p$ to $\theta = 2\pi$). (11)

As shown in Figure 1(b), the value of v at the time the switch is closed, V_c', must be continuous, otherwise i_c would have to be infinitely large. The value of v at the time the switch is opened, V_c, must be continuous for the same reason. Equations (10) and (11) can be solved readily to meet these boundary conditions. For Equation (10), a non-oscillatory solution is assumed, i.e., it is assumed that

$$\frac{1}{4}\left[\frac{1}{Q_C'} + \frac{1}{Q_L}\right]^2 > \frac{\omega_r^2}{\omega_0^2}\left[1 + \frac{R_L}{R_C} + \frac{R_L}{R_B}\right]. \quad (12)$$

For Equation (11), an oscillatory solution is assumed, i.e., it is assumed that

$$\frac{1}{4}\left[\frac{1}{Q_C} + \frac{1}{Q_L}\right]^2 < \frac{\omega_r^2}{\omega_0^2}\left[1 + \frac{R_L}{R_C}\right]. \quad (13)$$

If these inequalities are not satisfied, the solutions given below are still correct. Trigonometric identities may be used to remove the resulting imaginary arguments.

Solutions

The solutions of Equations (10) and (11) are, respectively,

$$\frac{v}{V_B} = \frac{R_L}{R_B}\left(\frac{\omega_r}{\beta_c\,\omega_0}\right)^2$$

$$+\left[e^{+\alpha_c\theta_p}\operatorname{csch}\sqrt{\alpha_c^2-\beta_c^2}\,\theta_p\,\frac{V_C}{V_B}-\coth\sqrt{\alpha_c^2-\beta_c^2}\,\theta_p\,\frac{V_C'}{V_B}\right.$$

$$-\left(e^{+\alpha_c\theta_p}\operatorname{csch}\sqrt{\alpha_c^2-\beta_c^2}\,\theta_p-\coth\sqrt{\alpha_c^2-\beta_c^2}\,\theta_p\right)$$

$$\left.\frac{R_L}{R_B}\left(\frac{\omega_r}{\beta_c\,\omega_0}\right)^2\right]e^{-\alpha_c\theta}\sinh\sqrt{\alpha_c^2-\beta_c^2}\,\theta+$$

$$\left[\frac{V_C'}{V_B}-\frac{R_L}{R_B}\left(\frac{\omega_r}{\beta_c\,\omega_0}\right)^2\right]e^{-\alpha_c\theta}\cosh\sqrt{\alpha_c^2-\beta_c^2}\,\theta,$$

$$(\text{valid from } \theta=0 \text{ to } \theta=\theta_p), \tag{14}$$

and

$$\frac{v}{V_B}=\left[e^{+\alpha_0(2\pi-\theta_p)}\csc\sqrt{\beta_0^2-\alpha_0^2}\,(2\pi-\theta_p)\,\frac{V_C'}{V_B}\right.$$

$$\left.-\cot\sqrt{\beta_0^2-\alpha_0^2}\,(2\pi-\theta_p)\,\frac{V_C}{V_B}\right]e^{-\alpha_0(\theta-\theta_p)}\sin\sqrt{\beta_0^2-\alpha_0^2}\,(\theta-\theta_p)$$

$$+\frac{V_C}{V_B}e^{-\alpha_0(\theta-\theta_p)}\cos\sqrt{\beta_0^2-\alpha_0^2}\,(\theta-\theta_p),$$

$$(\text{valid from } \theta=\theta_p \text{ to } \theta=2\pi). \tag{15}$$

Here

$$\alpha_c=\frac{1}{2}\left[\frac{1}{Q_C'}+\frac{1}{Q_L}\right], \tag{16}$$

$$\alpha_0=\frac{1}{2}\left[\frac{1}{Q_C}+\frac{1}{Q_L}\right], \tag{17}$$

$$\beta_c=\frac{\omega_r}{\omega_0}\sqrt{1+\frac{R_L}{R_C}+\frac{R_L}{R_B}}, \tag{18}$$

$$\beta_0=\frac{\omega_r}{\omega_0}\sqrt{1+\frac{R_L}{R_C}}. \tag{19}$$

Two additional boundary conditions are required in order to determine the values of V_c and V_c' as functions of various circuit parameters. Possibly the easiest boundary conditions to use are that the values of i_L at both $\theta = \theta_p$ and $\theta = 2\pi$ shall be continuous. This development will now be carried out.

If one uses Equation (14) for v/V_B, the equation for i_L is

$$\frac{R_C\, i_L}{V_B} = \frac{R_C}{R_B} - \left(1 + \frac{R_C}{R_B}\right)\frac{v}{V_B} - Q_C \frac{d\left(\frac{v}{V_B}\right)}{d\theta}$$

$$= \frac{R_C}{R_B}\left(\frac{\omega_r}{\beta_c\,\omega_0}\right)^2 + \left[e^{+\alpha_c\theta_p}\,\mathrm{csch}\,\sqrt{\alpha_c^2-\beta_c^2}\,\theta_p\,\frac{V_C}{V_B} - \coth\sqrt{\alpha_c^2-\beta_c^2}\,\theta_p\,\frac{V_C'}{V_B}\right.$$

$$\left. - \left(e^{+\alpha_c\theta_p}\,\mathrm{csch}\,\sqrt{\alpha_c^2-\beta_c^2}\,\theta_p - \coth\sqrt{\alpha_c^2-\beta_c^2}\,\theta_p\right)\frac{R_L}{R_B}\left(\frac{\omega_r}{\beta_c\,\omega_0}\right)^2\right]$$

$$\left[-\left(Q_C\alpha_c - \frac{Q_C}{Q_L}\right)e^{-\alpha_c\theta}\sinh\sqrt{\alpha_c^2-\beta_c^2}\,\theta\right.$$

$$\left. - Q_C\sqrt{\alpha_c^2-\beta_c^2}\,e^{-\alpha_c\theta}\cosh\sqrt{\alpha_c^2-\beta_c^2}\,\theta\right]$$

$$+\left[\frac{V_C'}{V_B} - \frac{R_L}{R_B}\left(\frac{\omega_r}{\beta_c\,\omega_0}\right)^2\right]\left[-\left(Q_C\alpha_c - \frac{Q_C}{Q_L}\right)e^{-\alpha_c\theta}\cosh\sqrt{\alpha_c^2-\beta_c^2}\,\theta\right.$$

$$\left. - Q_C\sqrt{\alpha_c^2-\beta_c^2}\,e^{-\alpha_c\theta}\sinh\sqrt{\alpha_c^2-\beta_c^2}\,\theta\right],$$

$$(\text{valid from } \theta = 0 \text{ to } \theta = \theta_p). \qquad (20)$$

If one uses Equation (15) for v/V_B, the equation for i_L is

$$\frac{R_C\, i_L}{V_B} = -\frac{v}{V_B} - Q_C\frac{d\left(\frac{v}{V_B}\right)}{d\theta}$$

$$= \left[e^{+\alpha_0(2\pi-\theta_p)} \csc \sqrt{\beta_0^2-\alpha_0^2}\,(2\pi-\theta_p) \frac{V_C'}{V_B} \right.$$

$$\left. - \cot \sqrt{\beta_0^2-\alpha_0^2}\,(2\pi-\theta_p) \frac{V_C}{V_B} \right]$$

$$[-(1-Q_C\alpha_0)\, e^{-\alpha_0(\theta-\theta_p)} \sin \sqrt{\beta_0^2-\alpha_0^2}\,(\theta-\theta_p)$$

$$- Q_C \sqrt{\beta_0^2-\alpha_0^2}\, e^{-\alpha_0(\theta-\theta_p)} \cos \sqrt{\beta_0^2-\alpha_0^2}\,(\theta-\theta_p)]$$

$$+ \left[\frac{V_C}{V_B} \right] [-(1-Q_C\alpha_0)\, e^{-\alpha_0(\theta-\theta_p)} \cos \sqrt{\beta_0^2-\alpha_0^2}\,(\theta-\theta_p)$$

$$+ Q_C \sqrt{\beta_0^2-\alpha_0^2}\, e^{-\alpha_0(\theta-\theta_p)} \sin \sqrt{\beta_0^2-\alpha_0^2}\,(\theta-\theta_p)],$$

$$(\text{valid from } \theta=\theta_p \text{ to } \theta=2\pi). \qquad (21)$$

Since i_L is continuous when the switch is closed, substitute $\theta = 0$ in Equation (20) and $\theta = 2\pi$ in Equation (21), equate these expressions, and simplify. The result is Equation (23) below. Likewise, since i_L is continuous when the switch is opened, substitute $\theta = \theta_p$ in Equations (20) and (21), equate, and simplify. The result is Equation (22) below.

$$\left[\frac{R_C}{2\,Q_C R_B} + \sqrt{\alpha_c^2-\beta_c^2} \coth \sqrt{\alpha_c^2-\beta_c^2}\,\theta_p \right.$$

$$\left. + \sqrt{\beta_0^2-\alpha_0^2} \cot \sqrt{\beta_0^2-\alpha_0^2}\,(2\pi-\theta_p) \right] \frac{V_C}{V_B}$$

$$- [\sqrt{\beta_0^2-\alpha_0^2}\, e^{+\alpha_0(2\pi-\theta_p)} \csc \sqrt{\beta_0^2-\alpha_0^2}\,(2\pi-\theta_p)$$

$$+ \sqrt{\alpha_c^2-\beta_c^2}\, e^{-\alpha_c\theta_p} \operatorname{csch} \sqrt{\alpha_c^2-\beta_c^2}\,\theta_p] \frac{V_C'}{V_B}$$

$$= \left[\frac{R_C}{Q_C R_B} - \frac{R_L}{R_B} \left(\frac{\omega_r}{\beta_c\,\omega_0} \right)^2 (\alpha_c - \sqrt{\alpha_c^2-\beta_c^2}\,\{\coth \sqrt{\alpha_c^2-\beta_c^2}\,\theta_p \right.$$

$$\left. - e^{-\alpha_c\theta_p} \operatorname{csch} \sqrt{\alpha_c^2-\beta_c^2}\,\theta_p\}) \right]. \qquad (22)$$

$$[\sqrt{\alpha_c^2-\beta_c^2}\, e^{+\alpha_c\theta_p} \operatorname{csch} \sqrt{\alpha_c^2-\beta_c^2}\, \theta_p$$

$$+ \sqrt{\beta_0^2-\alpha_0^2}\, e^{-\alpha_0(2\pi-\theta_p)} \csc \sqrt{\beta_0^2-\alpha_0^2}\, (2\pi-\theta_p)\,] \frac{V_C}{V_B}$$

$$+ \left[\frac{R_C}{2\,Q_C R_B} - \sqrt{\alpha_c^2-\beta_c^2} \coth \sqrt{\alpha_c^2-\beta_c^2}\, \theta_p\right.$$

$$\left. - \sqrt{\beta_0^2-\alpha_0^2} \cot \sqrt{\beta_0^2-\alpha_0^2}\, (2\pi-\theta_p)\right] \frac{V_C'}{V_B}$$

$$= \left[\frac{R_C}{Q_C R_B} - \frac{R_L}{R_B}\left(\frac{\omega_r}{\beta_c\,\omega_0}\right)^2 (\alpha_c + \sqrt{\alpha_c^2-\beta_c^2}\,\{\coth \sqrt{\alpha_c^2-\beta_c^2}\, \theta_p\right.$$

$$\left. - e^{+\alpha_c\theta_p} \operatorname{csch} \sqrt{\alpha_c^2-\beta_c^2}\, \theta_p\}) \right] . \qquad (23)$$

Simultaneous Equations (22) and (23) complete the solution. If the values of the circuit parameters and operating conditions are specified, V_C/V_B and V_C'/V_B can be determined by means of Equations (22) and (23). With these boundary values determined, the voltage, v, can be specified by means of Equations (14) and (15). The inductor current, i_L, can be specified by Equations (20) and (21). From these expressions, the various other circuit voltages and currents can be obtained by simple manipulation. Finally, with the circuit voltages and currents determined, the energy storage and conversion can be obtained.

For some values of the circuit parameters, difficulty may be experienced in obtaining the solutions. For certain other values of the circuit parameters, the solutions given above may be simplified considerably. Solutions for these special values of circuit parameters are considered in detail in Appendix I.

Approximate Solution

The solutions given above for the linear-power-transfer circuit shown in Figure 1(a) are too complex to permit a general study of the circuit performance. However, the general circuit performance can be studied if all circuit losses are neglected. Although this is a highly idealized condition, considerable insight can be gained concerning the performance of a practical circuit. The case where the circuit

losses are neglected is considered in detail in Appendix I (case 5). Of particular interest is the expression for the voltage v, present across the circuit elements. As indicated in Appendix I (case 5), $v/V_B = 1.0$ for $\theta = 0$ to $\theta = \theta_p$. For $\theta = \theta_p$ to $\theta = 2\pi$, the solution for v/V_B given in Appendix I (case 5) is repeated below.

$$\frac{v}{V_B} = -A \sin \frac{\omega_r}{\omega_0}(\theta - \theta_p) + \cos \frac{\omega_r}{\omega_0}(\theta - \theta_p)$$

$$= -\sqrt{1 + A^2} \sin\left\{\frac{\omega_r}{\omega_0}(\theta - \theta_p) - \cot^{-1} A\right\},$$

$$\text{(valid from } \theta = \theta_p \text{ to } \theta = 2\pi), \tag{24}$$

where $$A = \frac{\frac{\omega_r}{\omega_0}\theta_p + \sin \frac{\omega_r}{\omega_0}(2\pi - \theta_p)}{1 - \cos \frac{\omega_r}{\omega_0}(2\pi - \theta_p)}.$$

This equation is sufficiently simple to permit interpretation and evaluation. First, critical values of the circuit parameters ω_r/ω_0 and θ_p will be examined.

It is seen that v/V_B becomes infinitely large when

$$\frac{\omega_r}{\omega_0}(2\pi - \theta_p) = 2\pi n. \tag{25}$$

Here n is a nonnegative integer. Equation (25) is properly labeled as the resonance condition even though resonance is generally obtained for non-integral values of ω_r/ω_0. If θ_p is small, resonance is obtained when ω_r/ω_0 has approximately an integral value. The resonance condition will now be examined qualitatively.

For $n = 0$, and provided $\theta_p < 2\pi$, $\omega_r/\omega_0 = 0$. In this event, as shown in Figure 2(a), v/V_B does not change while the switch is open. Although for this case v/V_B does not become infinitely large, the current through the inductor does become infinitely large. For $n = 1$, resonance is obtained when ω_r/ω_0 and θ_p are adjusted so that v/V_B completes exactly one cycle of oscillation during the time the switch is open. For larger values of n, similar conditions hold with v/V_B completing

multiple cycles of oscillation during the time the switch is open. [See Figure 2(e) for $n = 2$.] Figures 2(b) and 2(d) show typical wave shapes existing for between-resonance conditions.

For resonance operation, v/V_B builds up to an indefinite amplitude as additional energy is stored in the capacitor each time the switch is closed. This mode of operation violates the original assumption of steady-state condition. Therefore, the above material concerning resonance operation is valid only as a limiting situation.

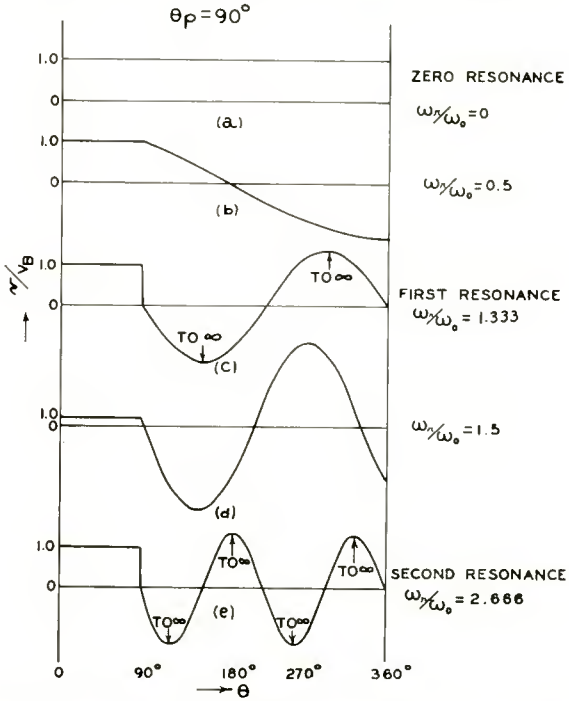

Fig. 2—Typical voltage wave shape for lossless linear-power-transfer circuit.

From Equation (24), it is seen that the amplitude of v/V_B cannot be smaller than unity. The necessary and sufficient condition that the amplitude of v/V_B equal unity is that

$$\frac{\omega_r}{\omega_0}\theta_p + \sin\frac{\omega_r}{\omega_0}(2\pi - \theta_p) = 0. \tag{26}$$

For $\theta_p \to 0$, Equation (26) is satisfied when $\omega_r/\omega_0 = \frac{1}{2}, \frac{3}{2}, \ldots\ldots$

If θ_p is greater than approximately 60 degrees, Equation (26) cannot be satisfied, and the amplitude of v/V_B is then always greater than unity.

If a value of θ_p is chosen, the variation of the amplitude factor [see Equation (24)] of v/V_B can be determined as a function of ω_r/ω_0. This variation of the amplitude factor is shown in Figure 3. During the time the switch is open, v/V_B will have the shape of a segment of a sine wave (see Figure 2). The amplitude factor gives the amplitude of this sine wave, although, if the segment of the sine wave is a small fraction of a cycle, v/V_B will not reach the maximum value indicated

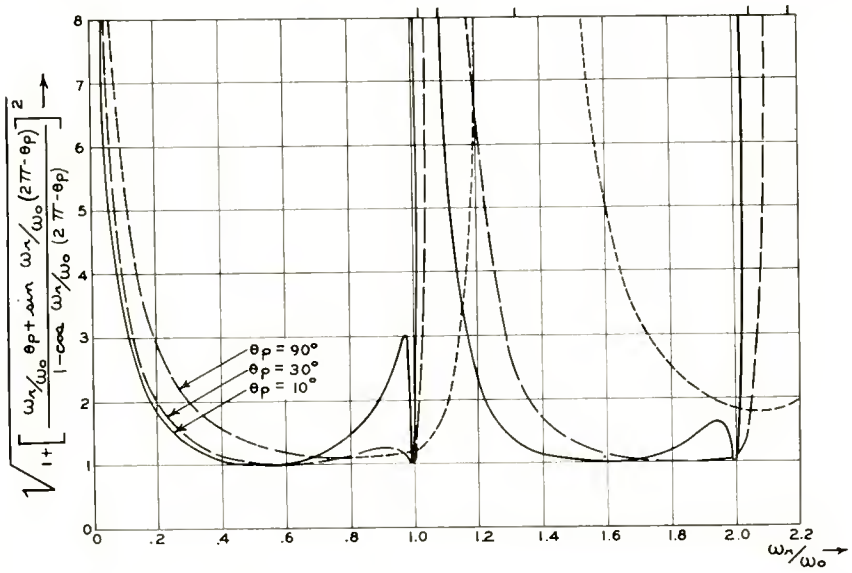

Fig. 3—Amplitude function of a lossless linear-power-transfer circuit.

by the amplitude factor. The phase angle of the segment of a sine wave used to define v/V_B is shown in Figure 4. This phase angle is measured with respect to a negative sine wave starting at $\theta = \theta_p$.

If θ_p is small, Figure 3 indicates that a secondary finite maximum of the amplitude factor occurs when ω_r/ω_0 is somewhat less than an integral value. The secondary maximum occurs at the same value of ω_r/ω_0 which produces the phase angle maximum shown in Figure 4. For the highly idealized limit, $\theta_p = 0$, the phase-angle maximum approaches 180 degrees and the secondary-amplitude maximum approaches infinity. A further study of the situation reveals that the resonant maximum and secondary maximum are closely related. The resonant maximum is produced by closing the switch when the voltage

across the capacitor, V_C', is zero and the current through the inductor, I_L', is positive. The current through the inductor, therefore, increases each time the switch is closed, and the amplitude increases indefinitely. To produce the secondary maximum, the switch is again closed when V_C' is approximately zero (actually slightly negative). Now, however, I_L' is negative. Consequently, when the switch is closed, the inductor stored energy is initially returned to the battery, and the amplitude has a finite steady-state value. The steady-state amplitude is smaller for larger values of θ_p since more energy can be returned from the inductor to the battery. Indeed, for a large enough value of θ_p, no secondary maximum is found; the critical value of θ_p is approximately

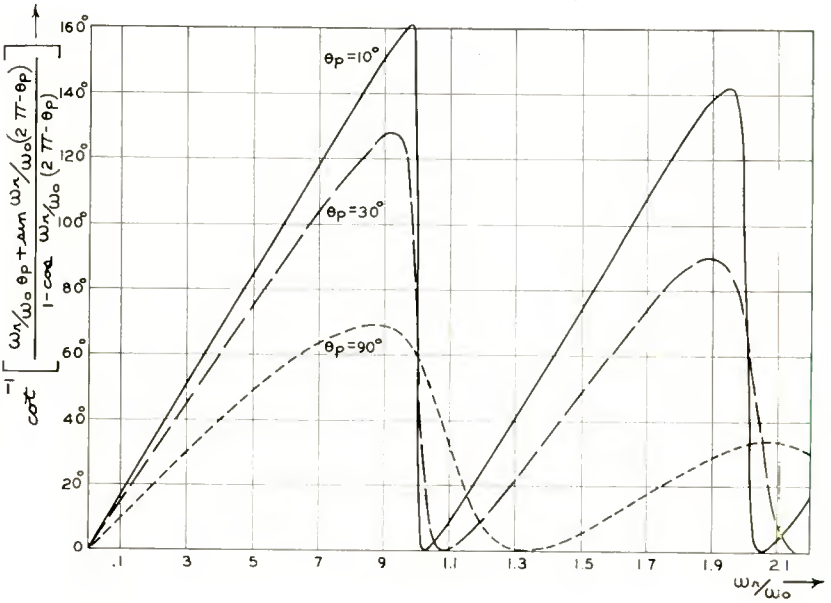

Fig. 4—Phase function of a lossless linear-power-transfer circuit.

the same as that for which the amplitude of v/V_B is always greater than unity, as discussed above.

In the usual type of electric oscillator circuit, feedback is used to maintain oscillations. Consequently, the operating frequency must equal the circuit resonant frequency; $\omega_r/\omega_0 = 1.0$. In this situation, the maximum value of the circuit voltage is not larger than the battery voltage when θ_p is small. However, if a separate source of excitation is used and if the circuit is resonated at a frequency somewhat higher than the operating frequency, the maximum value of the circuit voltage may be considerably larger than the battery voltage. This is one reason

why the peak of the alternating plate voltage of a class C amplifier is sometimes larger than the supply voltage.

Although all the preceding investigation was devoted to the parallel circuit of Figure 1(a), the results are readily transformed to a series circuit by applying the principles of circuit duality. L and R_L become a capacitor with a shunt conductor, and this combination is in series with an inductor (dual of C) and another conductor (dual of R_C). The voltage source with its series resistor becomes a current source with its shunt conductor in the dual circuit. The switch in the dual circuit alternately short circuits the series circuit or connects it to the current generator. Voltages and currents in the original circuit become currents and voltages, respectively, in the dual circuit.

Measurements and Calculations

It is important to determine how well the preceding solutions apply to a practical circuit. For this purpose, the circuit[1] shown in Figure 5 was utilized. A small direct-current motor, governor-regulated, drove

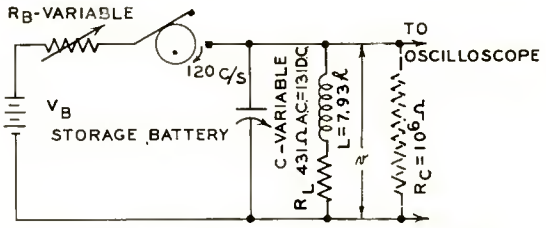

Fig. 5—Linear-power-transfer test circuit.

a cam which operated the switch at 120 cycles per second. The switch contacts were moved to vary the time the switch was closed. Resistance was added in the battery circuit to change the value of R_B. A low-loss, fixed, air-core inductor was used with a variable capacitor to form the parallel circuit. The capacitor was varied to adjust ω_r. A direct-current-coupled oscilloscope was used to determine the voltage wave form of v. Oscilloscope photographs for a variety of different operating conditions and circuit parameters are shown in Figures 6, 7, 8, and 9. These results will be discussed in some detail.

The first item of interest is the resonant condition shown in Figures 6(g), 6(m), 7(g), 7(m), 8(j), 8(m), 9(j), and 9(m). This resonant operation was obtained by adjusting the capacitor until the peak value

[1] Several attempts were made to use vacuum tubes to simulate a perfect switch with only limited success. The circuit shown follows a suggestion by I. Wolff, RCA Laboratories Division, Princeton, N. J., to use a mechanical switch which had been developed for other equipment. Although the operation of the mechanical switch was erratic as compared with a vacuum tube circuit, the final results were quite good.

of v was maximum. The measured values of ω_r/ω_0 which produce resonant operation are tabulated in Table 1 together with similar values of ω_r/ω_0 computed using the approximate condition of Equation (25). Although circuit losses are neglected in Equation (25), the agreement between measured and computed values of ω_r/ω_0 is quite good. Com-

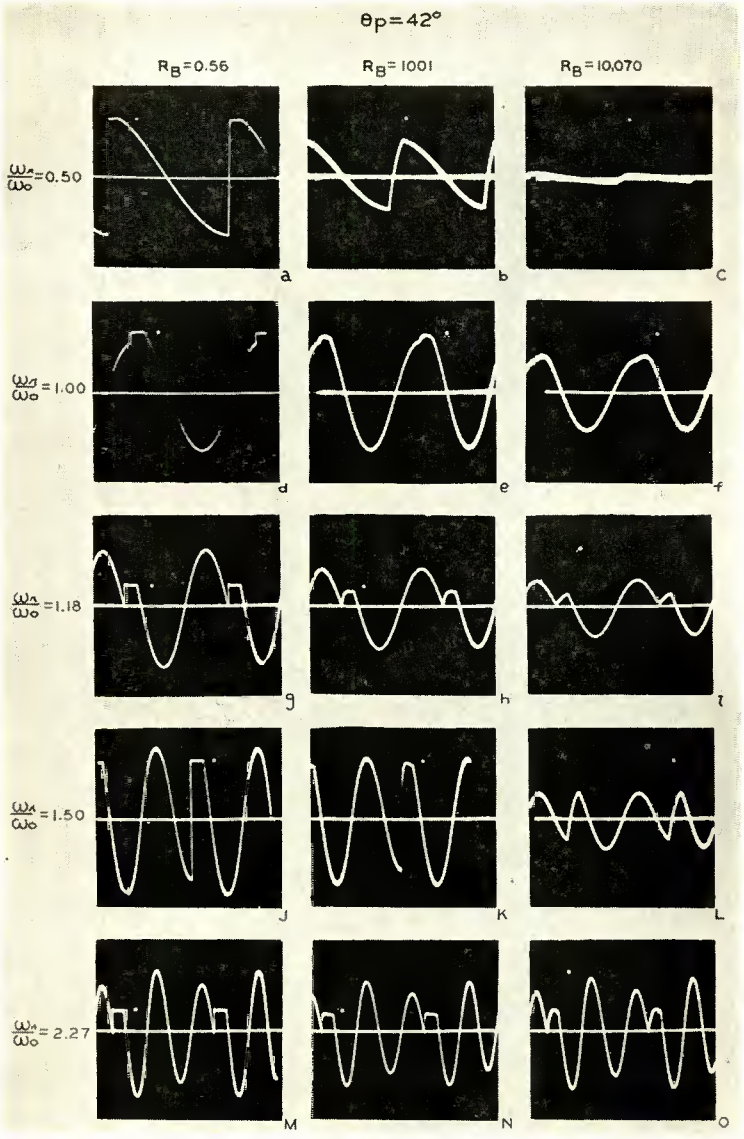

Fig. 6—Oscillograms of v/V_B for different operating parameters. White dot represents $v/V_B = 1.00$.

puted values of ω_r/ω_0 for resonant operation and including circuit losses are not tabulated in Table 1 because these computations can only be made by trial and error process. It was mentioned above that if circuit losses were neglected, resonance was obtained when $V_C' = 0$, provided also that I_L' was positive. The resonant conditions shown in the

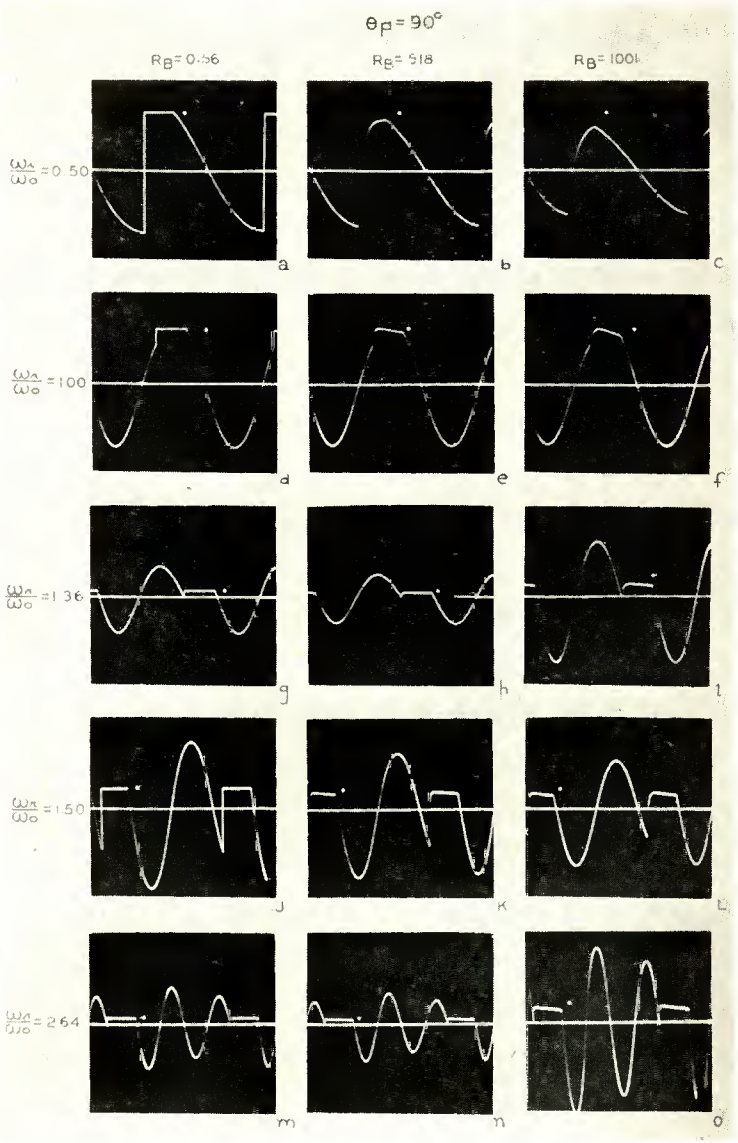

Fig. 7—Oscillograms of v/V_B for different operating parameters. White dot represents $v/V_B = 1.00$.

appropriate photographs of Figures 6, 7, 8, and 9 substantiate this statement. V_C' is approximately zero even though circuit losses were present and even though R_E was varied over a wide range. Although no proof is available, it would appear that even when circuit losses

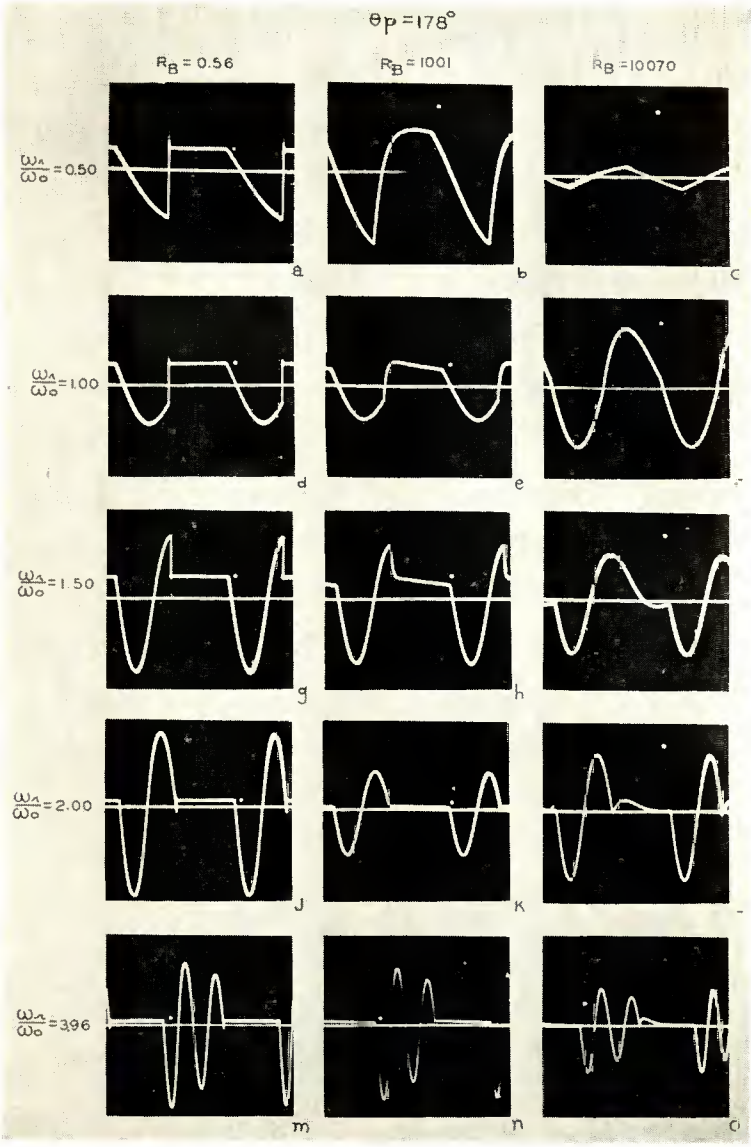

Fig. 8—Oscillograms of v/V_B for different operating parameters. White dot represents $v/V_B = 1.00$.

are present, resonance, i.e., maximum of peak value of v, is obtained when $V_C' = 0$.

In order to carry out calculations of the operating conditions shown in Figures 6, 7, 8, and 9, it was necessary to determine the correct

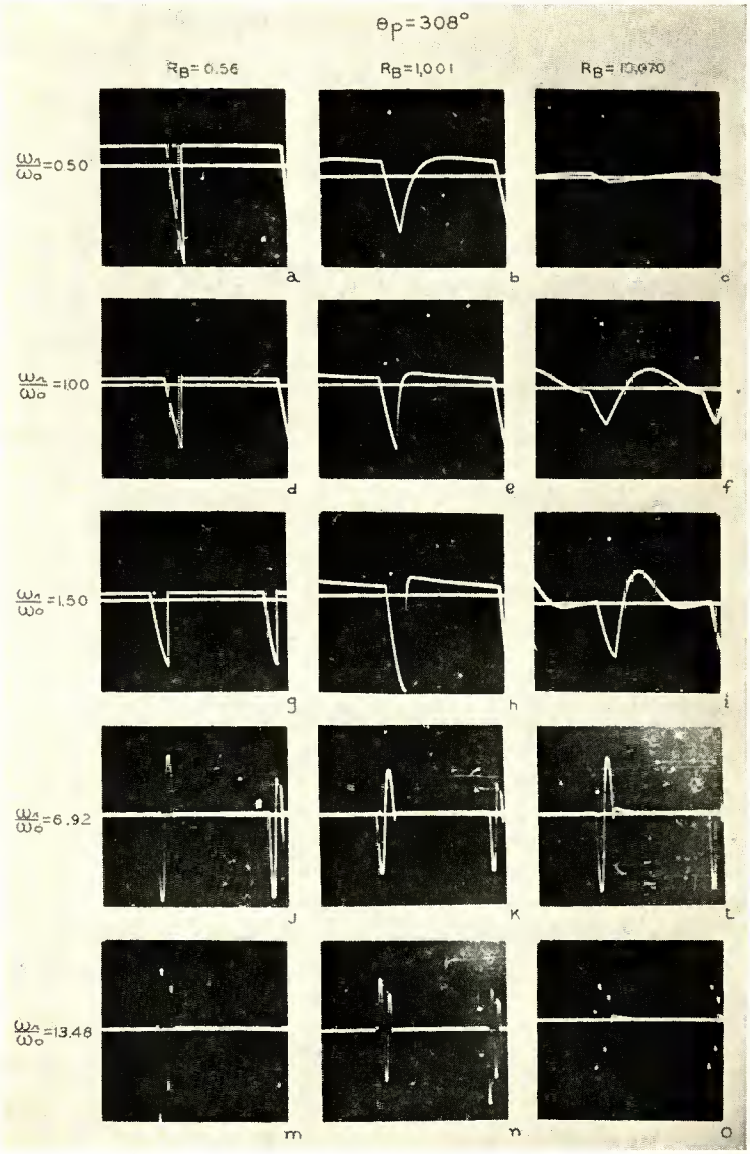

Fig. 9—Oscillograms of v/V_B for different operating parameters. White dot represents $v/V_B = 1.00$.

value of the circuit parameters. Measurement of R_L was complicated by its dependence upon frequency. With direct current, the value of R_L was 131 ohms. With alternating current, values of R_L of 684 ohms and 2,134 ohms were obtained at 120 and 1,000 cycles per second, respectively. As a compromise, the value of R_L was determined by measuring the decrement, α_0, from several oscillograms. From the average value of α_0, $Q_L = 13.87$ and $R_L = 431$ ohms were obtained.

Difficulty was also experienced in determining the correct value of θ_p. For the initial circuit adjustment, the desired value of θ_p was obtained by adjusting the switch contacts until the proper average voltage was present across a resistive load. The resistive load was then replaced by the tuned circuit, and the photographs were taken. It was subsequently found that this method of determining θ_p was not sufficiently accurate. Direct measurement of θ_p from oscillograms also was not sufficiently accurate. The final method used for determining θ_p was an indirect one. It is indicated above that, at resonance, $V_C'/V_B = 0$. The value of ω_r/ω_0 for resonance can be measured accurately. Therefore, trial and error calculations can be used until a value of θ_p is obtained for which $V_C'/V_B = 0$. This value of θ_p is then used in all other calculations. Normally, this method is sufficiently accurate so that values of θ_p can be determined to tenths of a degree.

Table 1—Tabulation of Computed and Measured Values of ω_r/ω_0 for First and Second Resonance

Resonant Number	θ_p	Computed Approx. ω_r/ω_0 (Eq. 25)	Measured ω_r/ω_0
1	42°	1.131	1.18
2	42°	2.262	2.27
1	90°	1.333	1.36
2	90°	2.667	2.64
1	178°	1.978	2.00
2	178°	3.956	3.96
1	308°	6.92	6.92
2	308°	13.84	13.48

Using values of R_L and θ_p determined as indicated above, computed values of V_C/V_B and V_C'/V_B agreed with the measured values within a few per cent except for calculations of oscillograms of Figure 9. In this case, since θ_p is so large, the direct-current rather than the alternating-current resistance of the coil becomes significant. Calculations using $R_L = 431$ ohms gave poor agreement with measurement whereas calculations using $R_L = 131$ ohms gave much better agreement.

Conclusions

From the preceding data, it is seen that the analytic results are capable of yielding detailed and accurate solutions for a circuit configuration involving a battery, perfect switch, and a parallel resonant circuit. As an example, Figure 10 shows typical measured and computed wave shapes. The analytic results will therefore be useful for studying any circuit that approximates the indicated circuit configuration. In many vacuum tube circuits, the operation of the vacuum

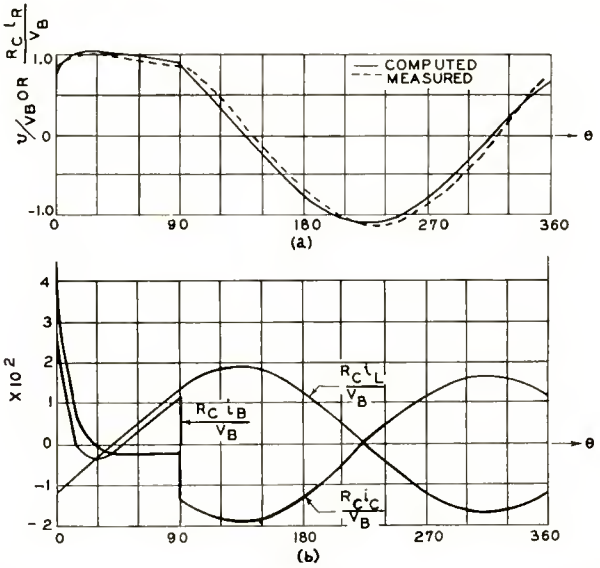

Fig. 10—Computed and measured voltage and currents for linear-power-transfer test circuit of Figure 5 with $\theta_p = 90°$, $\omega_r/\omega_o = 1$, $R_n = 1{,}001\Omega$. See Figure 7f for oscillogram.

tube is analogous to a switch.[2] The major discrepancy in this analogy is that a switch is a bidirectional current carrying device whereas the vacuum tube conducts current in only one direction. However, in some vacuum tube circuits the flow of current is unidirectional for other reasons. In those cases, the switch analogy can be used if the vacuum tube operates over a small enough portion of its characteristic so that the vacuum tube voltage and current are essentially linearly related. If this linear relationship is not valid, then the battery and tube combination can be looked upon as a nonlinear power source, $I_B = F(v)$, during the time the tube is conducting. In this event,

[2] This includes a gas tube which is closely analogous to a switch, provided that the operation of the gas tube is in the forward direction.

Equation (10) of the original development must be replaced by a new equation. This equation, developed from Equation (8), is:

$$\frac{d^2(v/V_B)}{d\theta^2} + \left[\frac{1}{Q_c} + \frac{1}{Q_L} - \frac{1}{\omega_0 C} F'(v)\right] \frac{d(v/V_B)}{d\theta}$$

$$+ \left(\frac{\omega_r}{\omega_0}\right)^2 \left[\left(1 + \frac{R_L}{R_C}\right) \frac{v}{V_B} - \frac{R_L}{V_B} F(v)\right] = 0. \qquad (27)$$

If $F(v)$ is known and can be expressed analytically, Equation (27) will, in general, yield a nonlinear differential equation. If a solution of this differential equation is available, a composite solution can be obtained in the same manner as that used for the linear power source. It is more probable that a solution of the nonlinear differential equation will not be available, at least not in such a form as to permit mathematical manipulation. In this event, it is believed that an approximate solution may be possible by dividing the $F(v)$ characteristic into linear regions, by solving the resulting linear differential equation for each region, and by obtaining a composite solution by matching the boundary conditions. Once a composite solution has been obtained, Fourier analysis can be used to obtain a series solution that may be used for further mathematical manipulation.

The subdivided cycle method of solution employed in this paper may be useful for obtaining solutions in similar problems. The resulting solution is usually relatively simple compared to a single solution for the entire operating cycle.

Although no extensive calculations have been made, it is the opinion of the writer that the switch analogue solutions can be applied quantitatively to oscillators, class C amplifiers, and many pulsed circuits. The writer has used the results contained in this paper to analyze quantitatively the sinusoidal and nonsinusoidal operation of separately excited and self-excited circuits employing a secondary-emitter tube.

Appendix I

Solutions for Special Values of Circuit Parameters

In the main body, the solution of the linear-power-transfer circuit is contained in Equations (22) and (23) in conjunction with Equations (14) and (15). However, for certain special values of the circuit parameters, the equations referred to may not be adequate. For certain other special values of the circuit parameters, the solution may be simplified considerably. In this appendix, five cases of special values of the circuit parameters will be considered and solutions obtained.

Case 1—When $\sqrt{\beta_0^2 - \alpha_0^2}\ (2\pi - \theta_p) = n\pi$ or $\sqrt{\alpha_c^2 - \beta_c^2}\ \theta_p = i\,n\pi$.

For this case, the simultaneous Equations (22) and (23) become linearly dependent, with the result that a single relationship between V_C/V_B and V_C'/V_B is obtained. This condition is brought about because V_C/V_B and V_C'/V_B are no longer independent variables under the condition specified above. A new set of independent variables is required. A convenient pair consists of V_C/V_B and $R_C\,I_L/V_B$. (I_L is the current through the inductor L when the switch is opened, i.e., at $\theta = \theta_p$.) Each solution of the differential Equations (10) and (11) involves two arbitrary constants. These arbitrary constants are determined by using the boundary conditions that at $\theta = \theta_p$, $v/V_B = V_C/V_B$, and $R_C i_L/V_B = R_C I_L/V_B$. Both v/V_B and $R_C i_L/V_B$ are continuous at $\theta = \theta_p$. The resulting solutions, which may be compared with Equations (14) and (15), are

$$\frac{v}{V_B} = \frac{R_L}{R_B}\left(\frac{\omega_r}{\beta_c\,\omega_0}\right)^2 + \left[\left\{\frac{V_C}{V_B} - \frac{R_L}{R_B}\left(\frac{\omega_r}{\beta_c\,\omega_0}\right)^2\right\}\left\{-\frac{\left(Q_C\alpha_c - \frac{Q_C}{Q_L}\right)}{Q_C\sqrt{\alpha_c^2 - \beta_c^2}}\,e^{+\alpha_c\theta_p}\cosh\sqrt{\alpha_c^2 - \beta_c^2}\,\theta_p - e^{+\alpha_c\theta_p}\sinh\sqrt{\alpha_c^2 - \beta_c^2}\,\theta_p\right\} - \left\{\frac{R_C\,I_L}{V_B} - \frac{R_C}{R_B}\left(\frac{\omega_r}{\beta_c\,\omega_0}\right)^2\right\}\left\{\frac{1}{Q_C\sqrt{\alpha_c^2 - \beta_c^2}}\,e^{+\alpha_c\theta_p}\cosh\sqrt{\alpha_c^2 - \beta_c^2}\,\theta_p\right\}\right]e^{-\alpha_c\theta}\sinh\sqrt{\alpha_c^2 - \beta_c^2}\,\theta$$

$$+\left[\left\{\frac{R_C I_L}{V_B} - \frac{R_C}{R_B}\left(\frac{\omega_r}{\beta_c\,\omega_0}\right)^2\right\}\left\{-\frac{1}{Q_C\sqrt{\alpha_c^2 - \beta_c^2}}\,e^{+\alpha_c\theta_p}\sinh\sqrt{\alpha_c^2 - \beta_c^2}\,\theta_p\right\} - \left\{\frac{V_C}{V_B} - \frac{R_L}{R_B}\left(\frac{\omega_r}{\beta_c\,\omega_0}\right)^2\right\}\left\{-\frac{\left(Q_C\alpha_c - \frac{Q_C}{Q_L}\right)}{Q_C\sqrt{\alpha_c^2 - \beta_c^2}}\,e^{+\alpha_c\theta_p}\sinh\sqrt{\alpha_c^2 - \beta_c^2}\,\theta_p - e^{+\alpha_c\theta_p}\cosh\sqrt{\alpha_c^2 - \beta_c^2}\,\theta_p\right\}\right]e^{-\alpha_c\theta}\cosh\sqrt{\alpha_c^2 - \beta_c^2}\,\theta$$

$$\text{(valid from } \theta = 0 \text{ to } \theta = \theta_p\text{)}, \qquad \text{(1-1)}$$

and

$$\frac{v}{V_B} = -\frac{1}{Q_C\sqrt{\beta_0^2-\alpha_0^2}}\left[\frac{R_C I_L}{V_B} + (1-Q_C\alpha_0)\frac{V_C}{V_B}\right]$$

$$e^{-\alpha_0(\theta-\theta_p)}\sin\sqrt{\beta_0^2-\alpha_0^2}\,(\theta-\theta_p)$$

$$+\frac{V_C}{V_B}e^{-\alpha_0(\theta-\theta_p)}\cos\sqrt{\beta_0^2-\alpha_0^2}\,(\theta-\theta_p)$$

$$\text{(valid from } \theta=\theta_p \text{ to } \theta=2\pi). \qquad (1\text{-}2)$$

V_C/V_B and $R_C I_L/V_B$ are next determined by applying the additional boundary conditions that v/V_B and $R_C i_L/V_B$ are also continuous at $\theta = 0\ (2\pi)$. These boundary conditions yield the following simultaneous equations which replace Equations (22) and (23).

$$\left[\frac{\left(Q_C\alpha_c - \frac{Q_C}{Q_L}\right)}{Q_C\sqrt{\alpha_c^2-\beta_c^2}}e^{+\alpha_c\theta_p}\sinh\sqrt{\alpha_c^2-\beta_c^2}\,\theta_p + e^{+\alpha_c\theta_p}\cosh\sqrt{\alpha_c^2-\beta_c^2}\,\theta_p\right.$$

$$+\frac{(1-Q_C\alpha_0)}{Q_C\sqrt{\beta_0^2-\alpha_0^2}}e^{-\alpha_0(2\pi-\theta_p)}\sin\sqrt{\beta_0^2-\alpha_0^2}\,(2\pi-\theta_p)$$

$$\left.-e^{\alpha_0(2\pi-\theta_p)}\cos\sqrt{\beta_0^2-\alpha_0^2}\,(2\pi-\theta_p)\right]\frac{V_C}{V_B}$$

$$+\left[\frac{1}{Q_C\sqrt{\alpha_c^2-\beta_c^2}}e^{+\alpha_c\theta_p}\sinh\sqrt{\alpha_c^2-\beta_c^2}\,\theta_p + \frac{1}{Q_C\sqrt{\beta_0^2-\alpha_0^2}}\right.$$

$$\left.e^{-\alpha_0(2\pi-\theta_p)}\sin\sqrt{\beta_0^2-\alpha_0^2}\,(2\pi-\theta_p)\right]\frac{R_C I_L}{V_B}$$

$$=-\frac{R_L}{R_B}\left(\frac{\omega_r}{\beta_c\,\omega_0}\right)^2\left\{1-\frac{\left(Q_C\alpha_c-\frac{Q_C}{Q_L}\right)}{Q_C\sqrt{\alpha_c^2-\beta_c^2}}e^{+\alpha_c\theta_p}\sinh\sqrt{\alpha_c^2-\beta_c^2}\,\theta_p\right.$$

$$\left. - e^{+\alpha_c \theta_p} \cosh \sqrt{\alpha_c^2 - \beta_c^2}\, \theta_p \right]$$

$$+ \frac{R_C}{R_B} \left(\frac{\omega_r}{\beta_c\, \omega_0} \right)^2 \frac{1}{Q_C \sqrt{\alpha_c^2 - \beta_c^2}}\, e^{+\alpha_c \theta_p} \sinh \sqrt{\alpha_c^2 - \beta_c^2}\, \theta_p, \qquad (1\text{-}3)$$

$$\left[- \frac{\dfrac{R_C Q_C}{R_L Q_L}}{Q_C \sqrt{\alpha_c^2 - \beta_c^2}}\, e^{+\alpha_c \theta_p} \sinh \sqrt{\alpha_c^2 - \beta_c^2}\, \theta_p - \frac{\dfrac{R_C Q_C}{R_L Q_L}}{Q_C \sqrt{\beta_0^2 - \alpha_0^2}} \right.$$

$$\left. e^{-\alpha_0 (2\pi - \theta_p)} \sin \sqrt{\beta_0^2 - \alpha_0^2}\, (2\pi - \theta_p) \right] \frac{V_C}{V_B}$$

$$+ \left[- \frac{\left(Q_C \alpha_c - \dfrac{Q_C}{Q_L} \right)}{Q_C \sqrt{\alpha_c^2 - \beta_c^2}}\, e^{+\alpha_c \theta_p} \sinh \sqrt{\alpha_c^2 - \beta_c^2}\, \theta_p + e^{\alpha_c \theta_p} \cosh \sqrt{\alpha_c^2 - \beta_c^2}\, \theta_p \right.$$

$$- \frac{(1 - Q_C \alpha_0)}{Q_C \sqrt{\beta_0^2 - \alpha_0^2}}\, e^{-\alpha_0 (2\pi - \theta_p)} \sin \sqrt{\beta_0^2 - \alpha_0^2}\, (2\pi - \theta_p)$$

$$\left. - e^{-\alpha_0 (2\pi - \theta_p)} \cos \sqrt{\beta_0^2 - \alpha_0^2}\, (2\pi - \theta_p) \right] \frac{R_C I_L}{V_B}$$

$$= - \frac{R_C}{R_B} \left(\frac{\omega_r}{\beta_c\, \omega_0} \right)^2 \left[1 - e^{+\alpha_c \theta_p} \cosh \sqrt{\alpha_c^2 - \beta_c^2}\, \theta_p \right.$$

$$\left. + \frac{Q_C \alpha_c}{Q_C \sqrt{\alpha_c^2 - \beta_c^2}}\, e^{+\alpha_c \theta_p} \sinh \sqrt{\alpha_c^2 - \beta_c^2}\, \theta_p \right]. \qquad (1\text{-}4)$$

Equations (1-3) and (1-4) may be used in place of Equations (22) and (23). However, for the special case under consideration here,

i.e., when $\sqrt{\beta_0^2 - \alpha_0^2}\,(2\pi - \theta_p) = n\pi$ or $\sqrt{\alpha_c^2 - \beta_c^2}\,\theta_p = in\pi$, the above equations must be used to obtain a solution. If desired, valid equations connecting V_C/V_B, V_C'/V_B, and $R_C I_L/V_B$ can be obtained readily by using Equations (20), (21), (1-1), or (1-2).

Case 2—When $\sqrt{\beta_0^2 - \alpha_0^2} = 0$ or $\sqrt{\alpha_c^2 - \beta_c^2} = 0$.

As was mentioned in the main body, the solutions and equations are correct, regardless of whether $\sqrt{\beta_0^2 - \alpha_0^2}$ and $\sqrt{\alpha_c^2 - \beta_c^2}$ are rea or imaginary, provided that suitable transformations are made from hyperbolic to trigonometric functions or vice versa. The solutions and equations are also correct if $\sqrt{\beta_0^2 - \alpha_0^2}$ and $\sqrt{\alpha_c^2 - \beta_c^2}$ are zero, provided this limiting case is approached properly; this can be accomplished by replacing cos and cosh functions by unity and sin and sinh functions by their arguments whenever the limit is required.

Case 3—When $R_B = 0$.

For this ideal case where the battery internal resistance, R_B, is zero, the battery current may be infinitely large. Consequently, a discontinuity in v/V_B is permissible at $\theta = 0$ since v/V_B must always be unity immediately after the switch is closed. Also, v/V_B must be unity during the time the switch is closed, so the solution from $\theta = 0$ to $\theta = \theta_p$ is $v/V_B = 1.0$. Since v/V_B must be continuous at $\theta = \theta_p$, $V_C/V_B = 1.0$. Equations for V_C'/V_B, $R_C I_L/V_B$, and $R_C I_L'/V_B$ are to be determined next.

During the time the switch is closed, i.e., from $\theta = 0$ to $\theta = \theta_p$, the following equation is valid.

$$L\frac{di_L}{dt} + R_L i_L = V_B. \qquad (1\text{-}5)$$

The solution of this differential equation has one arbitrary constant. This constant may be determined from the boundary condition that $R_C i_L/V_B = R_C I_L'/V_B$ at $\theta = 0$. The final solution is

$$\frac{R_C i_L}{V_B} = \frac{R_C}{R_L}\left[1 - e^{-\frac{\theta}{Q_L}} + \frac{R_L}{R_C}\,\frac{R_C I_L'}{V_B}\,e^{-\frac{\theta}{Q_L}}\right]. \qquad (1\text{-}6)$$

Using the boundary condition that $R_C i_L/V_B = R_C I_L/V_B$ at $\theta = \theta_p$, one obtains the following relation between $R_C I_L/V_B$ and $R_C I_L'/V_B$.

$$\frac{R_C I_L}{V_B} = \frac{R_C}{R_L}\left[1 - e^{-\frac{\theta_p}{Q_L}} + \frac{R_L}{R_C}\,\frac{R_C I_L'}{V_B}\,e^{-\frac{\theta_p}{Q_L}}\right] \qquad (1\text{-}7)$$

$R_C I_L/V_B$ can be obtained by substituting $\theta = \theta_p$ into Equation (21), and $R_C I_L'/V_B$ can be obtained by substituting $\theta = 2\pi$ into the same equation. The results are

$$\frac{R_C I_L}{V_B} = Q_C\alpha_0 - 1 - Q_C\sqrt{\beta_0^2 - \alpha_0^2}\left[\frac{V_C'}{V_B}\,e^{+\alpha_0(2\pi-\theta_p)}\csc\sqrt{\beta_0^2-\alpha_0^2}\,(2\pi-\theta_p) - \cot\sqrt{\beta_0^2-\alpha_0^2}\,(2\pi-\theta_p)\right], \qquad (1\text{-}8)$$

$$\frac{R_C I_L'}{V_B} = \frac{V_C'}{V_B}\left[Q_C\alpha_0 - 1 - Q_C\sqrt{\beta_0^2-\alpha_0^2}\cot\sqrt{\beta_0^2-\alpha_0^2}\,(2\pi-\theta_p)\right] + Q_C\sqrt{\beta_0^2-\alpha_0^2}\,e^{-\alpha_0(2\pi-\theta_p)}\csc\sqrt{\beta_0^2-\alpha_0^2}\,(2\pi-\theta_p). \qquad (1\text{-}9)$$

Substitute (1-8) and (1-9) into (1-7) and solve for V_C'/V_B.

$$\frac{V_C'}{V_B} = e^{+\frac{\theta_p}{Q_L}}\left\{1 - Q_C\alpha_0 + \frac{R_C}{R_L}\left(1 - e^{-\frac{\theta_p}{Q_L}}\right) + Q_C\sqrt{\beta_0^2-\alpha_0^2}\left[e^{-\frac{\theta_p}{Q_L}-\alpha_0(2\pi-\theta_p)}\csc\sqrt{\beta_0^2-\alpha_0^2}\,(2\pi-\theta_p) - \cot\sqrt{\beta_0^2-\alpha_0^2}\,(2\pi-\theta_p)\right]\right\}$$

$$\left\{1 - Q_C\alpha_0 - Q_C\sqrt{\beta_0^2-\alpha_0^2}\left[e^{+\frac{\theta_p}{Q_L}+\alpha_0(2\pi-\theta_p)}\csc\sqrt{\beta_0^2-\alpha_0^2}\,(2\pi-\theta_p) - \cot\sqrt{\beta_0^2-\alpha_0^2}\,(2\pi-\theta_p)\right]\right\}^{-1} \qquad (1\text{-}10)$$

Substitute (1-10) into (1-8).

$$\frac{R_C I_L}{V_B} = e^{+\frac{\theta_p}{Q_L}}\left\{-(1 - 2Q_C\alpha_0 + Q_C^2\beta_0^2)\,e^{-\frac{\theta_p}{Q_L}} - \frac{R_C}{R_L}\left(1 - e^{-\frac{\theta_p}{Q_L}}\right)Q_C\sqrt{\beta_0^2-\alpha_0^2}\,e^{+\alpha_0(2\pi-\theta_p)}\csc\sqrt{\beta_0^2-\alpha_0^2}\,(2\pi-\theta_p)\right\}$$

$$\left\{1 - Q_C\alpha_0 - Q_C\sqrt{\beta_0^2 - \alpha_0^2}\left[e^{+\frac{\theta_p}{Q_L} + \alpha_0(2\pi - \theta_p)}\csc\sqrt{\beta_0^2 - \alpha_0^2}\,(2\pi - \theta_p)\right.\right.$$

$$\left.\left. - \cot\sqrt{\beta_0^2 - \alpha_0^2}\,(2\pi - \theta_p)\right]\right\}^{-1} \qquad (1\text{-}11)$$

Substitute (1-11) into (1-7) and solve for $R_C I_L'/V_B$.

$$\frac{R_C I_L'}{V_B} = e^{+\frac{\theta_p}{Q_L}}\left\{-(1 - 2\,Q_C\alpha_0 + Q_C^2\beta_0^2)\right.$$

$$\frac{R_C}{R_L}\left(1 - e^{-\frac{\theta_p}{Q_L}}\right)\left[1 - Q_C\alpha_0 + Q_C\sqrt{\beta_0^2 - \alpha_0^2}\,\cot\sqrt{\beta_0^2 - \alpha_0^2}\,(2\pi - \theta_p)\right]\Big\}$$

$$\left\{1 - Q_C\alpha_0 - Q_C\sqrt{\beta_0^2 - \alpha_0^2}\left[e^{+\frac{\theta_p}{Q_L} + \alpha_0(2\pi - \theta_p)}\csc\sqrt{\beta_0^2 - \alpha_0^2}\,(2\pi - \theta_p)\right.\right.$$

$$\left.\left. - \cot\sqrt{\beta_0^2 - \alpha_0^2}\,(2\pi - \theta_p)\right]\right\}^{-1} \qquad (1\text{-}12)$$

Equations (1-10), (1-11), and (1-12) together with the fact that $V_C/V_B = 1.0$ complete the solution of this case. During the time the switch is closed $v/V_B = 1.0$, and while the switch is open v/V_B can be obtained by using either Equation (15) or (1-2). During the time the switch is closed $R_C i_L/V_B$ can be obtained by using Equation (1-6); while the switch is open $R_C i_L/V_B$ can be obtained by using Equation (21).

If, now, in addition to $R_B = 0$, $\sqrt{\beta_0^2 - \alpha_0^2}\,(2\pi - \theta_p) = n\pi$, then Equation (1-10) indicates that $V_C'/V_B = (-1)^n\, e^{-\alpha_0(2\pi - \theta_p)}$. This result can be obtained by direct reasoning since V_C'/V_B must now be an odd or even power of -1 times the value of V_C/V_C $(= 1.0)$ times the exponential decay factor. For the conditions just specified, Equation (1-11) simplifies to

$$\frac{R_C I_L}{V_B} = \frac{\dfrac{R_C}{R_L}\left(1 - e^{-\frac{\theta_p}{Q_L}}\right)}{1 - (-1)^n\, e^{-\frac{\theta_p}{Q_L} - \alpha_0(2\pi - \theta_p)}}. \qquad (1\text{-}13)$$

Case 4—When $R_G = \infty$ and $R_L = 0$.

If the circuit elements are lossless, $R_G = \infty$, and $R_L = 0$. For this case, then, the derived circuit constants have the following values [see Equations (5), (6), (7), (16), (17), (18), and (19) respectively]:

$$Q_C = \infty, \tag{1-14}$$

$$Q_L = \infty, \tag{1-15}$$

$$Q_C' = \omega_0 C R_B \tag{1-16}$$

$$\alpha_c = \frac{1}{2\,Q_C'} \tag{1-17}$$

$$\alpha_0 = 0, \tag{1-18}$$

$$\beta_c = \frac{\omega_r}{\omega_0}, \tag{1-19}$$

$$\beta_0 = \frac{\omega_r}{\omega_0}. \tag{1-20}$$

For convenience, the following quantity is introduced:

$$\gamma_c = \sqrt{\alpha_c^2 - \beta_c^2}. \tag{1-21}$$

Simplified solutions are obtainable by direct substitution of the above values into different equations. Thus, Equations (14) and (15) become

$$\frac{v}{V_B} = \left[e^{+\alpha_c \theta_p} \operatorname{csch} \gamma_c \theta_p \frac{V_C}{V_B} - \coth \gamma_c \theta_p \frac{V_C'}{V_B} \right] e^{-\alpha_c \theta} \sinh \gamma_c \theta + \frac{V_C'}{V_B} e^{-\alpha_c \theta} \cosh \gamma_c \theta$$

$$\text{(valid from } \theta = 0 \text{ to } \theta = \theta_p). \tag{1-22}$$

$$\frac{v}{V_B} = \left[\csc \frac{\omega_r}{\omega_0} (2\pi - \theta_p) \frac{V_C'}{V_B} - \cot \frac{\omega_r}{\omega_0} (2\pi - \theta_p) \frac{V_C}{V_B} \right] \sin \frac{\omega_r}{\omega_0} (\theta - \theta_p)$$

$$+ \frac{V_C}{V_B} \cos \frac{\omega_r}{\omega_0} (\theta - \theta_p)$$

(valid from $\theta = \theta_p$ to $\theta = 2\pi$). (1-23)

Simultaneous Equations (22) and (23) become

$$\left[\frac{\omega_0}{\omega_r} \alpha_c + \frac{\omega_0}{\omega_r} \gamma_c \coth \gamma_c \theta_p + \cot \frac{\omega_r}{\omega_0} (2\pi - \theta_p) \right] \frac{V_C}{V_B}$$

$$- \left[\csc \frac{\omega_r}{\omega_0} (2\pi - \theta_p) + \frac{\omega_0}{\omega_r} \gamma_c e^{-\alpha_c \theta_p} \operatorname{csch} \gamma_c \theta_p \right] \frac{V_C'}{V_B}$$

$$= 2 \frac{\omega_0}{\omega_r} \alpha_c. \quad (1\text{-}24)$$

$$\left[\frac{\omega_0}{\omega_r} \gamma_c e^{+\alpha_c \theta_p} \operatorname{csch} \gamma_c \theta_p + \csc \frac{\omega_r}{\omega_0} (2\pi - \theta_p) \right] \frac{V_C}{V_B}$$

$$+ \left[\frac{\omega_0}{\omega_r} \alpha_c - \frac{\omega_0}{\omega_r} \gamma_c \coth \gamma_c \theta_p - \cot \frac{\omega_r}{\omega_0} (2\pi - \theta_p) \right] \frac{V_C'}{V_B}$$

$$= 2 \frac{\omega_0}{\omega_r} \alpha_c. \quad (1\text{-}25)$$

Similarly, Equations (1-1) and (1-2) and simultaneous Equations (1-3) and (1-4) become, respectively,

$$\frac{v}{V_B} = \left[\left(2 - 2 \frac{R_B I_L}{V_B} - \frac{V_C}{V_B} \right) \frac{\alpha_c}{\gamma_c} e^{+\alpha_c \theta_p} \cosh \gamma_c \theta_p \right.$$

$$\left. - \frac{V_C}{V_B} e^{+\alpha_c \theta_p} \sinh \gamma_c \theta_p \right] e^{-\alpha_c \theta} \sinh \gamma_c \theta$$

$$- \left[\left(2 - 2 \frac{R_B I_C}{V_B} - \frac{V_C}{V_B} \right) \frac{\alpha_c}{\gamma_c} e^{+\alpha_c \theta_p} \sinh \gamma_c \theta_p \right.$$

$$-\frac{V_C}{V_B} e^{+\alpha_c \theta_p} \cosh \gamma_c \theta_p \Bigg] e^{-\alpha_c \theta} \cosh \gamma_c \theta$$

(valid from $\theta = 0$ to $\theta = \theta_p$). (1-26)

$$\frac{v}{V_B} = -2 \frac{\omega_0}{\omega_r} \alpha_c \left[\frac{R_B I_L}{V_B} \right] \sin \frac{\omega_r}{\omega_0} (\theta - \theta_p) + \frac{V_C}{V_B} \cos \frac{\omega_r}{\omega_0} (\theta - \theta_p)$$

(valid from $\theta = \theta_p$ to $\theta = 2\pi$). (1-27)

$$\left[\frac{\alpha_c}{\gamma_c} e^{+\alpha_c \theta_p} \sinh \gamma_c \theta_p + e^{\alpha_c \theta_p} \cosh \gamma_c \theta_p \right.$$

$$\left. - \cos \frac{\omega_r}{\omega_0} (2\pi - \theta_p) \right] \frac{V_C}{V_B} + \left[2 \frac{\alpha_c}{\gamma_c} e^{+\alpha_c \theta_p} \sinh \gamma_c \theta_p \right.$$

$$\left. + 2 \frac{\omega_0}{\omega_r} \alpha_c \sin \frac{\omega_r}{\omega_0} (2\pi - \theta_p) \right] \frac{R_B I_L}{V_B} = 2 \frac{\alpha_c}{\gamma_c} e^{+\alpha_c \theta_p} \sinh \gamma_c \theta_p \quad (1\text{-}28)$$

$$\frac{\omega_r}{2 \omega_0 \alpha_c} \left[\frac{\omega_r}{\omega_0 \gamma_c} e^{+\alpha_c \theta_p} \sinh \gamma_c \theta_p + \sin \frac{\omega_r}{\omega_0} (2\pi - \theta_p) \right] \frac{V_C}{V_B}$$

$$+ \left[\frac{\alpha_c}{\gamma_c} e^{+\alpha_c \theta_p} \sinh \gamma_c \theta_p - e^{+\alpha_c \theta_p} \cosh \gamma_c \theta_p + \cos \frac{\omega_r}{\omega_0} (2\pi - \theta_p) \right] \frac{R_B I_L}{V_B}$$

$$= 1 - e^{+\alpha_c \theta_p} \cosh \gamma_c \theta_p + \frac{\alpha_c}{\gamma_c} e^{+\alpha_c \theta_p} \sinh \gamma_c \theta_p. \quad (1\text{-}29)$$

Case 5—When $R_C = \infty$, $R_L = 0$, and $R_B = 0$.

If both circuit elements and battery are lossless, the solution reduces to a simple form. During the time the switch is closed, i.e., from $\theta = 0$ to $\theta = \theta_p$, $v/V_B = 1.0$ for the same reasons indicated for Case 3. Therefore, $V_C/V_B = 1.0$. V_C'/V_B, $\dfrac{I_L}{\omega_r C V_B}$, and $\dfrac{I_L'}{\omega_r C V_B}$ can be obtained from Equations (1-10), (1-11), and (1-12) respectively, provided the limiting values are approached in a suitable manner.

Another method of obtaining the values of V_C'/V_B and $\dfrac{I_L}{\omega_r C V_B}$ is to time-average v/V_B from $\theta = 0$ to $\theta = 2\pi$ using Equations (1-23) and (1-27) and to equate the result to zero. In any event, the following solutions are obtained for these boundary values:

$$\frac{V_C'}{V_B} = \frac{\dfrac{\omega_r}{\omega_0}\theta_p \sin\dfrac{\omega_r}{\omega_0}(2\pi - \theta_p)}{1 - \cos\dfrac{\omega_r}{\omega_0}(2\pi - \theta_p)} - 1, \tag{1-30}$$

$$\frac{I_L}{\omega_r C V_B} = \frac{\dfrac{\omega_r}{\omega_0}\theta_p + \sin\dfrac{\omega_r}{\omega_0}(2\pi - \theta_p)}{1 - \cos\dfrac{\omega_r}{\omega_0}(2\pi - \theta_p)}. \tag{1-31}$$

$$\frac{I_L'}{\omega_r C V_B} = \frac{\dfrac{\omega_r}{\omega_0}\theta_p \cos\dfrac{\omega_r}{\omega_0}(2\pi - \theta_p) + \sin\dfrac{\omega_r}{\omega_0}(2\pi - \theta_p)}{1 - \cos\dfrac{\omega_r}{\omega_0}(2\pi - \theta_p)}. \tag{1-32}$$

The expression for v/V_B during the time the switch is open is

$$\frac{v}{V_B} = -A \sin\frac{\omega_r}{\omega_0}(\theta - \theta_p) + \cos\frac{\omega_r}{\omega_0}(\theta - \theta_p)$$

$$= -\sqrt{1 + A^2}\sin\left\{\frac{\omega_r}{\omega_0}(\theta - \theta_p) - \cot^{-1}A\right\}$$

(valid from $\theta = \theta_p$ to $\theta = 2\pi$), (1-33)

where $A = \dfrac{\dfrac{\omega_r}{\omega_0}\theta_p + \sin\dfrac{\omega_r}{\omega_0}(2\pi - \theta_p)}{1 - \cos\dfrac{\omega_r}{\omega_0}(2\pi - \theta_p)}$.

The current through the capacitor and inductor during the time the switch is open can be readily obtained from Equation (1-33). At the moment that the switch is closed, an infinitely large capacitor current (provided $V_C' \neq V_B$) is required to change the capacitor voltage to V_B. During the time the switch is closed, the capacitor current is zero. During the same period, the inductor current changes linearly from the value I_L' at $\theta = 0$ to the value I_L at $\theta = \theta_p$. These two quantities are related to each other by the following expression:

$$\frac{I_L}{\omega_r C V_B} = \frac{I_L'}{\omega_r C V_B} + \frac{\omega_r}{\omega_0} \theta_p. \tag{1-34}$$

RCA TECHNICAL PAPERS†

Second Quarter, 1952

Any request for copies of papers listed herein should be addressed to the publication to which credited.*

"Adjustment Procedure for Kinescope Ion-Trap Magnets," *RCA Application Note AN-153*, RCA Tube Department, Harrison, N. J. (April) 1952

"An Analysis of the Injection Locking of Magnetrons Used in Amplitude-Modulated Transmitters," J. S. Donal, Jr. and K. K. N. Chang, *RCA Review* (June) 1952

"Anomalous Interference Films on Glass by Chemical Treatment," F. H. Nicoll, *Jour. Opt. Soc. Amer.* (April) 1952

"An Aural Monitor for Frequency Modulation," J. L. Hathaway and R. E. Lafferty, *Proc. I.R.E.* (May) 1952

"Azimuth Film Calibration," M. Rettinger, *Audio. Eng.* (April) 1952

"The Control of Frequency Response and Stability of Point-Contact Transistors," B. N. Slade, *RCA Licensee Bulletin LB-867* (June 19) 1952

"A Crystal Ringing Circuit for Color Synchronization," J. Avins, *RCA Licensee Bulletin LB-863* (May 20) 1952

"A Deluxe TV-Audio Console Custom Built by RCA for NBC Studios," R. W. Byloff, *Broadcast News* (May-June) 1952

"Ferromagnetic Spinels Containing Lithium," R. S. Weisz, *Ceramic Industry* (April and May) 1952

"A Four-Purpose Communication-Receiver Auxiliary," G. D. Hanchett, Jr. and K. G. Bucklin, *QST* (April) 1952

"Germanium P-N-P Junction Transistors," L. D. Armstrong, J. I. Pantchechnikoff, C. W. Mueller, and R. R. Law, *RCA Licensee Bulletin LB-868* (June 23) 1952

"Heater-Cathode Leakage Hum Reduction by Means of a Shielded Heater," K. R. DeRemer and H. Johnson, *RCA Licensee Bulletin LB-861* (May 5) 1952

"Horizontal-Deflection-Output and High-Voltage Transformer RCA-230T1 for 18-Kilovolt Kinescope Operation," *RCA Application Note AN-154*, RCA Tube Department, Harrison, N. J. (April) .. 1952

"The Host Crystal Luminescence of Zinc Sulfide Phosphors," R. H. Bube, *Jour. Chem. Phys.* (April) 1952

"How to Handle Film in Your TV Station," W. L. Murray, *Broadcast News* (May-June) 1952

"Increasing Tube Reliability in Industrial Circuits," D. G. Koch, *Product Eng.* (June) 1952

"Interference from Harmonics of Sound-IF and Picture-IF Signals," J. R. Meagher, *RCA Radio and Television Service News*, (May-June) 1952

"NBC Converts El Capitan for TV Theatre," *Broadcast News* (May-June) 1952

"A New All-Purpose Television Camera," A. Reisz, *Tele-Tech* (April) 1952

"Noise Factor Considerations and Measurement Techniques at UHF," B. Harris and A. T. Brennan, *RCA Licensee Bulletin LB-866* (June 5) 1952

† Report all corrections or additions to RCA Review, Radio Corporation of America, RCA Laboratories Division, Princeton, N. J.

* *RCA Licensee Bulletins* are not published and are issued only as a service to licensees of the Radio Corporation of America.

"Occurrence of Ferromagnetism in Spinels," R. S. Weisz, *Ceramic Age* (April) 1952
"Optical-Magnetic Sound 16mm Projector," G. A. del Valle and F. L. Putzrath, *Jour. S.M.P.T.E.* (April) 1952
"Pack-Carried Television Station," L. E. Flory, W. S. Pike, J. E. Dilley, and J. M. Morgan, *Electronics* (June) 1952
"Pattern-Testing the TFU-24B UHF Antenna," E. H. Shively, *Broadcast News* (May-June) 1952
"Planetary Position Effect on Short-Wave Signal Quality," J. H. Nelson, *Elec. Eng.* (May) 1952
"The Plasmatron, A Continuously Controllable Gas-Discharge Developmental Tube," E. O. Johnson and W. M. Webster, *Proc. I.R.E.* (June) 1952
"P-N Junctions by Impurity Introduction Through an Intermediate Metal Layer," L. D. Armstrong, *RCA Licensee Bulletin LB-869* (June 23) 1952
"Practical TVI Filter," J. Owens, *Radio-Electronics* (May) 1952
"The Preparation of Single and Multiple P-N Junctions in Single Crystals of Germanium," A. R. Moore, *RCA Licensee Bulletin LB-860* (April 25) 1952
"Production Testing of Multiplier Phototubes," R. W. Engstrom, R. G. Stoudenheimer, and A. M. Glover, *Nucleonics* (April) 1952
"Some New Ultra-High-Frequency Power Tubes," P. T. Smith, *RCA Review* (June) 1952
"Some Types of Omnidirectional High-Gain Antennas for Use at Ultra-High Frequencies," J. Epstein, D. W. Peterson, and O. M. Woodward, Jr., *RCA Review* (June) 1952
"Static Magnetic Matrix Memory and Switching Circuits," J. A. Rajchman, *RCA Review* (June) 1952
"Studies of Externally Heated Hot Cathode Arcs, Part II—The Anode-Glow Mode," W. M. Webster, E. O. Johnson, and L. Malter, *RCA Review* (June) 1952
"A Survey of Transistor Development," B. N. Slade, *RCA Licensee Bulletin LB-862* (May 19) 1952
"The Synchro-screen as a Stage Setting for Motion Picture Presentation," B. Schlanger, W. A. Hoffberg, and C. R. Underhill, Jr., *Jour. S.M.P.T.E.* (June) 1952
"A Technical Solution of Magnetic Recording Cost Reduction," K. Singer and H. C. Ward, *Jour. S.M.P.T.E.* (April) 1952
"Televised Films—A Review of Current and Proposed Methods," P. J. Herbst, *Broadcast News* (May-June) 1952
"Transistor Oscillators," R. O. Endres, R. P. Moore, Jr., and E. A. Oser, *RCA Licensee Bulletin LB-865*, (May 23) 1952
"Trouble Shooting 'Tough' Sets or 'Dogs'," J. R. Meagher, *TV Servicing*, Supplement I (May) 1952
"TV Facilities for NBC Hollywood Studio 'D'," *Broadcast News* (May-June) 1952
"TV Pattern for the Future," R. F. Guy, *Radio-Electronics* (May) .. 1952
"Twin-Drum Film-Drive Filter System for Magnetic Recorder-Reproducer," C. E. Hittle, *Jour. S.M.P.T.E.* (April) 1952
"Use of Thoriated-Tungsten Filaments in High-Power Transmitting Tubes," R. B. Ayer, *Proc. I.R.E.* (May) 1952
"A Video Test Signal Generator," H. Borkan, J. G. Reddeck, and W. C. Morrison, *RCA Licensee Bulletin LB-859* (April 4) 1952
"Zinc-Magnesium Oxide and Zinc-Magnesium Sulfide Phosphors," *Jour. Electro-Chem. Soc.* (April) 1952
"A 7000-Megacycle Developmental Magnetron for Frequency Modulation," H. K. Jenny, *RCA Review* (June) 1952

AUTHORS

ORVILLE E. DOW received the B.S. degree in Electrical Engineering from the University of Colorado in 1928, and in the same year joined the Transmitter Research and Development Laboratory of RCA Communications, Inc. Since 1942 he has been with the Radio Systems Research Laboratory of RCA Laboratories Division at Rocky Point, L. I., N. Y. Mr. Dow is a member of Tau Beta Pi, Sigma Tau, and an Associate Member of the Institute of Radio Engineers.

RICHARD O. ENDRES studied engineering at Tulsa University and majored in communications at Purdue University, receiving the B.S. degree in Electrical Engineering in 1948. He joined the Engineering Products Department of the RCA Victor Division at Camden, N. J. in the same year. His work in the Advanced Development Section since that time has been on applied research. Mr. Endres is presently doing graduate study at Pennsylvania University, and is an Associate Member of the Institute of Radio Engineers.

JOHN R. FORD received the B.S. degree in Electrical Engineering from the Massachusetts Institute of Technology. In 1940 he joined RCA as a design engineer at Camden, N. J. In 1944 he became a systems engineer with the Government Radar Engineering Section of the Engineering Products Department. Mr. Ford is presently on an extended assignment in New Mexico.

L. J. GIACOLETTO received the B.S. degree in Electrical Engineering from Rose Polytechnic Institute, Terre Haute, Indiana, in 1938, and the M.S. degree in Physics from the State University of Iowa in 1939. From 1939 to 1941, while a Teaching Fellow in the department of Electrical Engineering at the University of Michigan, he engaged in frequency-modulation research. He received the Ph.D. degree in Electrical Engineering from the University of Michigan in 1952. He was associated with the Collins Radio Company during the summers of 1937 and 1938, and with the Bell Telephone Laboratories in 1940. From 1941 to 1945 he served with the Signal Corps and returned to inactive status as a major in the Signal Corps Reserve in May, 1946. Since June, 1946, he has been serving as a research engineer at RCA Laboratories Division, Princeton, N. J. Dr. Giacoletto is a member of the American Association for the Advancement of Science, Gamma Alpha, Iota Alpha, Phi Kappa Phi, Tau Beta Pi, and Sigma Xi.

EDWIN A. GOLDBERG received the degrees of B.S. in E.E. and M.S. in E.E. in 1938 and 1940 at the University of Texas. From 1938 to 1939 he was employed on a field seismograph crew by the Magnolia Petroleum Co. He joined the RCA Manufacturing Co. in 1940 as a student engineer, and was assigned to the Research Division in 1941. He was transferred to Princeton in 1942 with RCA Laboratories Division. Mr. Goldberg is a Member of Eta Kappa Nu, Tau Beta Pi, Sigma Xi, and the American Institute of Electrical Engineers.

EUGENE B. HERMAN is a graduate of Pennsylvania State College with B.S. and M.S. degrees in Physics. Following the completion of his academic training in 1949, he joined the RCA organization as a design engineer on FM altimeters. He is now a member of the Microwave Componants Group of the Government Radar Engineering Section, Engineering Products Department.

NATHANIEL I. KORMAN received the B.S. degree in General Engineering from Worcester Polytechnic Institute in 1937. He then entered Massachusetts Institute of Technology under a Charles A. Coffin Fellowship and received the M.S. degree in Electrical Engineering in 1938. Later the same year he joined RCA as a student engineer. His early engineering activities were in the field of advanced development work on FM transmitters and associated equipment. He is now Assistant Manager of the Government Radar Engineering Section in charge of its development activities. He is Chairman of the Ground Based surveillance Radar Sub-panel of the Research and Development Board of the U. S. Department of Defense. Mr. Korman is a member of Sigma Xi.

JEROME KURSHAN received the B.A. degree with honors in Mathematics and Physics from Columbia University in 1939 and was an assistant in Physics there during that year. From 1939 to 1943 he was an assistant in Physics at Cornell University where he received the Ph.D. degree in 1943. Since then he has been with the RCA Laboratories Division at Princeton, working on FM magnetrons, special receiving tube problems and, more recently, on transistors and semiconductor physics. Dr. Kurshan is a member of Phi Beta Kappa, Sigma Xi, the American Physical Society and the Institute of Radio Engineers.

RAYMOND P. MOORE, JR. received the B.S. degree in Physics from Rensselaer Polytechnic Institute, in 1948. In the same year, he joined the RCA Victor Division at Camden, N. J. At present Mr. Moore is working in the Advanced Development Section of the Engineering Products Department on problems in applied research.

E. A. OSER received the Ph.D. degree in Experimental Physics at the University of Goettingen, Germany, in 1935. From 1935 to 1937 he worked on nuclear physics at Victoria University, Manchester, England. Since 1937, except for two years spent as a development engineer (1942-1944), he has been engaged in patent practice. In 1944 he joined the Patent Department of Farnsworth Television and Radio Corporation, at Fort Wayne, Indiana, and from 1947 to 1952 he was associated with the Patent Department of Radio Corporation of America in Camden, New Jersey. He is presently associated with the Patent Department of Hughes Aircraft Company at Culver City, California. Dr. Oser has been concerned primarily with inventions in the electronic field, including semi-conductor devices and transistor circuits.

ROLF W. PETER received the M.S. degree in Electrical Engineering in 1944, and the Ph.D. degree in Radio Engineering in 1948 from the Swiss Federal Institute of Technology in Zurich, Switzerland. From 1946 to 1948 he was Assistant Professor of Radio Engineering at the Swiss Federal Institute of Technology. In 1948 he joined the RCA Laboratories Division in Princeton, N. J., where he has been engaged in research on traveling-wave tube amplifiers. Dr. Peter is a Member of Sigma Xi and a Senior Member of the Institute of Radio Engineers.

JOHN C. TURNBULL received the B.S. degree from the Massachusetts Institute of Technology in 1934 and the Ph.D. degree in Physics from Brown University in 1938. From 1939 to 1941, he was engaged in research on glass problems for Glass Container Association. From 1942 to 1945, he was associated with the M.I.T. Radiation Laboratory and the Radio Research Laboratory in Cambridge, Mass. Since 1945, he has been with the Tube Department of the RCA Victor Division at Lancaster, Pa. engaged in glass technology. Dr. Turnbull is a member of the American Ceramic Society and the American Physical Society.

RICHARD C. WEBB received the B.S. degree in Electrical Engineering from the University of Denver in 1937, and the M.S. degree in 1944 and the Ph.D. degree in 1951 from Purdue University. From 1937 to 1939 he was associated with the Mountain States Telephone and Telegraph Company in Denver, Col., and from 1939 to 1945 he was an instructor and research assistant at Purdue. In 1945 he joined the Research Department of RCA Laboratories Division at Princeton, N. J. From January 1950 to June 1951 he was on leave of absence from RCA, first at Iowa State College and later at Purdue. Since August 1952 he has been on leave of absence from RCA working at the Institute of Industrial Research of the University of Denver. Dr. Webb is a member of the Society of Motion Picture and Television Engineers, the Institute of Radio Engineers, Tau Beta Pi, Eta Kappa Nu, and Sigma Xi.